PROTECTING HEALTHY CELLS AGAINST THE NEGATIVE EFFECTS OF RADIATION THERAPY FOR LUNG CANCER

APPROVED BY SUPERVISORY COMMITTEE

_____
Jerry W. Shay, PhD

_____
Sandeep Burma, PhD

_____
Ralph DeBerardinis, MD, PhD

_____
Carole Mendelson, PhD

_____
Woodring E Wright, PhD

DEDICATION

Graciously and humbly written in honor of my Giddo and his Aida.

PROTECTING HEALTHY CELLS AGAINST THE NEGATIVE EFFECTS OF RADIATION THERAPY FOR LUNG CANCER

by

MARIAM A. EL-ASHMAWY

DISSERTATION

Presented to the Faculty of the Graduate School of Biomedical Sciences

The University of Texas Southwestern Medical Center

In Partial Fulfillment of the Requirements

For the Degree of

DOCTOR OF PHILOSOPHY

The University of Texas Southwestern Medical Center

Dallas, Texas

May, 2017

PROTECTING HEALTHY CELLS AGAINST THE NEGATIVE EFFECTS OF RADIATION THERAPY FOR LUNG CANCER

MARIAM EL-ASHMAWY, PhD

The University of Texas Southwestern Medical Center at Dallas, 2015

JERRY W. SHAY, PhD

Although radiation therapy is a commonly used treatment for many human diseases including cancer, ionizing radiation produces reactive oxygen species that can damage both cancer and healthy cells. Synthetic triterpenoids, including CDDO-Me, act as anti-inflammatory, antioxidant modulators primarily by inducing the Nrf2/ARE pathway. In the documented series of experiments, I show that CDDO-Me can be used as a radioprotector in normal non-cancerous human lung and breast epithelial cells, whereas CDDO-Me does not further protect cancer lines from radiation-induced cytotoxicity, nor does it protect experimentally transformed human bronchial epithelial cells with progressive oncogenic manipulations. Additionally, CDDO-Me protects human lymphocytes against radiation-induced DNA damage. As part of these studies

other compounds (RTA-408, TA-65, and Yel-002) were also tested for radioprotective effects in epithelial and cancer cells as well as human lymphocytes. A therapeutic window exists in which CDDO-Me protects normal cells from radiation by activating the Nrf2 pathway, but does not protect experimentally transformed or cancer cell lines. This suggests that use of this oral available, non-toxic class of drug can protect non-cancerous healthy cells during radiotherapy, potentially resulting in better outcomes with less toxicity for patients.

The effects of radiation and DNA damage in traditional two-dimensional (2D) cell culture conditions *in vitro* may not recapitulate tissue responses as modeled in three-dimensional (3D) organotypic culture systems since important signals, provided by the extracellular matrix and microenvironment, are lost in 2D monolayer cultures. While irradiating premalignant HBECs in traditional 2D culture significantly increased cancer progression phenotypes, irradiation in 3D culture reduced radiation-induced transformation compared to 2D. Furthermore, 3D cell culture conditions did not affect cell killing, the ability of cells to survive in a colony formation assay, and proliferation rates after radiation—implying there was no obvious selection against any cells in or dissociated from 3D conditions. My findings indicate that culture conditions are crucial for cellular responses to radiation and can affect cancer progression. If 3D culture is a more biologically representative model compared to 2D cultures, then current studies assessing transformation and radiation may be overestimating radiation risks using standard 2D culture methods.

Acknowledgments

I would like to express the deepest gratitude and appreciation to my mentors Drs. Jerry W. Shay and Woodring E. Wright for their support and guidance over the past four years. The members of the lab have been critical in my success, especially Dr. Oliver Delgado, who trained me from the moment I joined lab and was a great mentor and friend. Huge thanks to Aadil Kaisani and Sang Bum Kim for keeping me company and helping me troubleshoot. Kimberly Batten and Crystal Cornelius for balancing me out. Krishna Luitel for his exuberant curiosity and strong work ethic. Ronald Bozeman, Jennifer Peters-Hall, Melissa Coquelin, Summer Baron, Andrew Ludlow. Ehsan Sayed and Laura Yuan for making me laugh and keeping me company during our adventures, both in and out of lab. Most importantly, merci beaucoup to my dear friend Jerôme Robin, without whom I would have been lost and definitely bored.

Profound thanks to my thesis committee members Drs. Sandeep Burma, Ralph Deberardinis, and Carole Mendelson, for always making time in their busy schedules to nurture my progress throughout this journey. Our collaborators Drs. John Minna and Michael Story for help and support with irradiation experiments, NSCOR support, reagents, and for help planning and designing crucial experiments. Their labs' members have also been invaluable, Boning Gao, Seongmi Park, Michael Peyton, and Luc Girard. I would also like to acknowledge The Genomics Shared Resource and Cancer Center Support Grant for conducting microarray experiments. Many thanks to Sarah Gonzales-van Horn and David Farrar in Department of Immunology for facilitating the initial human lymphocyte experiments and re-teaching me how to draw blood after I'd long forgotten. Thanks to Brandon Probst, Lyndsey McCauley, Deborah Ferguson, and Chris Wigley from Reata Pharmaceuticals (Irving, TX) for important discussions and reagents.

The entire staff and support at the NASA Space Radiation Laboratories at Brookhaven National Laboratory (Upton, New York), especially Peter Guida, Adam Rusek, and Chiara LaTessa for making my time in Long Island fun, educational, and memorable. The Howard Hughes Medical Institute Gilliam Fellowship and everyone at HHMI who have followed my path and supported my progress over eight years—Maryrose Franko, Megan Lassig, Makeda Richardson, and David Asai. The Medical Scientist Training Program administrators and staff—Robin Downing, Stephanie Robertson, Charletha Jordan, and Drs. Andrew Zinn and James Amatruda.

All my classmates for late night vent sessions, help with protocols, emergency reagents, and hypothetical science experiments, without which I would never been able to complete a dissertation. This especially goes to Gina Aloisio, for being my science soulmate and the most positive, brilliant, talented, beautiful, and helpful and supportive person I have ever have the honour of being friends with.

Finally, my parents Amina and Ahmed deserve the greatest recognition for their continual support, example, and motivation, and my sister and best friend Laila, for being there even when she was halfway across the world. My family has pushed me to the edge while making sure I was able to balance there without ever falling off. I love you.

TABLE OF CONTENTS

Prior Publications

2015 **El-Ashmawy M**, Luitel K, Batten K, Shay JW. (2015) Organotypic culture in three-dimensions prevents radiation-induced cancer progression in the lung. *In progress*.

2014 **El-Ashmawy M**, Delgado O, Cardentey A, Wright W, Shay JW. (2014) CDDO-Me protects normal lung and breast epithelial cells but not cancer cells from radiation. *PLoS ONE*, 9(12): e115600.

2012 Conrad CD, McLaughlin KJ, Huynh TN, **El-Ashmawy M**, Sparks M. (2012) Chronic stress and a cyclic regimen of estradiol administration separately facilitate spatial memory: relationship with hippocampal CA1 spine density and dendritic complexity. *Behavioral Neuroscience*, 126:142-56.

List Of Figures

List Of Tables

List Of Appendices

List Of Abbreviations

2D – two dimensional

3D – three dimenstional

3D-CRT – three dimensional conformal radiation therapy

^{56}Fe – iron 56

ABL – abelson murine leukemia viral oncogene homolog 1

ACE – angiotensin-converting enzyme

ADAMTS6 – A disintegrin and metalloproteinase with thrombospondin type 1 motif 6

ADC – adenocarcinoma

ADH – antidiuretic hormone

AIM – anti-inflammatory or anti-oxidative modulator

AKT – protein kinase B

ALI – air liquid interface

ALK – anaplastic lymphoma kinase

AP1 – activator protein-1

ARE – antioxidant response element

ATP – adenosine triphosphate

BCL2 – B-cell lymphoma 2

BCR – breakpoint cluster region

BMI1 – B lymphoma Mo-MLV insertion region 1 homolog proto-oncogene, polycomb ring finger

BMP4 – bone morphogenic protein

CC10 – Clara cell protein 10

CDDO-Me – oleana-1,9 (11)-dien-28-oicacid, 2-cyano-3,12-dioxo-, methyl ester; bardoxolone-methyl; RTA-402

CDK4 – cyclin-dependent kinase 4

CDKN2A p16^{INK14a} – cyclin dependent kinase inhibitor p16

CLK1 – CDC-like kinase 1

COX – cyclooxygenase

^{137}Cs – cesium 137

CT – computerized tomography

DAPI – 4',6-diamidino-2-phenylindole

DMF – dose modifying factor

DMSO – dimethyl sulfoxide

DNA – deoxyribonucleic acid

DPPC – phospholipid dipalmitoyl phosphatidylcholine

DSB – double-strand break

ECM – extracellular matrix

EdU – 5-ethynyl-2'-deoxyuridine

EGFR – epidermal growth factor receptor

EM – electromagnetic

EthD1 – ethidium D1

FDA – Food and Drug Administration

FDR – false detection rate

FGF10 – fibroblast growth factor 10

FOXA2 – forkhead box protein

G1 – gap 1 (phase of mitosis)

GST1 – glutathione S-transferase

GUSB – glucuronidase beta

Gy – gray

^{+}H – proton

H&E – hematoxylin and eosin

HBEC – human bronchial epithelial cell

HER2 – v-Erb-B2 avian erythroblastic leukemia viral oncogene homolog 2

HIF1α – hypoxia inducible factor

HMEC – human mammary epithelial cell

HO1 – heme oxygenase

HRE – hypoxia response element

HPRT1 – hypoxanthine phosphoribosyltransferase 1

HSP90AM1 – heat shock protein 90kDa alpha class B member 1

hTERT – human telomerase reverse transcriptase

Hz – hertz

HZE – high charge and energy

IMRT – Intensity-modulated radiation therapy

^{131}I – iodine 131

IR – ionizing radiation

IκK – I kappa B kinase

JAK – janus kinase

JUN – jun proto-oncogene

K-Ras – v-Ki-ras2 Kirsten rat sarcoma viral oncogene homolog

Keap1 – kelch-like ECH-associated protein

KSFM – keratinocyte serum free media

LC_{50} – median lethal concentration

LCC – large cell carcinoma

LET – linear energy transfer

LOH – loss of heterozygosity

MAPK – mitogen-activated protein kinase

MDM2 – mouse double minute 2 homolog

MEF – mouse embryonic fibroblast

MeV/n – mega electronvolt per nucleon

mTOR – mammalian target of rapamycin

MYC – v-myc avian myelocytomatosis viral oncogene homolog

NADPH – nicotinamide adenine dinucleotide phosphate

NASA – National Aeronautics and Space Administration

NCRP – National Council of Radiation Protection and Measurement

NFκB – nuclear factor kappa beta

NQO1 – NADPH dehydrogenase quinone

Nrf2 – nuclear factor erythroid-derived 2 -like 2

NSAID – nonsteroidal anti-inflammatory drug

NSCLC – non-small cell lung cancer

PAGE – polyacrylamide gel electrophoresis

PBS – phosphate buffered saline

PD – population doubling

P_{ef} – plating efficiency

PHA-L – phytohaemagglutinin

PI3K – phosphatidylinositol-4,5-bisphosphate 3-kinase

PNEC – pulmonary neuroendocrine cells

PRX1 – peroxiredoxin

PTHrP – parathormone-related peptide

qRT-PCR – quantitative reverse transcription polymerase chain reaction

RAB6A – Ras-related GTP binding protein

Ral/RalGEF – Ras-like small GTPase

RB – retinoblastoma 1 protein

RNA – ribonucleic acid

ROS – reactive oxygen species

RPMI – Roswell Park Memorial Institute

S – synthesis (phase of mitosis)

SCC – squamous cell carcinoma

SCLC – small cell lung cancer

SDS – sodium dodecyl sulfate

SF – surviving fraction

SHH – sonic hedgehog

shRNA – short hairpin RNA

SIRT2 – sirtuin 2

SP-C – surfactant protein C

SPE – solar particle event

SPRY2 – sprouty homolog proteins

STAT – signaling transducer and activator of transcription

SVC – superior vena cava

TA – telomerase activator

TGF-β – transforming growth factor beta

TNM – tumor nodes mets

TP53 (p53) – tumor proteins p53

TTF1 – thyroid transcription factor

UV – ultraviolet

VEGF – vascular epitheilial growth factor

WR – radiation weighting factor

γ - gamma radiation

CHAPTER ONE

Introduction to Respiratory Biology, Lung Cancer, and Radiation

1.1 Respiratory Biology

The human lung is part of the respiratory system, a complex network of airways responsible for gas exchange between the circulatory system and exogenous environment. The respiratory system is composed of two functional and structural components: the air-conducting, or central airway, and the respiratory, or peripheral airway (**Figure 1.1**). The chest cavity and rib cage protect the lung externally, while the diaphragm and other smaller intercostal muscles control ventilation. The reticular formation and brainstem within the central nervous system regulates breathing, sending innervation via the vagus and phrenic nerves and pulmonary plexus [147].

After a deep inhale, air rushes quickly through the nasal cavity, where specialized olfactory sensing cells smell the air, and a system of conchae create eddies in the air flow to contribute to turbulent precipitation of particulate matter and help warm the air. From the nose, air travels past the pharynx to the larynx, where a system of irregularly shaped cartilaginous plates give way to the trachea. Up to twenty C-shaped cartilaginous rings give this short tube structure and rigidity with an underlying system of smooth muscles and fibroelastic tissues for flexibility when swallowing [147]. A specialized pseudostratified epithelium lines the trachea and upper airway, specifically suited for conditioning and filtering inhaled air (**Figure 1.2A**). Continuously beating ciliated columnar cells allow particulate matter or potential pathogens to be expelled using motile cilia projected from their apical surface. Coating the epithelial surface is a continually moving layer of mucus, produced by secretory goblet cells, which offer protection by

catching airborne debris as well as moisten and humidify inhaled air. Basal cells, which hug the bottom layers of the central airway in close vicinity to the basal lamina, help anchor the pseudostratified epithelium to the matrix and protect the stroma from the exogenous environment [181]. Basal cells play a crucial role in regenerating and repopulating the upper airway after injury or normal cell turnover; this will be further discussed in the following section [35]. Another interesting cell type found throughout the central airway are the innervated, columnar pulmonary neuroendocrine cells (PNEC), responsible for sensing hypoxia in the airway and transmitting this information to nervous system. Sometimes found in clusters called neuroepithelial bodies, PNECs are usually found in the highest densities where the trachea bifurcates into bronchi and subsequent branch points [35].

In line with the sternal angle, at the level of the fifth thoracic vertebra where the trachea bifurcates, is a longitudinal cartilaginous ridge known as the carina; the mucous membrane here is the most sensitive area of the trachea/larynx and is responsible for triggering cough reflexes. The trachea bifurcates into the left and right primary bronchi, which continue to branch into smaller bronchi and bronchioles after entering the lobes of the lung, forming the bronchial tree (**Figure 1.1**). These primary bronchi have a similar cellular composition as the trachea, although smaller in diameter, with fewer cartilaginous rings. Due to the spatial constraints of the heart in the chest cavity, fewer lobar (secondary) branches exist on the left side of the lung. The left bronchus, leading to the left lung, divides into two left lobes, whereas the right bronchus, leading to the right lung, divides into three right lobes [147]. Each lobar bronchus further bifurcates into tertiary and various segmented bronchi. Segmental bronchi compose distinct bronchopulmonary segments, separated by a layer of connective tissue, and are capable of functioning completely independently of one another. Within the intrapulmonary bronchi, small

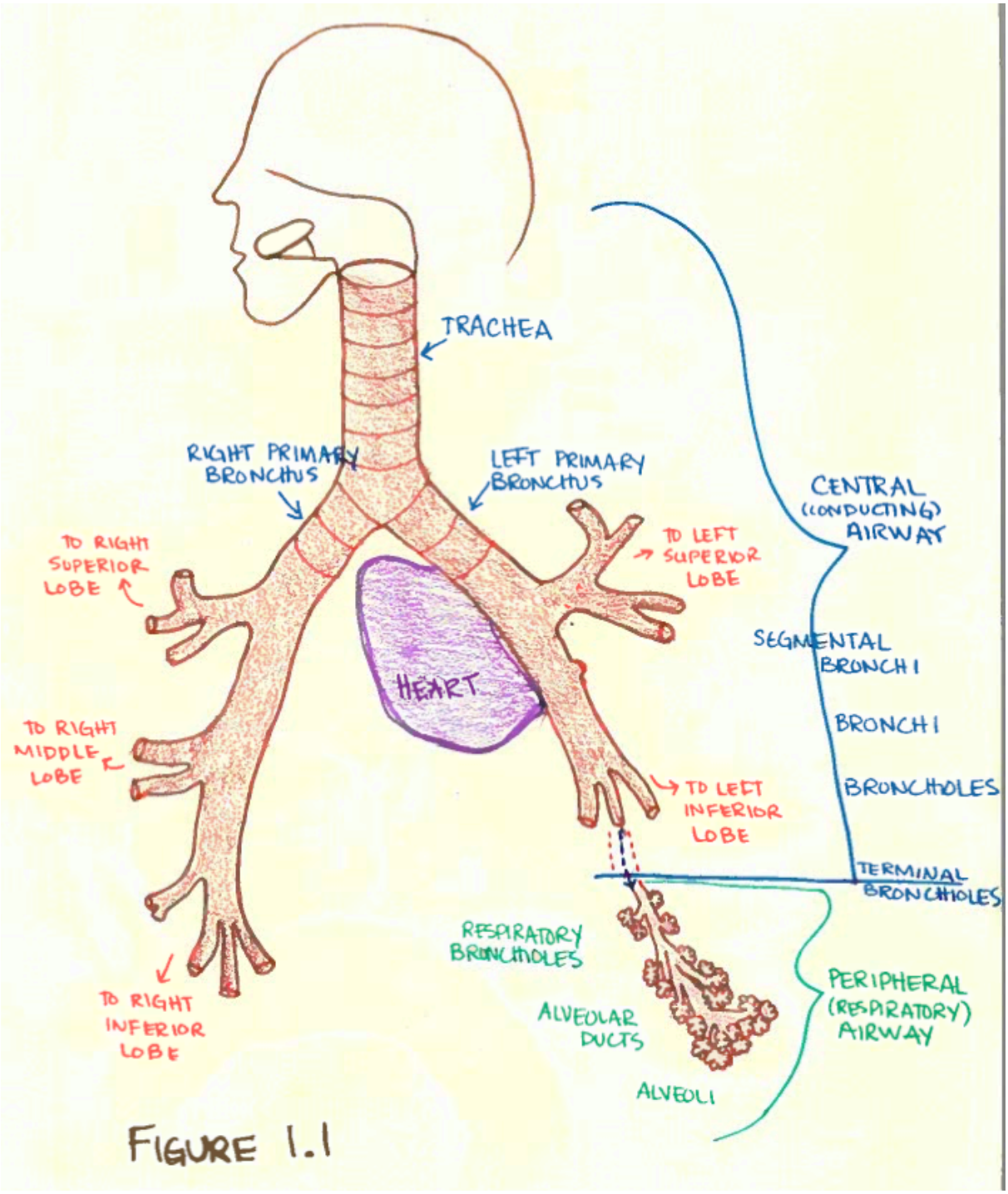

Figure 1.1: Central and Peripheral Airways of the Lung

islands of cartilage and submucosal glands are present with spiral bands of smooth muscle to keep the airway open [147].

As bronchi dive and branch deeper into the lung, bronchioles appear. These structures have no cartilage with well-developed smooth musculature to help with lung recoil. A shift in the epithelial composition also occurs at this point—transitioning from columnar to cuboidal, with a gradual reduction in the fluid-producing goblet and ciliated cells (**Figure 1.2A**). Specialized dome-shaped secretory club (formerly Clara) cells appear, which produce the surface-active agent (CC10) responsible for detoxification and degrading the mucus produced in the upper airway. Along with a few ciliated cuboidal cells, club cells compose the majority of lower airway epithelium, and a subset of these cells may also serve as stem-like regenerative cells capable of repopulating the lower airways [35]. These changes in epithelial composition reflect enhanced mucus clearance and prevent substantial mucus penetration of the deeper respiratory lung tissue. Continued branching eventually gives rise to terminal bronchioles, with a very thin smooth muscle layer and highly irregularly shaped lumen. The conducting segment, which ends at the terminal bronchioles, consists of a branching system where the combined diameters from each branch are larger than the previous branch. While air rushes through the initial conducting segments, it slows as the airways taper with each successive split. By the time it reaches the respiratory components, the air is flowing rather slowly, which helps facilitate gas exchange.

Once air has been cleaned, humidified, and funneled through the conducting component, it enters the respiratory zone where oxygenation and carbon dioxide exchange takes place (**Figure 1.1**). Respiratory bronchioles, emerging from each terminal bronchiole, can be distinguished by the presence of thin-walled outcroppings—up to a dozen alveolar ducts—lined

by squamous epithelium. Alveolar ducts contain multiple septated saccular alveoli, separated by an interalveolar septum, and are lined with cuboidal cells and smooth muscle that allow for constriction of the ducts. Alveoli, the primary sites for gas exchange, are the end of the continuous branched network and completes the tubule structure of the lung [147]. Surrounding the semi-circular shaped alveoli is a very thin connective tissue layer containing capillaries. Apart from the airway tree in the respiratory system, there is a corresponding circulatory vascular tree composed of capillaries from branching blood vessels originating from the bronchial and pulmonary arteries [147]. These arteries follow the tracheal branches, intertwining until both terminate at alveoli, where they can trade their gaseous contents.

Many specialized cell types within alveolar architecture facilitate the various functions of gas exchange (**Figure 1.2B)**. Covering over ninety-five percent of the alveolar wall, the type I pneumocyte is a squamous epithelial cell whose role is conducting air between the alveolus and blood; their thin nucleus and extension of flattened cytoplasm allows for maximum gas exchange [35]. Type II pneumocytes specialize in the production of surfactant lipoproteins, composed of the phospholipid dipalmitoyl phosphatidylcholine (DPPC). Surfactant acts as a detergent by disrupting the intermolecular forces between water and the air/water interface, decreasing surface tension in the alveolus and preventing collapse of the structure. This decreases the amount of work necessary for breathing (compliance), as well as minimizes transudation of fluid from the pulmonary capillaries into the alveolar space, protecting against pulmonary edema [238]. Often found in the corners of alveoli, type II cells are cuboidal/pyramidal in morphology with characteristic lamellar bodies. Their frothy, vacuolated cytoplasm is the site of surfactant storage, which must be continuously replenished due to rapid metabolism in the lungs. Additional cells types include endothelial cells and pericytes, fibroblasts, as well as alveolar macrophages that

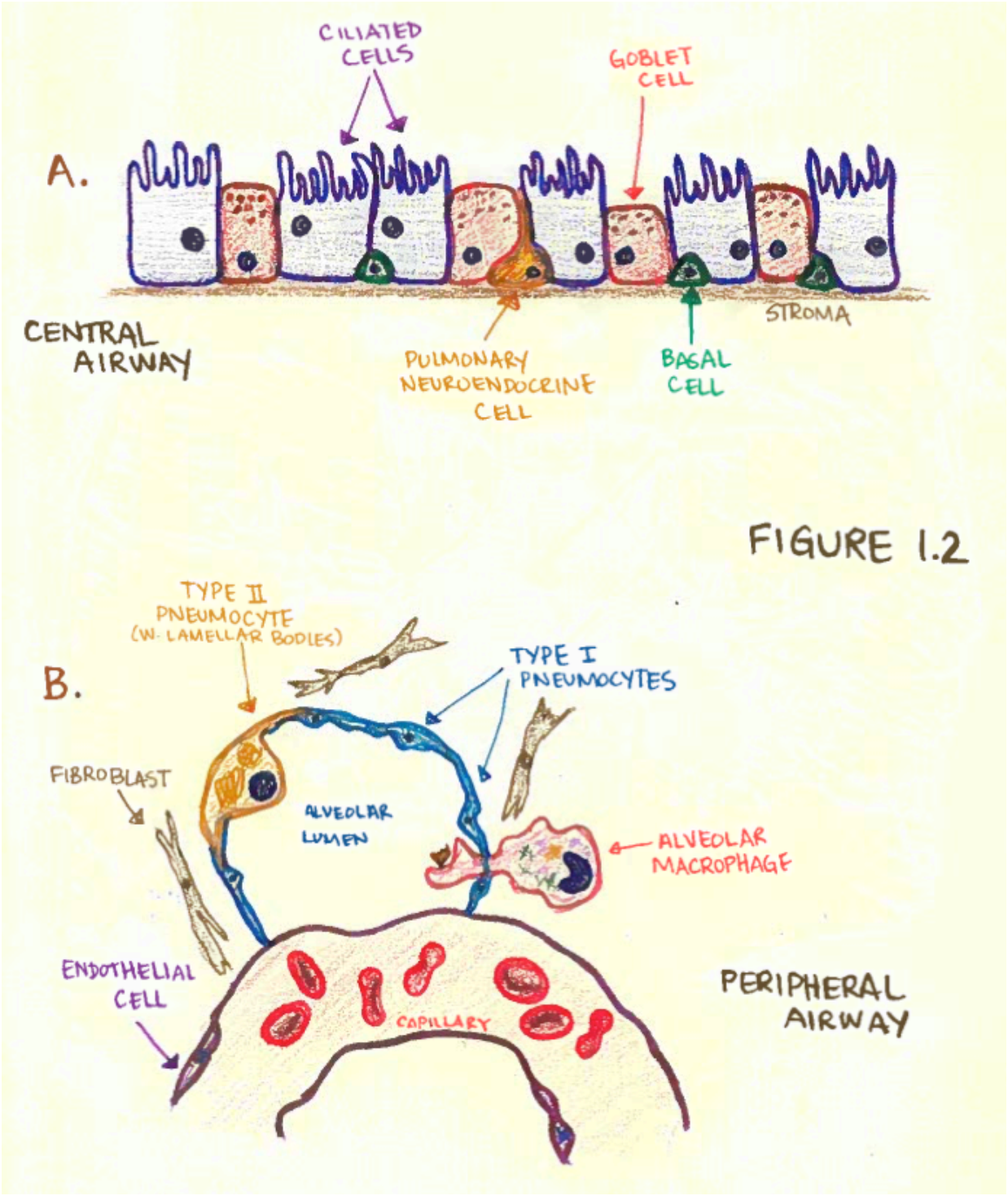

Figure 1.2: Epithelial Cell Types of the Central and Peripheral Airway

migrate across the alveolar epithelium to scavenge and phagocytose foreign particles that have penetrated the alveolus (**Figure 1.2B**). A rich capillary network surrounds alveoli, and gas exchange within the alveolus depends on the vasculature and architecture within the lung, and this can be affected by many factors. Gasses diffuse across the alveolar-capillary membrane, the rate of which depends on the pressure gradient, surface area, distance, and size and solubility of the gas. In disease states, ventilation and gas exchange can be affected, leading to inadequate oxygenation of the blood and tissues [239].

Surrounding the outer surface of the lung and adjoining blood vessels, bronchi, and nerves, is the visceral pleura, composed of mesothelium. The parietal pleura is attached to the chest wall, and this pleural cavity contains a small amount of pleural fluid between the two serous membranes, allowing the lung to expand in the chest cavity during ventilation without friction, as well as allowing greater inflation of the alveoli during breathing [147].

A continuous efflux of fluid from the capillaries to the interstitial space is removed by lymphatic drainage along a series of nodes and vessels, which follow bronchi, arteries, and veins. Distally, the pulmonary (intra-pulmonary) nodes and bronchopulmonary (hilar) lymph nodes are first in line to receive drainage, depending on the lobe from which drainage is occurring; these primary nodes are interspersed throughout the lung tissue along airway branch points (**Figure 1.4**). These lead to tracheobronchial (carinal) nodes located around the bifurcation of the trachea into main bronchi. Flowing proximally, paratracheal nodes situated along either side of the trachea lead fluid to either the bronchomediastinal lymphatic trunk and/or deep cervical (scalene) node. From these central locations, lymphatic fluid from the lungs rejoins the circulation via the brachiocephalic vein or thoracic duct [147]. The lymphatic system is especially important for filtering pathogens that have accessed the lung, containing the spread of diseases, and the

importance of these routes will become evident when staging of lung cancers is discussed in later sections (**Figure 1.4).**

Clinical inspection of the chest wall should reveal a smooth and convex chest with the trachea midline in healthy people. Accessory muscles, such as the sternocleidomastoid, abdominal wall, and intercostal muscles, are not used during respiration, and both sides of the chest should expand equally. Normally, sound is conducted through the airways to the pleura to the chest wall, so the vibrations of sounds are felt (tactile fremitus) when placing hands on the chest wall. Percussion of a healthy chest should be resonant. Auscultation of the lung with the diaphragm of a stethoscope normally reveals uniform breath sounds bilaterally. Different breath sounds (vesicular < 200 Hz < bronchial < 1000 Hz < tracheal <1500 Hz) are heard best over different areas of the lungs and are present at different times during inspiration or expiration. The presence of other adventitious sounds can indicate pathology; for example, “fine crackles” or dry rales may indicate heart failure, infections, or cancer [16].

1.2 Lung Development & Regeneration

Fetal development of the lung during gestation requires the complex integration of multiple regulatory factors to form an organ with a functional air-blood interface for respiration and gas exchange at the moment of birth. This dynamic process requires interaction between cells from multiple lineages and the environment [133]. Although development is a continuous process, lung development is divided into five developmental stages based on anatomical and histological characteristics: embryonic, psuedoglandular, canalicular, saccular, alveolar.

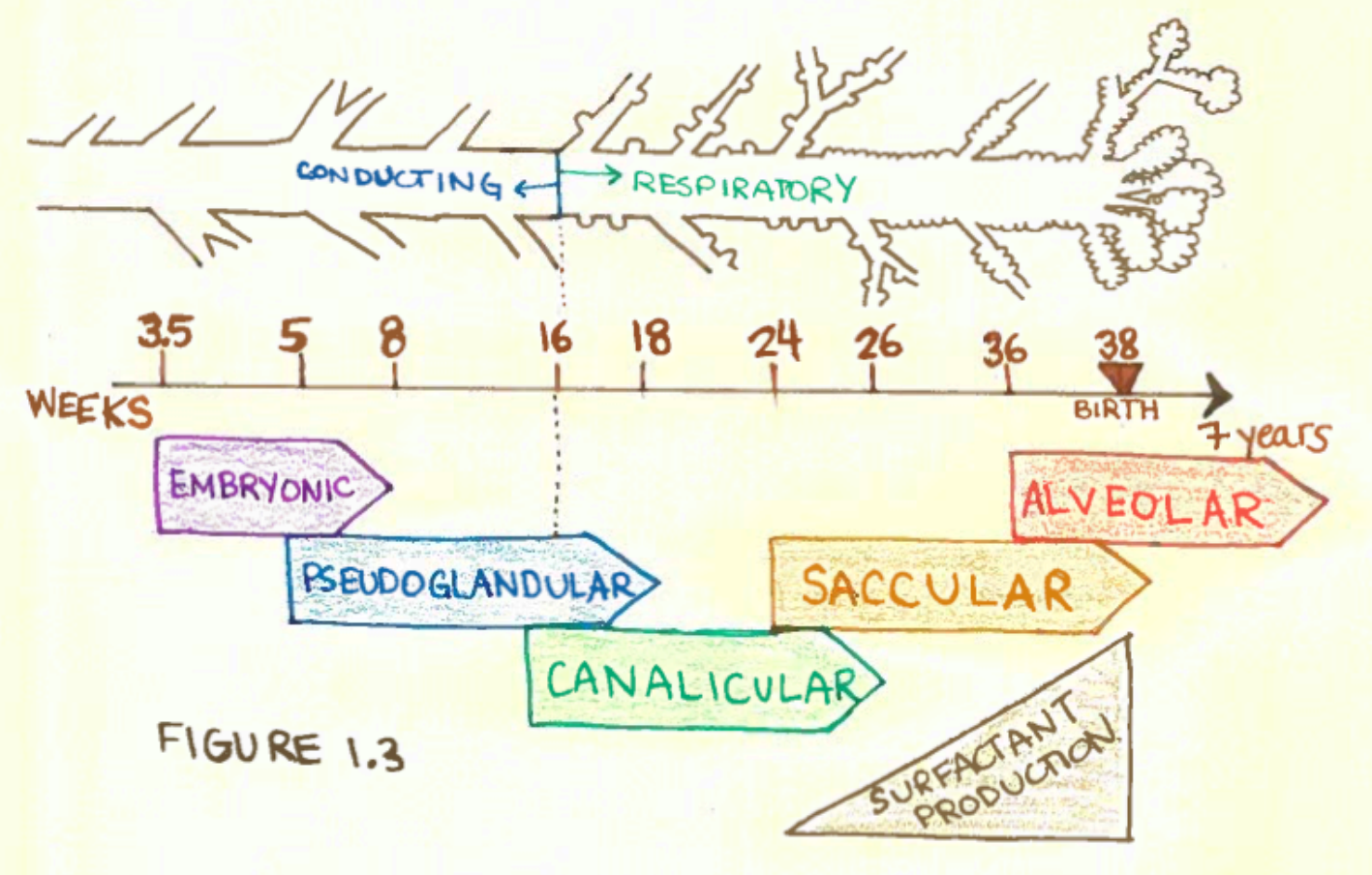

Figure 1.3: Overview of Lung Developmental Stages

Embryonic and psuedoglandular stages elaborate the conducting airways; vascularization and differentiation of airway epithelium to form of a thin blood-air interface occurs during the later stages (**Figure 1.3)**. Postnatally, continued growth and rapid expansion of the lungs allows for maximal surface area for ventilation [101, 183].

During the embryonic stage of lung development, two tubes develop from the interior forgut endoderm separated by longitudinal septum, eventually forming the trachea and esophagus [133, 183]. The respiratory tract develops from endoderm of the ventral foregut, from which the laryngo-tracheal groove arises as a ventral outpouching. The proximal portion will give rise to the larynx and trachea. The caudal portion of the laryngo-tracheal groove forms two ventrolateral buds, which will form the left and right primary bronchi, and these buds continue to branch and grow into adjacent splanchnic mesoderm [101]. Branching morphogenesis to form the conducting airways as well as the terminal alveolar compartments characterizes the psuedoglandular stage of lung development. Nearby mesenchyme signals primordial lung buds the using transcription factor gradients; particularly, fibroblast growth factor (FGF10) from neighboring cardiac mesoderm has been shown to be an essential signal for lung cell fate and branching morphogenesis; loss of the FGF signaling network results in complete lack of branching [101, 143, 192, 234]. Opposing gradients of forkhead box protein (FOXA2) and thyroid transcription factor (TTF1) delineate the region from which budding will occur [115]. To balance pro-branching signals, the sprouty homolog family of proteins (SPRY2) limit outgrowth and control the sizes of lung buds by acting as a negative regulator of FGF signaling for chemotaxis and proliferation [134, 234]. FGF secretion is further regulated by other signaling pathways, including bone morphogenic protein (BMP4), sonic hedgehog (SHH), transforming growth factor beta (TGF-β), and retinoic acid [25][11]. Fibronectin, an important extracellular

matrix (ECM) component, is responsible for guiding formation and directing new branch points [184]. Additionally during the pseudoglandular stage, the lining of proximal airways begins to differentiate into ciliated and goblet cells, and smooth muscle begins to differentiate from surrounding mesenchyme. The culmination of these factors, as well as many others, allow for the branching to be regulated in both a temporal and spatial fashion throughout the early stages of lung morphogenesis [25].

Lung tissue starts to form around the bronchial tree around the fifth week of gestation. The development of early respiratory components, including respiratory bronchioles and alveolar ducts, commences after branching morphogenesis during the canalicular stage (**Figure 1.3**) [183]. During this time, different peripheral cell types—such as the club cell and type II pneumocyte—differentiate from the airway epithelium while the lumens of established airways dilate [133]. Capillaries formed from the neighboring mesenchyme begin to invade the developing respiratory endoderm, and endothelial cells differentiate in proximity to the airway epithelium [210]. Transition of the lung from being fluid-filled to air-filled and resulting formation of alveolar sacs, arising from the ducts, marks the beginning of the saccular stage [133]. Type I pneumocytes line the alveolar sacs, although there is inefficient gas exchange at this stage due to the still thickened septa separating the capillaries. Type II pneumocytes begin to secrete surfactant as early as twenty weeks of gestation, although this is usually not enough to prevent atelectasis in pre-maturely born infants [183, 238]. Human lungs are required to perform their respiratory functions at birth, signifying the beginning of the alveolar stage, which continues postnatally until several years past birth. Expanding populations of type II pneumocytes secrete surfactant and act as the basal cell, from which type I pneumocytes arise [101, 133]. Maturation of alveoli includes the thinning and shrinkage of septa dividing the

airways and capillaries, while the existing network of vessels is remodeled and modified to allow for efficient gas exchange [143, 210].

Lung developmental processes during morphogenesis, while complex and not fully understood, are important for cellular differentiation and regeneration. Exposure to potential environmental injury, exogenous toxins, and pathogens requires the ability of an organ system to respond to cellular damage. Generation of new cells is integral for proper tissue homeostasis, repair, and maintenance of the adult human lung throughout a lifetime.

The ability of a tissue to regenerate depends on specialized stem cells within the population. Some organs—especially the gastrointestinal tract, skin, and hematopoietic system—must constantly renew themselves, resulting in localized niches harboring dedicated multipotent stem cells. These tissue stem cells have the ability to undergo long-term self-renewal in addition to producing a population of transient amplifying daughter cells. In organ systems with high turnover rates, transient amplifying cells serve as progenitors capable of reconstituting all cell types necessary within a tissue; although these oligopotent stem cells have higher proliferation rates compared to their parental tissue stem cells, they have limited self-renewal capacity [173, 236]. Other tissues—such as the lung, pancreas, or liver—maintain themselves without a dedicated, undifferentiated stem cell population. Rather, these organs harbor normally quiescent differentiated cells that can function as stem cells after serious damage to repopulate certain cellular compartments [236]. These facultative stem cells are thought to recapitulate developmental processes, proliferating and transdifferentiating in response to regenerative cues from the environment [173, 180].

Although the presence of "lung stem cells" has been hotly debated, especially in regard to cancer, the prominent view is that different kinds of stem cells are used depending on the region within the respiratory system. Since the trachea and primary buds each arise from distinctive morphogenic processes, large conducting airways utilize separate stem cells from the distal bronchioles and alveoli. Within the central airway, basal cells act as a multipotent stem cell for the pseudostratified epithelium—giving rise to ciliated and goblet cells as well as self-renewing the basal compartment [231]. After airway injury, it is postulated that basal cells respond by spreading and covering the basal lamina, forming apical intercellular junctions to restore the airway barrier, then proliferating and differentiating into the other cells types necessary for reconstituting the upper airway epithelium (**Figure 1.2A)** [180]. Within the peripheral airway, lineage-tracing experiments in mice have shown that a subset of less differentiated club cells (club-variant cells) have the ability to proliferate and regenerate lower epithelium after chemically-induced injury, capable of regenerating all regional epithelial cells except PNECs [157, 231]. However, club-variant cells do not give rise to either type I or II pneumocytes present in alveoli. Although ciliated cells are unable to self-renew or differentiate after injury, some investigations have shown that goblet cells have the ability to respond to injury in a progenitor-like capacity [53, 175]. Within the past decade, evidence has mounted for a bronchioalveolar stem cell in mice—an extremely rare cell expressing both CC10 protein as well as surfactant protein C (SP-C) of type II pneumocytes, present at the junctions of bronchioalveolar ducts [68, 231]. Purified populations of these dual-expressing cells are able to give rise to bronchial and alveolar cell types, although a subset of type II pneumocytes express low levels of CC10 [2, 174]. Furthermore, type II pneumocytes can self-renew and differentiate into type I cells, both in steady-state conditions or in response to injury [231]. Depending on the assay utilized, model

system, or region of the airway, it seems that several cellular populations have the capacity to regenerate a majority of lung cell types and/or self renew, and it is still unclear which cellular populations function as definitive stem cells in the lung.

1.3 Cancer Statistics

Cancer will kill over half a million people in 2015 and is currently the second leading cause of death in the United States [202]. It is responsible for one in eight deaths worldwide—this global cancer burden is expected to virtually double by the year 2030. Though slightly higher for men than women, lifetime risk of being diagnosed with an invasive cancer is forty percent [90]. This likely represents a combinatorial effect of multiple influences, including endogenous hormones and genetic susceptibility; environmental pollution and occupational exposure to carcinogens, such as radon, asbestos, or radiation; or lifestyle factors, such as tobacco, diet/nutrition, drug use, and alcohol consumption.

Tobacco smoke is one of the main culprits responsible for causing cancers, especially lung cancers. In 1964, the United States Surgeon General finally announced that smoking causes lung cancer, after almost a decade of controversial investigations [237]. Some estimate that ninety percent of lung cancers are due to tobacco smoke, and when combined with other risk factors, the synergism with tobacco can push the total attributable risk to one hundred percent [6]. The smoke produced by tobacco, as well as the chemical additives in cigarettes, culminate in a complex assembly of over four thousand chemicals and toxic carcinogens, which can damage DNA by causing adducts or mutations.

In the year 2015, it is estimated that almost a quarter million new cases of lung cancer will be diagnosed, representing fifteen percent of all new cancer cases. However, malignancies

of the lung and bronchus account for almost thirty percent of all cancer deaths, regardless of gender, making it a major public health problem [202]. This means that more people die of lung cancer than of prostate, breast, and colon cancers collectively. The average age of diagnosis is sixty-eight years old, and two-thirds of all people diagnosed are sixty-five or older. Although men are more susceptible to lung cancers than women, the average lifetime risk of developing lung cancer is approximately one in fifteen, regardless of gender [212].

Over the course of the past three decades, there have been marked improvements in the survival of cancer patients, mainly due to developments in treatment protocols, discovery of targeted therapies, and advances in screening and diagnostic testing. This is mostly evident in breast, colon, and prostate cancers, which have lengthened patient survival by standardizing early detection methods. A dichotomy arises when including cancers such as lung or pancreatic in the comparison, where advances have been sluggish with abysmally low survival rates. Five-year survival rates are entirely dependent on the tumor stage at time of diagnosis, with a seventeen percent overall combined five-year survival rate for all stages of lung cancer (**Table 1.1**). This drops to only four percent with advanced disease, which must be taken into account since more than half of cases are diagnosed after the tumor has progressed to metastatic, late stage disease—mainly due to lack of early detection methods. Even annual screening using chest X-rays do not reduce lung cancer deaths in participants who had no increased risk of cancer [152]. The only promise is early detection with screening using spiral computed tomography—in adult smokers with an increased risk of developing lung cancer, this has shown to reduce lung cancer deaths by up to twenty percent [57, 146].

In the following sections, the pathological, clinical, and genetic attributes of cancer, as well as potential therapeutic modalities, will be reviewed. Although each organ system harbors

its own multitude of cancer types, only those pertaining to the lung and respiratory system will be discussed.

1.4 Pathology of Neoplasia

Normal tissues exist in a state of homeostasis whereby cell growth and death are balanced in a tightly controlled equilibrium; mitotic activity and the rate of tissue turnover are highly dependent on the tissue type. For example, the lung turns over very slowly, with average turnover time more than four months (compared to only four hours in the gut) [17]. Disequilibrium of these tightly regulated tissue regeneration pathways, due to environmental or genetic factors, can lead to devastating pathologic processes such as cancer.

Originating from the Latin for swelling or mass, a tumor can refer to cancer, or unrelated masses such as hematomas, abscesses, or benign neoplasms. Neoplasm, simply meaning "new growth," implies a biological cellular overgrowth whereby a group of cells grows faster and independent from the surrounding cells; this process can be benign, a microscopic precancerous precursor, or result in a malignant cancer [222]. Malignancy necessitates the ability of cells invade and spread, either locally or systemically (metastasis). Neoplasms no longer respond to physiologic stimuli, which would normally limit cell growth, such as contact inhibition, resulting in uncoordinated growth. Abnormal cellular and tissue architecture, as well as the precise number and arrangement of cells allows for diagnosis by histologic evaluation.

An overgrowth of tissue in response to a physiologic or pathologic stimulus, known as hyperplasia, occurs within the framework of normal regulatory mechanisms, such as hormonal signaling. The growth is coordinated with normal architecture, and when the stimulus is removed, growth usually stops, followed by regression. The difference between this process and

neoplastic growth is that neoplasia are a clonal outgrowth of abnormal cells resulting from epigenetic and genetic mutations. Aberrant signaling pathways combined with compromised regulatory mechanisms within cells resulting in overgrowth [222]. The two are related, however, in that hyperplasia often progresses to neoplasia. If the provoking stimulus remains, increased cell mass and rates of mitosis create additional opportunities for mutations and clonal outgrowth.

The conversion of one specialized cell type into another, transdifferentiation known as metaplasia, can be adaptive and reversible and is usually in response to noxious stimuli. However, metaplasia also provides opportunities for neoplasia to arise, with a notable example of smokers' bronchial epithelium undergoing squamous metaplasia, which may eventually develop into squamous cell carcinoma. While metaplasia is still not well understood, this phenomenon may be due to associated hyperplasia, or perhaps because noxious stimuli (smoking) may be carcinogenic itself. Dysplasia refers to abnormal cytoarchitecture and misarrangement of cells arising from deranged growth. Atypical cells with loss of normal progressive maturation and tissue organization characterize epithelial dysplasias. These lesions may regress, or can progress into carcinomas if they transgress normal tissue boundaries past the basement membrane [222].

Histogenic categorization of tumors based on their cellular differentiation depends on whether cells are of epithelial or mesenchymal origin. In general, malignant epithelial tumors are termed *carcinomas*, and those derived from glandular epithelium begin with the prefix *adeno-*. Malignant tumors of mesenchymal origin are generally termed *sarcomas* (i.e. *osteosarcoma* = malignant tumor of the bone). The different kinds of lung cancers will be elaborated upon in the following section.

Clinically, tumors are categorized based on the degree to which they have invaded or spread to surrounding areas. Tumor grade, determined via biopsy, describes the histological appearance of the cells—if the cells look abnormal, lack tissue architecture, or appear undifferentiated, or have penetrated the basement membrane (refer to **Figure 1.2**). Grading serves as an indicator of how quickly a tumor might grow and/or spread [222]. Tumor stage, on the other hand, describes the size and spread of a tumor from where it originated; stage is highly correlated with prognosis and long-term patient survival (**Table 1.1**).

Stage 0 (also termed *carcinoma in situ*): This stage indicates the lesion is where it started and is not spreading. This is often considered a precursor to malignant cancer, as the tumor has not technically invaded through the basement membrane into surrounding tissue.

Stage I: The tumor is still small (<2 cm) and is located only in the tissue of origin. Stage I tumors have not spread to any lymph nodes or surrounding tissues.

Stage II: Tumors have grown in size (2-7 cm). Usually these involve nearby lymph nodes (pulmonary/hilar nodes), although some advanced stage II cancers of the lung may spread to one of the main bronchi, surrounding muscles, or tissue without lymph involvement.

Stage III: Known as locally advanced disease, these cancers are found in the tissue of origin and distant lymph nodes. This stage has two subtypes:

IIIa have unilaterally spread to lymph nodes in the middle chest, or to surrounding tissue such as pleura, chest wall, or mediastinum.

IIIb have bilaterally spread to either middle chest or supra-clavicular lymph nodes, or spread to another major adjacent structure (esophagus, trachea, heart).

Stage IV: The most advanced stage, this indicates the cancer has metastasized to a distant site affecting other parts of the body.

These stages are useful for clinical designation of the cancer severity. This system parallels with tumor/node/metastasis (TNM) characterization for tumor stage (refer to **Figure 1.4**).

Table 1.1

Stage	5-year Survival
I	56%
II	34%
III	10%
IV	4%

Table 1.1: Five-year survival rates for lung cancer by histological stage.

(adapted from American Cancer Society, 2014)

1.5 Lung Cancer; Clinical Presentations

A quarter million new cases of bronchogenic cancers will be diagnosed this year in the United States alone, with over 1.2 million cases worldwide.

Lung cancers vary based on histologic, clinical, and neuroendocrine characteristics, with a main dichotomy separating non-small cell lung cancers (NSCLC) from small-cell lung cancers (SCLC), an important distinction mainly for treatment purposes. NSCLCs include adenocarcinoma, squamous cell and large cell carcinomas, and account for over eighty percent of all lung cancer diagnoses. These patients may have metastases at the time of diagnosis but are able to be treated surgically if the tumors are resectable. Conversely, SCLCs almost always have metastases at the time of diagnosis, although these tumors are highly responsive to radio-chemotherapy. Molecular and genetic differences separate lung cancer subtypes, and although there is some specificity as to which genes are disrupted amongst lung cancer subtypes, genetic alterations including mutations, deletions, or chromosomal amplifications are common events—these will be elaborated upon in the following section [114]. Additionally, each type differs in its histogenesis, location and appearance, severity, and pattern of spread. A summary of some the different types of lung cancers are visually represented in (**Figure 1.4**).

Squamous cell carcinomas (SCC) are centrally located, in relation to a large stem bronchus, and usually present in older male smokers. Often preceded for years by squamous metaplasia and dysplasia, the sequence of molecular changes parallels and presumably causes histologic progression to cancer [116]. SCC can be characterized histologically by the presence of focal keratinization, or squamous pearls, and intercellular bridges. Often times anucleated squamous cells (ghost cells) are found with keratinous or necrotic debris with surrounding

neutrophils and erythrocytes, a phenomenon known as tumor diathesis [239]. These tumors may undergo central necrosis, cause obstruction, and are predisposed to atelectasis (lung collapse) and infection. SCCs grow slowly and spread first to the hilar lymph nodes.

Adenocarcinomas (ADC) are peripheral tumors, not related to a large bronchus, and are the most common type of lung cancer, especially in women and nonsmokers. These malignant epithelial tumors with glandular differentiation and/or mucin production may develop from pre-existing lesions known as atypical adenomatous hyperplasias. The nuclei of tumor cells are round with nuclear grooving and prominent nucleoli, often with eccentric placement within delicately wispy vacuolated cytoplasm [239]. ADCs can have different histological patterns, including acinar, papillary, or solid. They grow more slowly and can be smaller in size that SCC, but tend to metastasize early and widely. The precursor lesion for ADC is known as adenocarcinoma in situ, and occurs peripherally as a single nodule growing along preexisting structures (known as lepidic spreading) in a monolayer without invading or destroying the alveolar architecture. ADCs are more likely than other kinds of lung cancer to be contained in one area, sometimes taking years to become invasive from a confined, asymptomatic cancer.

Small cell carcinomas (or oat-cell carcinomas), found centrally, are highly aggressive and effectively incurable due to widespread metastases. Of all the lung cancers, small cell is almost always caused by tobacco and is rare in non-smokers. Arising from PNECs lining the central airway, the progression and genesis of this tumor mimic other neuroendocrine tumors, including those found in children. Small tumor cells have fine, granular chromatin, often described as “salt and pepper” nuclei with scarce cytoplasm. The nuclei of small cell tumors exhibit prominent nuclear molding, so the nuclei of cells appear like a stack of coins or beads on a string, and “crush artifact,” or streaks of chromatin extending from an otherwise intact nucleus [239]. High

cell volumes and constant turnover result in abundant necrosis and apoptosis in these tumors, so nuclear material and cell debris often clings to blood vessel walls. When staining with H&E, this can cause blood vessels to appear blue, known as the Assopardi effect. Small cell carcinomas commonly arise in the main stem bronchi and spread easily due to constant flow of blood and lymph throughout the lung, with early involvement of lymph nodes.

Large cell carcinomas (LCC) are highly malignant, undifferentiated epithelial tumors with poor prognoses, often found peripherally. The tumors are characterized by large cells with vesicular nuclei, prominent nucleoli, and no obvious glandular or squamous differentiation [222]. LCC are rarely diagnosed since most tumors exhibit some type of differentiated lineage and fall into another category when staining for histological markers. While it is currently unclear, these large cell tumors probably represent poorly differentiated cells and thus especially aggressive forms of either squamous or adenocarcinomas.

Pleural mesothelioma, most commonly associated with asbestos or radon exposure, can arise from either the visceral or parietal pleura. The development of asbestos-related mesothelioma requires a long latent period, up to forty-five years, and is commonly associated with pleural effusions. After diffuse spreading and growth of the lesion along the pleura, the lung eventually becomes encased in a thick fleshy tumor; half of patients die within a year of diagnosis.

Apart from primary tumors developing in the tissue itself, the lung is the most common site of metastatic tumors arising from elsewhere in the body, usually from breast, colon, stomach, pancreas, and kidney. Carcinomas and sarcomas can spread via blood vessels or lymphatics, or by direct invasion through nearby structures. Metastases present as multiple discreet nodules

scattered throughout the peripheral lung parenchyma, as opposed to primary lung lesions, which are usually ill-defined, unilateral, and solitary.

Malignancy can present in many ways, and each person's history and symptoms may manifest as a unique clinical presentation. Most lung cancers are insidious and aggressive, usually discovered late in the course of the disease since there are no effective screening methods for early diagnosis; only fifteen percent are diagnosed at an early stage (stages I, II). Common signs or symptoms of general malignancy are unusual fatigue, loss of appetite/taste for food, fevers, weight loss, and/or night sweats. Since tumors produce symptoms by obliterating, obstructing, and invading normal tissue function, much of the presentation depends on the involved organ, with localizing symptoms such as palpable masses, jaundice, rectal bleeding, or headaches, etc. For lung masses, the occupied space results in obstruction of ventilation and decreased O_2 exchange, while invasion into vasculature can cause hemorrhage. The most common complaints of lung cancer patients include persistent cough, weight loss, and dyspnea.

Lung cancer masses can also manifest with less common presentations—for example, superior vena cava (SVC) syndrome, although this is a less common presentation, seen in approximately five percent of lung cancer patients. SVC syndrome occurs when obstruction or compression of the SVC blocks blood return to the heart, resulting in congestion and edema of the face and arms, cyanosis, plethora, dyspnea, and cough. This blockade also results in collateral venous formation: azygous veins, internal mammary veins, and intercostal veins become enlarged. Apical lung tumors, called Pancoast Tumors, can invade into local mediastinal structures such as the heart, aorta, or esophagus, or invade into the superior sympathetic ganglion, resulting in Horner's syndrome – the classic clinical triad of myosis, anhydrosis, and ptosis. Paraneoplastic syndromes also occur in up to ten percent of lung cancer patients, where

the cancer cells ectopically secrete hormones or cytokines. For example, SCCs are associated with release of parathyroid-related peptide (PTHrP), resulting in humoral hypercalcemia of malignancy [222]. SCLC cells may secrete antidiuretic hormone (ADH), resulting in hyponatremia and confusion; SCLCs can also produce adrenocorticotropic hormone, resulting in Cushing's disease with edema, weight gain, buffalo hump, and hyperglycemia. Rarely, patients develop muscle weakness from an autoimmune condition known as Lambert-Eaton myasthenic syndrome, when antibodies released from cancer cells react at the neuromuscular junction [222].

While most tumors follow similar patterns of metastasis, with bone, brain, liver, lung, and adrenals being common sites, initial sites of spread vary and parallel venous and lymphatic drainage form the area of tissue origin (**Figure 1.4**). Regional lymph node metastases are present in over half of lung cancer cases, and some may involve pleural or pericardial effusion. Lung tumors most commonly metastasize to liver, brain, bone, and adrenal glands. Lung cancers can appear as white-grey masses on a plain film chest X-ray, and computerized tomography (CT) scans to take better resolution images of the lung are usually used for diagnostic imaging.

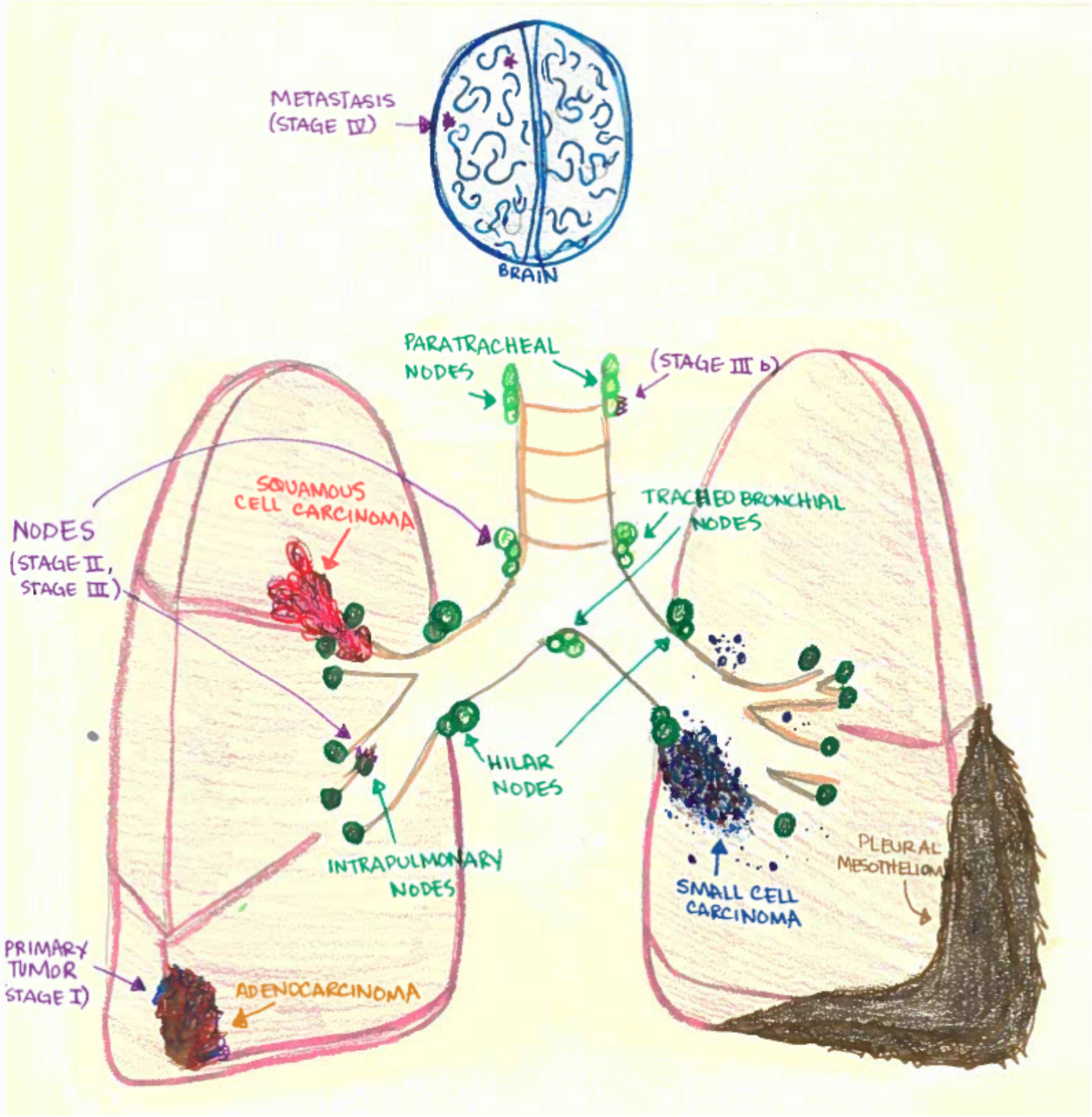

Figure 1.4: Lung Cancer Stages and Lymphatic Spread

1.6 Molecular Carcinogenesis

Carcinogenesis is a multi-step process, resulting from the accumulation of multiple non-lethal genetic mutations, which lead to growth and survival advantages. Inherited or acquired genetic mutations target major cell regulatory pathways to affect numerous characteristics. Through decades of research, the hallmarks of cancer, and several emerging new ones, have described the process whereby cells acquire malignant traits to become cancerous. These include sustained proliferation, resisting cell death, replicative immortality, induction of angiogenesis, and invasion/metastases. Some of the newer hallmarks described in the past decade have taken into regard microenvironmental and immune influences on tumor progression, as well as metabolism.

While each one of these alterations singularly seems quite detrimental to cell functioning, the truth is there are immense checkpoints with overlapping and interacting signaling pathways, amounting to an incredible redundancy. A cell may undergo hundreds of divisions throughout its lifespan, with mutations occurring at a rate of one in three hundred each time the genome is duplicated; however, cells have built in checkpoints for repair and are very efficient at checking for and repairing damaged and mutated cells. Consequently, multiple hits in oncogenes and tumor suppressors in multiple pathways are needed in order for cancer progression. Broad ranges of mutational combinations can lead to cancer, and when epigenetic, microRNA, inflammatory, and microenvironmental influences are added into this mix, the tumorigenic possibilities are literally infinite. There are, however, certain genetic pathways that are more frequently altered in human cancers, and below is a brief digest of molecular mechanisms pertaining to NSCLC carcinogenesis, in particular. A summary of these pathways and common genetic alterations found in lung cancer can be found in **Table 1.2**.

Table 1.2

Gene	% NSCLC	Alterations
KRAS	35	Activating oncogenic mutations.
MYC	20	Gene amplification, increased protein expression.
EGFR	50-90	Activating oncogenic mutations, amplification, increased protein expression.
TP53	70	Inactivating mutations, hemizygous deletion & LOH.
RB/p16	65-80	Inactivating mutations, deletions (LOH), loss of protein expression, DNA methylation.
ALK	4	Inversion and gene fusion with EML4.

Table 1.2: Common genetic alterations found in lung cancer.

Common pathways mutated in NSCLCs. LOH=Loss of heterozygosity. Percentages reflect the upper estimate of NSCLC with the indicated genetic mutation/alteration. [114]

A common mechanism by which cancer cells acquire growth autonomy is mutation of genes encoding for signaling pathways components. The most commonly mutated proto-oncogenes in all human tumors is the v-Ki-ras2 Kirsten rat sarcoma viral oncogene homolog, *RAS,* which encodes for a family of small G-proteins; these function as molecular switches and consist of four isoforms (HRas, KRas4a, KRas4b, NRas) [224]. Ras-GTPases are inactive when bound to GDP, but upon growth factor stimulation, GDP is exchanged for GTP, generating activated Ras. Ras-GTP can then bind to several downstream effectors and stimulate proliferation, differentiation, and survival pathways, notably stimulating the mitogen-activated protein kinase (RAS/RAF/MAPK), mammalian target of rapamycin (PI3K/AKT/mTOR), and Ras-like small GTPase (Ral/RalGEF) signaling pathways [47]. When oncogenic mutations hijack this robust signaling network, dysregulation results in overactive mitogenic signaling, decreased apoptosis, and induction of angiogenesis, all of which are hallmarks of cancer [47, 79]. In lung cancer, point mutations (G12G, G12V, G12D) in *KRas* are the most common, resulting in loss of intrinsic GTPase activity and constitutively active KRas signaling, with activation of the protein occurring in approximately thirty percent of NSCLC; additional mutations are found in cancers of the pancreas, colon, and biliary tract [60, 224]. Unfortunately, *KRas* mutations have been associated with worse overall survival in patients with NSCLC, even when detected in early stages [138]. The importance of the frequency and similarity/precision/ of KRas mutations in lung carcinogenesis will become especially clear when experimental designs are explained in future sections.

Overexpression of the *MYC* proto-oncogene family, consisting of c-Myc, l-Myc, n-Myc, and others, has been associated with twenty percent of human cancers. This nuclear transcription factor has been shown to regulate almost fifteen percent of all human genes, including cell cycle

and proliferation, apoptosis, metabolism, protein synthesis, DNA damage responses, and senescence. Originally discovered in Burkitt's lymphoma, aberrant c-Myc expression—through gene activation by chromosomal translocation, rearrangement, and amplification—results in tumorigenesis and sustained growth [29]. The primary functions of c-Myc are to arrest cellular differentiation and promote cell proliferation by regulating G1 phase transition of the cell cycle [8, 28].

Growth factor receptors transmit signals to intracellular proteins, which can then act in various compartments of the cell. Epidermal growth factor receptor (EGFR) belongs to ErbB family of tyrosine kinase receptors and is estimated to be aberrant in up to seventy percent of NSCLCs [82, 114]. This transmembrane protein is involved in regulating multiple cellular functions, including proliferation, survival, differentiation, vascularization. After extracellular binding of its ligand, EGF, the EGFR dimerizes and activates its intracellular tyrosine kinase domain, allowing for a signal transduction pathway through a cascade of downstream effectors. Most notable of its downstream targets are the mammalian target of rapamycin (PI3K/AKT/mTOR), mitogen-activated protein kinase (RAS/RAF/MAPK), and signaling transducer and activator of transcription (JAK/STAT) signaling pathways; these lead to increased cell survival by inhibition of apoptosis as well as increased proliferation [104, 189]. Increased gene copy number or amplification of gene products are common mechanisms for increased EGFR signaling [39, 82, 151] and activating mutations in *EGFR* lead to oncogenic transformation of lung epithelial cells *in vitro* [72]. In lung cancer, almost all EGFR mutations occur in ADC, and most commonly in young female non-smokers, with delE746-A750 frame deletion and L858R missense mutations being amongst the most common [33]. Interestingly,

EGFR and KRas signaling pathways overlap, and therefore are usually mutually exclusive due to their redundancy; mutations in only one or the other is found in a particular tumor—rarely both.

Loss of a tumor suppressor is another common occurrence in cancer, with *TP53* being the most frequently mutated. Regularly referred to as "the guardian of the genome," p53 responds to cellular stress by regulating cell cycle checkpoints, and p53 protects cells exposed to anoxia, oncogenic expression, and DNA damage against neoplastic transformation via three separate mechanisms [113, 119]. Normally, p53 is bound and inhibited by MDM2, but in times of DNA damage, p53 is released and acts as a transcription factor. First, p53 can induce quiescence by G1 arrest, allowing cells to attempt to repair damage and potentially renter the cell cycle. If DNA errors cannot be repaired, p53 can induce either senescence for permanent cell cycle arrest, or trigger programmed cell death via apoptotic pathways [245]. *TP53* is frequently mutated (up to seventy percent) in all cancers, and affect the DNA binding domain of p53, hindering its transcriptional activity [245]. Germline mutations in *TP53*, known as Li-Fraumeni syndrome, result in an autosomal dominant predisposition to tumor development at an early age, even in the absence of tobacco exposure [121, 135]. Investigation of NSCLC primary tumor and cell lines show that the short arm of chromosome 17 containing *TP53* are frequently deleted, often along with point mutations in the remaining allele [21, 30, 89, 213]. Although p53 mutations occur in over eighty percent of all lung cancers (including SCLCs), mutations are associated with a positive smoking history or exposure to environmental tobacco smoke, and the spectrum of mutations differs between smokers and non-smokers [88, 104, 116].

Normally, RB polices the G1-S checkpoint of the cell cycle, preventing transition during times of unrepaired DNA damage. While *RB1* is often inactivated in other cancers (including small cell carcinomas and its namesake, retinoblastoma), NSCLC alters this tumor suppressive

pathway by inactivating other targets as opposed to inactivating *RB* itself. The most commonly altered of these is the cyclin dependent kinase inhibitor p16 (CDKN2A) $p16^{INK14a}$ inhibits cyclin D1 dependent kinase phosphorylation of RB, preventing cell cycle progression. But $p16^{INK14a}$ is inactivated in almost eighty percent of NSCLC, with gene amplification or other overexpression of cyclin D1 [20].

1.7 Cancer Treatments; Oncology

There are three major modalities for treating cancer: surgery, radiation, and chemotherapy. If a tumor is diagnosed in stages I or II, surgery to remove the tumor is potentially curative. Generally, a lobectomy is performed via thoracoscopic surgery, whereby the surgeon inserts a tiny camera through a small incision in the chest and then can remove of a lobe or section of the lung through the scope without making a large cut. Even for patients whose tumors have been removed surgically, chemotherapy may be added afterwards, known as adjuvant chemotherapy. This is usually recommended to prevent latent cancer cells from returning or treat potential metastases. For patients with stage III lung cancers, which cannot be removed surgically, a combination of chemotherapy and high-dose radiation is recommended. By the time patients reach stage IV, chemotherapy is the main treatment option, and radiation is used only palliatively [66].

Almost two-thirds of all patients with NSCLC will receive radiation treatment during the course of their disease [220]. Using high-energy particles or waves to destroy or damage cells locally, radiotherapy's utility ranges from curative to palliative. Palliative radiation is commonly administered to relieve patient's symptoms, usually by shrinking tumors/metastases impinging on the brain, spine, or esophagus, which cause pain and interfere with their ability to function

[90]. Radiation sources for cancer treatment may be generated from machines, known as external-beam radiation therapy. Radioactive material can also be implanted in the body adjacent to tumors, called brachytherapy, or injected into the bloodstream, known as systemic radiation therapy [90]. Three dimensional conformal radiation therapy (3D-CRT) uses advanced computer software to precisely deliver the radiation to a specifically shaped area [90]. Intensity-modulated radiation therapy (IMRT) uses multiple smaller collimators, which deliver single doses of radiation; this allows for changes in the dose and intensity of radiation beams spatially or for adjustments between sessions. IMRT also increases the radiation dose in the desired areas (tumor) while reducing exposure to specific areas which might be more sensitive in the surrounding normal tissue, thus reducing risk of side effects [90]. It should be noted, however, that a larger overall volume of tissue is exposed to radiation with IMRT when compared with other delivery methods, and this has been shown to increase the incidence of secondary cancers [78].

When selecting the area for treatment, the whole tumor plus a small amount of normal tissue surrounding the tumor is included to account for the patient's body movement from breathing and normal organ movement, which can change between treatment sessions. This margin also ensures killing of cancer cells, which might have spread to the surrounding tissue, called microscopic local spread, and reduces the likelihood of relapse. Radiotherapy is usually delivered in fractions using small dose increments (1.8-3 Gy) five days a week to the tumor site, with total doses varying from 30 to 80 Gy depending on the cancer type and intention of treatment (curative vs. palliative). Common side effects of radiation include skin dryness or blistering and fatigue, and site-specific effects such as difficulty swallowing, dyspnea. Some patients develop a dry cough due to decreased surfactant production by type II pneumocytes.

Others develop interstitial inflammation in the lungs, a condition known as radiation pneumonitis, which can manifest as congestion, cough, dyspnea, fever, and chest pains [162]. If left untreated, pneumonitis can progress to radiation-induced fibrosis in the long term—characterized by collagen deposition and vascular damage [103]. Finally, patients undergoing radiation therapy are at an increased risk for developing secondary cancers later in life [78]. The importance of radiation-induced cancers, as well as the use of radioprotectors during radiation, will be more thoroughly addressed in the succeeding sections.

Chemotherapy, or the use of chemicals and drugs, has been designed to target cancer cells, while being as nontoxic as possible. Some current approaches rely on gene therapy to replace defective genes, such as with loss-of-function mutations, targeting surface tumor antigens to select only cancer cells, or to inhibit new blood vessel formation required for the growth of tumors. For example, the humanized monoclonal antibody bevacizumab (avastin) binds to and inactivates vascular epithelial growth factor (VEGF), thus inhibiting the growth of new blood vessels to solid tumors [58, 164]. The first of its class to be approved by the United States Food and Drug Administration (FDA) in 2004, bevacizumab and others similar to it are used in colorectal, breast, and lung cancers, even though bevacizumab has recently been withdrawn for breast cancer. Individualized therapy, using a patient's unique tumor profile, holds great promise and allows for identification of mutations in candidate genes that lead to better and more tailored drug combinations for that patient.

Promising uses for personalized therapies include tumors with specific growth factor receptor mutations, such as EGFR-positive lung cancers or HER2-positive breast cancers. Gefitinib (Iressa) competitively binds to the ATP binding site of EGFR, blocking tyrosine kinase activity [55]. Approved in 2003, it was the first selective EGFR family inhibitor, although the

FDA withdrew it two years later due to questions over whether it extended life. A newer version, erlontinib (Tarceva), has activity against HER1 and EGFR, and has been approved for use in NSCLC [22, 219]. The monoclonal antibody to EGFR, cetuximab (Erbitux), blocks EGFR by binding on the cell surface, whereas other small molecules bind the intracellular kinase domain of the receptor [160]. Another kinase inhibitor, crizotinib (Xalkori), is effective for the nine thousand new patients every year in the U.S. with a chromosomal rearrangement resulting in constitutively activated anaplastic lymphoma kinase (ALK), responsible for four percent of NSCLC (see **Table 1.1**) [196]. However, since cancer cells are constantly replicating and acquiring new mutations, they develop resistance, and many tumors eventually stop responding to these targeted therapies [107, 200].

Although single, directed agents can be very effective, they are insufficient at curing patients and must be combined with other conventional chemotherapies. This class of cytotoxic drugs acts by selectively killing proliferating cells by hindering mitosis. Platinum-based drugs, such as cisplatin and carboplatin, act by crosslinking DNA, resulting in significant damage and killing of cells once they reach the S-phase of the cell cycle. Although these compounds must be administered intravenously, platins are used frequently—they are first-line treatment in almost eighty percent of newly diagnosed advanced NSCLC cases [18]. Cisplatin can produce serious cytototoxicity and peripheral neuropathy, and if patients are not well hydrated, platins can accumulate in proximal tubule cells resulting in significant renal toxicity. Other common NSCLC chemotherapies that act during S-phase include the nucleoside analog gemcitabine (Gemzar), and the topoisomerase II inhibitor etoposide, which results in double-stranded DNA breaks [90]. Paclitaxel and docetaxel both belong to the taxane class of drug, which bind to preexisting microtubules and prevent their disassembly. Since a dynamic equilibrium is required

between the alpha-beta subunits to form functional microtubules, taxanes cause accumulation of inactive microtubules and thus inhibit mitosis. Another class of drug which acts on microtubules, the vinca alkaloids, including vinblastine, bind to tubulin alpha-beta heterodimers, preventing the formation of microtubules necessary for separating chromosomes during metaphase and anaphase of mitosis. Vinca drugs cause myelosuppression and neurotoxicity, presumably due to the ineffective neuron axonal transport of substrates.

All these classical cytotoxic drugs kill rapidly dividing cells, and this occurs in both normal and cancerous cells. Since some normal tissues, such as the bone marrow, gastrointestinal tract, and hair follicles, proliferate just as rapidly as cancer cells, these cells are also killed during treatment. As a result, patients often undergo severe side-effects, including myelosupression, gastrointestinal distress, and alopecia, although side effects depend on the type and dose of drugs given, and the length of time they are taken [90]. Furthermore, some cancer types, such as colon or lung cancers, can grow very slowly, and therefore this class of drug is not as effective for cells with a long doubling time. There is also mounting evidence of a sub-population of cancer stem cells, which are responsible for repopulating tumors even after they have been debulked by harsh chemotherapies. Courses of chemotherapy are usually administered in cycles of three to four weeks, with average two to three day treatment periods followed by a rest period [90].

1.8 Introduction to Radiation

Radiation is defined as energy—electromagnetic (EM) or particulate—emitted from a source. When this energy is sufficient to displace electrons, it is termed ionizing radiation (IR); this can cause energy transfer into biological material and result in breakage of chemical bonds [77]. Energy transferred per unit length of track, known as linear energy transfer (LET), impacts

the mechanistic actions of IR and translates into large differences in spatial distribution and resulting damage depending on the source. Electromagnetic radiation, such as gamma radiation (γ) or X-rays, is made up of waves of photons, which interact uniformly with matter. This results in less energy deposition, with ionization events uniformly scattered throughout the exposed area; EM radiation generally has a low LET and acts via indirect ionization of its targets. Conversely, when particulate radiation, consisting of subatomic or alpha particles and high charge and energy (HZE) particles such as proton or iron nuclei, impact matter, the energy is deposited centered along the particle's track, with dense clusters of ionization along the path. This results in higher amounts of energy deposited; though generally higher than EM, the LET values of particulate radiation depends on the species and nature of energized particle [77].

The critical target and main biologic effects of IR result principally from damage to DNA (**Figure 1.5**). When any form of radiation is absorbed in a cell, it can interact directly with cellular molecules, causing a cascade of reactions resulting in biological changes, although this is more common with high LET radiation. The most common effect of radiation is breakage of the DNA backbone; if both strands are disrupted, this double-strand break (DSB) can splinter DNA molecules in two. These have vast biological repercussions, including inaccurate repair or chromosomal aberrations (deletions/inversions/translocations) should the DSB be inefficiently or inaccurately repaired, or if fractured DNA is inappropriately rejoined [241]. These random alterations in genetic material resulting from energy deposition can have profound effects.

Alternatively, radiation can have indirect actions by reacting with other atoms in the cell to produce free radicals and other reactive species that can diffuse through the cell to have far-reaching consequences (**Figure 1.5**) [77]. The most abundant intercellular molecule, water, is usually the target of radiolysis, with a resulting hydroxyl free radicals acting as the principle

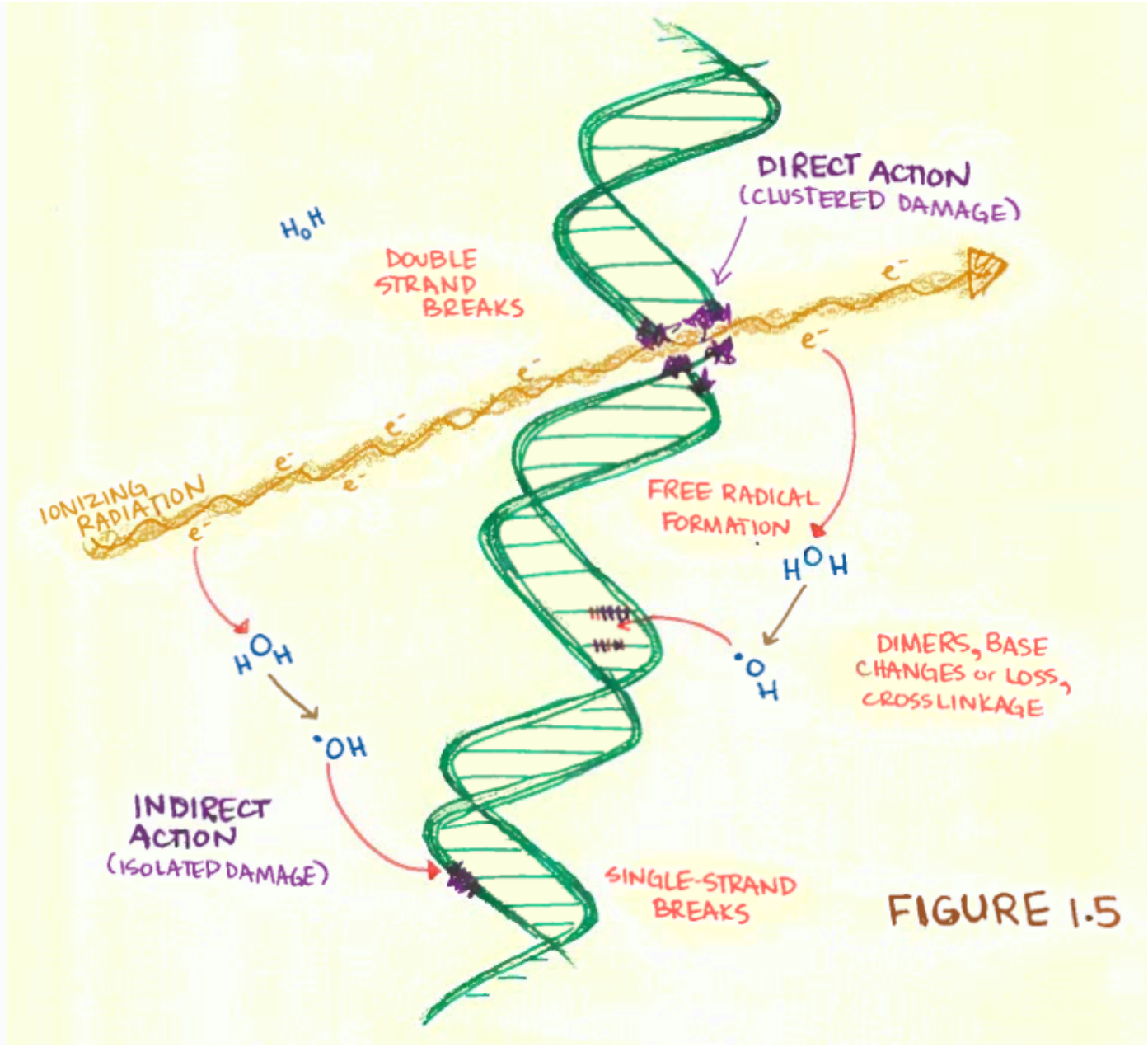

Figure 1.5: Radiation Mechanisms of Action

damaging species. This mechanism for radiation damage, production of reactive oxygen species (ROS) and free radicals in the cell, is highly dependent on oxygen concentrations, and therefore the effects of IR are potentiated at high O_2 concentrations whereas hypoxia shields tissues against IR [77, 177].

Although IR effectively destroys rapidly dividing tumor cells via these mechanisms, it also causes damage in healthy, noncancerous cells. Induction of complex DNA breaks, altered bases, chromosomal aberrations, and overwhelming reactive species result in mutagenesis, carcinogenesis, and cell death (**Figure 1.6**). Cancer risks associated with IR exposure have been analyzed from atomic bomb survivors after World War II and underground miners exposed to radon gas; additional observations of nuclear fallouts from reactors such as Chernobyl, Fukushima, or nuclear testing such as Castle Bravo, have given insight to the damaging, transformative, and long-lasting effects of radiation on biological processes [34, 95, 169]. While cancer incidence increases with higher doses of radiation for most tissues, the lung is remarkably susceptible to low doses of IR [131, 148, 211].

Although radiation-induced damage to healthy cells may not have been a major concern in the past, advances in genetic medicine, diagnostics, and general supportive care has resulted in increased survival, extending the lives of cancer patients sometimes up to twenty years or more past their original diagnoses. Since then, patients have begun to develop secondary cancers arising from normal tissue exposed to the damaging effects of IR that was part of their original therapy. Given the efficacy of radiotherapy, and its widespread use over the past century, a wealth of knowledge has accrued for secondary malignant neoplasms, especially for young patients treated with large-field radiotherapy that produced high cure rates. The best-documented link is with Hodgkin's lymphoma—patients surviving radiation treatments developing solid

tumors, especially breast cancers, within twenty years [15, 43]. A majority of radiotherapy-related secondary malignancies manifest as solid tumors within or near irradiated fields and are associated with latency periods of five to ten years; furthermore, there is a direct link between risk of lung cancer and increasing doses of radiation [37, 148, 155, 218]. Apart from cancer treatments, radiation is also used prior to bone marrow, stem cell, or organ transplantation for immunosuppression [162].

The diversity and range of radiation types are also a concern for United States National Aeronautics and Space Administration (NASA) and astronauts on long-term space missions. While exposure to damaging radiation on earth is limited due to the protective atmosphere and only low energy EM radiation, space radiation includes high-LET radiation fields; radiation-induced carcinogenesis is a primary limitation. Based on recommendations from the National Council of Radiation Protection and Measurement (NCRP), NASA limits astronauts' lifetime increased risk of radiation-induced death to three percent [36]. Exposure to galactic cosmic radiation composed of high-energy protons and HZE nuclei as well as solar particle events (SPE) can occur unexpectedly and have the capacity to penetrate engineered shielding [38, 50]. While shielding is effective against terrestrial radiation, effective countermeasures and radioprotective agents are needed to reduce the biological damage produced by the highly ionizing radiation found in space; radioprotectors will also have important implications in radiation oncology where there is an increased risk of secondary malignancies resulting from therapy.

1.9 Radioprotectors

The negative effects of radiation on normal tissue are responsible for radiation sickness, fibrosis, secondary cancers, and other toxic side effects in cancer patients treated with IR. Additionally, IR effects are a particularly important consideration for first responders to nuclear accidents, astronauts on long-term space missions, or any other situation where individuals are exposed to radiation. In recent years, there has been growing demand to develop protective agents against radiological/nuclear terrorism, and governments have invested into drug development with the intent of developing radioprotectors for military use [182].

Pharmacologically, there are three classes of drugs that have the potential to modulate the effects of radiation depending on the time they are administered in relation to IR exposure (**Figure 1.6**). Prophylactic radioprotectors are intended as countermeasures, used prior to anticipated exposure to prevent tissue damage. Mitigators, given during or after IR exposure, would prevent or ameliorate IR-induced damage prior to the onset of organ toxicity or irreversible long-term symptoms. The final category, therapeutic preparations, is useful for the delayed effects of radiation, once clinical signs and symptoms of radiation-induced damage (such as fibrosis, or secondary cancers) have already manifested [98, 182]. Ideally, the use of these therapeutic agents could improve the therapeutic ratio/margin of radiotherapy—selectively reducing radiation-induced injury in normal tissue without reducing tumoricidal efficacy. Few attempts to prevent damage have been made in the past due to possible tumor protection, enhanced tumor proliferation, development of resistance, or inter-individual variability in IR response [162]. Implementation of radioprotective agents has the potential to improve patients' quality of life by reducing the short- and long- term effects of radiation therapy.

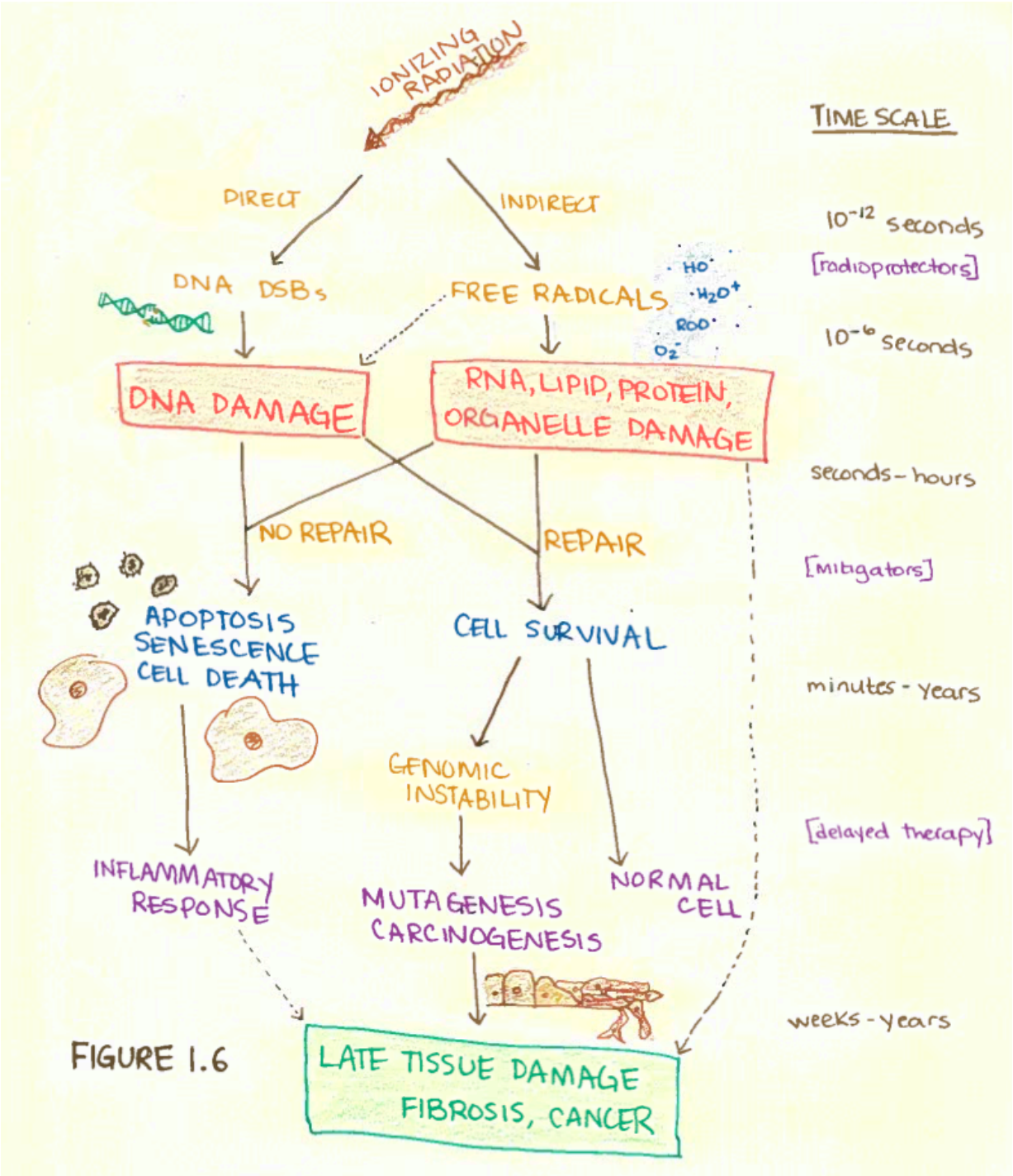

Figure 1.6: Effects of Ionizing Radiation on Living Cells

To ascertain the efficacy of potential protective factors, certain experimental measures are used to determine protection against clonogenic or apoptotic cell death, differentiation and mutagenesis, induction of ROS, lipid peroxidation or other biochemical changes; *in vivo* studies commonly include protection against IR-induced lethality due to hematopoietic or gastrointestinal injury. The most reliable and commonly used measure for a drug's efficacy is a dose modifying factor (DMF) or reduction factor. DMF is determined by irradiating with and without the agent at a range of radiation doses and comparing the dependent variable of interest (i.e. clonogenic survival).

Radioprotective agents generally function by preventing the indirect actions, or repairing direct actions, of IR-induced cell damage. Radioprotectors act by suppressing reactive compounds (free-radical scavenging), detoxifying, or stabilizing biomolecules to enhance repair and recovery of the cell [77, 110]. The most potent and effective radioprotectors are sulfhydryl compounds. However, toxicity of a compound often parallels radioprotective effects, so these synthetic agents produce serious side effects and are deemed too toxic at the doses required for radioprotection—the majority of synthetic radioprotectors are not suitable for human use due to severe nausea and vomiting [112, 228]. Plants and naturally derived products have promise due to their low toxicity, exerting radioprotection through similar antioxidant and free-radical scavenging mechanisms; however they exhibit mediocre protection compared to synthetic thiol compounds such as amifostine, and DMFs are rarely reported for naturally occurring compounds since they are usually invariably low (DMF < 1.3) [110, 235]. Despite over half a century of research, only two compounds (amifostine and palifermin) have overcome the obstacles of clinical approval by the FDA, sanctioned as radioprotective compounds for use during radiation

therapy, although currently there is still a lack of clinical data to support the use of any protective agent in an emergency scenario (i.e. nuclear accident, dirty bomb).

The current mainstay for acute radiation exposure is amifostine (Ethyol®; S-2[3-aminopropylamino-] ethylphosphorothioic acid; WR-2721), first approved by the FDA in 1996 for use with cisplatin-based chemoradiation [3]. Developed in the 1950s by the United States military as a WR (radiation weighting factor), this sulfhudryl-containing thiol substance and its radioprotective properties have been extensively investigated ever since [110]. Amifostine is converted to active metabolites both in the bloodstream (WR-1065) and then again intracellularly (WR-33278) [243]. Amifostine and its metabolites are thought to act as free radical scavengers to protect subcellular components from IR damage. Amifostine and WR-151327 protect against radiation-induced malignancies when administered prior to exposure to IR [70, 71, 139]. Hyperfractionated IR therapy in NSCLC patients receiving concurrent chemotherapy showed that amifostine only minimally reduced pain after chemoradiation, but did result in less dysphagia and less weight loss, although another report compiling thirty studies could make no conclusion regarding the efficacy of amifostine in preventing/reducing mucositis due to conflicting data [149, 186].

Since WR-1065 competes with oxygen for free radicals, the degree of radioprotection provided varies greatly depending on the oxygen content and tissue type, and at higher oxygen concentrations such as those found in the lung, protection is gradually lost [77]. In fact, lung protection factors with amifostine are amongst the lowest (DMF of 1 to 1.2), compared to tissues with intermediate levels of oxygen such as the bone marrow (DMF up to 3) [9]. As a hydrophilic phosphorothioate compound, amifostine does not readily cross cell membranes; it can only be

administered intravenously, and uptake and clearance of amifostine/WR-1065 into tissues varies extensively—again contributing to the differential protection of amifostine of different tissues [9]. For example, tumor tissues exhibit less uptake of WR-1065, and the lung and skin rapidly metabolize the drug within thirty minutes, whereas salivary glands can take up to three hours to eliminate it [197]. Although amifostine was first reported to be well tolerated and exhibit acceptable toxicity, cytotoxic effects are dose-dependent and can result in serious side effects including hypotension, somnolence, hypocalcemia, and neuropathies—often these are severe enough to limit the total administered dose to lower than necessary for maximal radioprotection [3, 9].

Palifermin (Kepivance®) recombinant human keratinocyte growth factor, is a newer radioprotector, approved for use in 2004 [4]. Palifermin has been shown to decrease the severity and duration of severe mucositis in patients receiving high doses of chemoradiation, or patients undergoing whole body IR for stem cell transplant [12, 170]. While this therapy has been approved as a radioprotector in leukemia and lymphoma, its mechanism of protection is by stimulating growth of cells in the mouth, stomach, and colon, thus helping to counteract and repair the detrimental effects of IR on mucosal tissue [4]. Since the data supporting palifermin for use in solid tumors is limited, there is a theoretical risk of stimulating tumor growth, and some patients experience adverse side effects like rash, pruritus, cough, and taste alterations [136].

Within the entire plant kingdom, it is assumed that over eight thousand naturally occurring antioxidants exist. The wealth of data existing for plant compounds and all their active ingredients is more than extensive. However, the largest category of potential radioprotectors is

polyphenols, which belonging to a larger class known as flavonoids [144]. Polyphenols can defend against ultraviolet (UV) radiation, pathogens, and provide protection against development of cancers, cardiovascular disease, diabetes, osteoporosis, and neurodegenerative diseases [154].

One of the most famous polyphenols is resveratrol (3,5,4'-trihydroxy-trans-stilbene), an anti-inflammatory anti-oxidant with multiple health benefits [194, 216]. Isolated from the skin of grapes (hence its fame as the antioxidant present in wine), resveratrol has been shown to ameliorate IR-induced hematopoietic injury in mice, preventing stem cell senescence and inhibiting chronic oxidative stress caused by irradiation, as well as reduce the frequency of IR-induced chromosomal aberrations in irradiated mouse bone marrow cells *in vivo* [26, 244]. Additionally, resveratrol can help mitigate follicle loss and ovarian damage as well as salivary gland damage induced by IR in rats [203, 204]. Low micromolar concentrations of resveratrol have been shown to be photoprotective against UV-B radiation [23]. In addition to protecting normal tissue, resveratrol has been shown to be a radio-sensitizer in prostate and cervical cancer—increasing apoptosis and inhibiting cyclooxygenases (COX1) and cell cycle progression [144, 190]. Resveratrol enhances IR-induced damage in NSCLC cells, acting by increasing ROS production, DNA DSBs, and inducing premature senescence [132]. Another anti-tumor property of resveratrol is inhibition of aromatase, which has been shown to protect against breast cancer [216]. Resveratrol can decrease activation of transcription factors important for inflammation and cell regulation, such as transforming growth factor-beta (TGF-β), nuclear factor kappa β (NFκβ), and activator protein (AP1), and induce apoptosis as well as harboring other antiproliferative activities [161].

Synthetic oleanane triterpenoids are a multifunctional non-cytotoxic class of organic compounds with the ability to activate cytoprotective and antioxidant pathways [83, 125, 129].

The radioprotective effects of triterpenoids have been well established, especially in the most commonly used and investigated triterpenoid CDDO (oleana-1,9 (11)-dien-28-oicacid, 2-cyano-3,12-dioxo). The ethylamide analogue of CDDO (CDDO-Ea) has been demonstrated to stabilize and activate Nrf2 in the colons of mice exposed to acute lethal doses of ionizing radiation resulting in increased survival [99]. Furthermore, its methyl ester (CDDO-Me) has been shown to be an effective radioprotector in human colonic epithelial cells [52, 99]. As the concentration of CDDO increases into the micromolar range, it can induce differentiation and inhibit cell proliferation, eventually leading to cell death via apoptosis through the nuclear factor kappa β (NFκβ) pathway [128]. At these doses, a CDDO analog significantly increases survival and decreases apoptosis in different tissues of lethally irradiated zebrafish embryos [40]. CDDO-Me has shown antitumor activity in lymphoma patients in a phase I human trial and prevents formation of estrogen receptor-negative mammary tumors in mouse models of breast cancer [84, 124]. Additionally, CDDO-Ea can prevent cancer progression in mouse models of lung and prostate cancer [123, 230]. Additional work by the Liby and Sporn group shows that CDDO compounds activate Nrf2 downstream effectors, such as heme oxygenase (HO1), as well as other pathways in both transgenic and wildtype mouse models [122, 124, 127].

Other flavonoids have been shown to modulate IR effects in cancer cells, and these effects can be compounded when administered with other agents. Genistein (4′,5,7-trihydroxyisoflavone), a major metabolite of soy present in miso, exhibits many anti-inflammatory antioxidant properties, free radical scavenging ability [223]. Clinically it reduces adverse effects in patients with prostate cancer, and *in vitro* genistein can induce cell cycle arrest, apoptosis, and impaired damage repair in irradiated prostate cancer cells [5, 221]. Conversely,

post-IR administration of genistein decreases frequency of IR-induced micronuclei, a measure of genotoxicity and cellular damage, in both mouse lung cells and fibroblast cultures [41]. The angiotensin-converting enzyme II (ACE) inhibitor captopril, a common antihypertensive drug containing a sulfhydryl group, has been shown to synergize with genistein, providing significant radioprotection in whole body irradiated mice [42]. Due to captopril's free radical scavenging properties, it also protects mice hematopoetic cells from radiation-induced DNA damage and genotoxicity [87]. Some groups have postulated that genistein reduces levels of inflammatory cytokines and IR-induced ROS, resulting in decreased DNA damage and functional deficits, while captopril acts through alternative mechanisms including copper chelation [24, 41, 214]. A number of other flavonoids can reduce micronuclei in irradiated blood cells [201].

Found in many edible plants including cherries as well as secreted by the pineal gland in the brain, melatonin (*N*-acetyl-5-methoxytryptamine) has been documented as a direct free-radical scavenger and indirect antioxidant with protective effects against IR-induced oxidative stress[94]. Pre-treatment of human lymphocytes with melatonin shows a reduction in IR-induced chromosomal aberrations and micronuclei formation, and additional *in vivo* investigations have confirmed that melatonin can protect mammalian cells from the geno- and cytotoxic effects of IR [226-228]. Several clinical reports indicate that melatonin administration can positively widen the therapeutic margin during radiotherapy for cancers. Side effects include sedation, reduced alertness, and depression [228].

Metformin, a biguanide drug used to treat type II diabetes, can mildly protect mouse fibroblasts (4 Gy) or splenic cells *in vivo* (7 Gy) when administered 24 hours after IR [140].

Vitamins and dietary antioxidants have well-documented protective properties. This is especially true for vitamin E (α-tocopherol monoglucoside), which has been shown to inhibit

radiation-induced transformation and mutagenesis, even when administered after IR [19]. Vitamin E also protects intestinal and bone marrow cells against low dose radiation and chromosomal damage as well as reduces radiation-induced fibrosis in patients undergoing therapy [110, 235]. Radioprotection by dietary vitamin A and β-carotene has also been demonstrated in multiple tissues of irradiated mice, and vitamin C can protect against radiation-induced chromosomal damage, even when administered after IR [185, 191]. Although these naturally occurring minerals and vitamins are less potent (DMFs of 1.1 to 1.2), their low toxicity offers a wider window of protection. Furthermore, their ability to provide protection when given after IR exposure may induce endogenous antioxidant systems or increased benefits from longer and repeated use.

Retinoic acid, the major bioactive metabolite of dietary vitamin A, plays an important role in cell development and differentiation, proliferation, and apoptosis, and possesses anti-oxidant effects. For these reasons, retinoic acid and its derivatives have been commonly employed over the past thirty years as potential chemotherapeutic or chemopreventive agents [46, 209]. Retinoids can induce differentiation of myeloid and leukemic cells and reverse premalignant epithelial lesions [31, 32, 85]. There are reports of the chemopreventative activity of retinoids in lung, liver, and breast cancers, and some have demonstrated that retinoic acid treatment can sensitize lung cancer cells to radiation [49, 64, 209]. Unfortunately, more recent chemoprevention trials show that retinoids do not reduce tumor formation, recurrences, or mortality in patients with early NSCLCs, and retinoic acid does not reduce the risk of developing NSCLCs [63, 96, 130]. Although retinoic acid may have therapeutic value as a radioprotector, more information is needed to understand the paradoxical effects of using retinoids in lung cancer treatments.

Commonly used in palliative cancer care, non-steroidal anti-inflammatory drugs (NSAID) are also widely used for their anti-inflammatory, anti-pyretic, and anti-clotting functions. As inhibitors of prostaglandin H synthase, NSAIDs block production of COX and prostaglandin enzymes, resulting in decreased arachaidonic acid signaling and pro-inflammatory metabolites—however, NSAIDs may also possess some manner of free radical scavenging properties [118]. Two NSAIDs, indomethacin and diclofenac sodium, each have been demonstrated to increase survival, protect hematopoietic cells and enhance recovery in irradiated mice, and these drugs act synergistically with sulfhydryl compounds (such as amifostine) for radioprotection of bone marrow [7, 54, 65, 106]. In addition to demonstrating significant protection against IR-induced esophagitis in opossums, indomethacin protects against radiation mucositis in human patients with head and neck cancers [150, 159]. Prostaglandin inhibitors can protect normal tissues against the deleterious effects of radiation by inducing G1 cell cycle arrest, thus minimizing the proportion of cycling cells to be damaged by radiation [69, 118, 159]. Although NSAIDs are widely used, they are associated with significant adverse gastrointestinal side effects such as ulceration, bleeding, and perforation due to prostaglandin necessity in the intestinal mucosa, and therefore frequency of use must be carefully monitored.

Although antioxidants/anti-inflammatory agents can prevent cellular damage and neutralize free radicals, generation of free radicals and damage to malignant cells is the mode of action for radiation and certain chemotherapies. This logically raises concerns that antioxidants may decrease the effectiveness, and therefore concurrent administration of oral antioxidants should be contraindicated, during cancer therapy. However, the current wealth of data suggest the opposite—most therapeutic modalities exhibit increased efficacy when administered with antioxidants [111]. Frequently the effects of radiation are synergistic when combined with

antioxidants, and patients not only tolerate standard treatments better due to fewer adverse side effects, but also tend to have a better quality of life. Antioxidants supplements may currently be underutilized in conventional oncologic treatments, and this provides fertile ground for the development and characterization of new radioprotectors. Furthermore, feasible radioprotectors must be designed with the desired application in mind. Uncontrolled radiation exposure from nuclear weapons or space travel present additional challenges from those in radiotherapy; high-LET radiation, gravitational effects, and timing of exposures require unique and innovative radioprotective approaches.

CHAPTER TWO

CDDO-Me Protects Normal Lung And Breast Epithelial Cells But Not Cancer Cells From Radiation

2.1 Introduction to Nrf2/ARE & CDDO-Me as a Radioprotector

Although radiation therapy is a common treatment for cancer patients, ionizing radiation (IR) produces reactive oxygen species (ROS) and is known to damage cellular components in healthy cells, leading to damaged bases and DNA breaks, resulting in chromosomal aberrations, mutagenesis, carcinogenesis, and cell death [14, 232]. Not only are these effects responsible for causing radiation sickness and other toxic side effects in cancer patients treated with ionizing or proton radiation therapy, they are a particularly important consideration for first responders to nuclear accidents, astronauts on long-term space missions, or any other situation where individuals are exposed to radiation.

A central cellular mechanism for dealing with oxidative stress, including response to radiation, is through induction of the Nrf2/ARE pathway, which is responsible for detoxifying cellular insults. Nuclear factor erythroid-derived 2 -like 2 (Nrf2) is a transcription factor that is normally bound by its cytoplasmic repressor Kelch-like ECH-associated protein (Keap1), which acts as a molecular oxidative sensor. When the level of reactive species in a cell reaches a certain threshold—say, for example, after exposure to ionizing radiation and subsequent free-radical formation—cysteine residues on Keap1 respond and result in a conformational shift of the Keap1 protein, thus inhibiting the ubiquitination and subsequent degradation of Nrf2 [141]. Newly synthesized Nrf2 is then unable to interact with Keap1, resulting in Nrf2 accumulation and phosphorylation until it translocates to the nucleus, where it binds to antioxidant response

elements (AREs) in the genome (**Figure 2.1**). AREs are responsible for the transcription of multiple antioxidative and cytoprotective genes. Some of the main transcriptional targets of Nrf2 include glutathione synthesis, ROS elimination, detoxification, multidrug resistance-associated proteins /efflux pumps, and NADPH synthesis [141, 176]. Nrf2 function is necessary for responding to cellular insult, and administration of factors downstream to Nrf2 can help attenuate fibrosis in other models of lung injury and fibrosis [76, 92]; this is especially true for response to IR damage, as Nrf2 deficiency decreases lifespan of thoracic irradiated animals [217].

Interestingly, the Nrf2 pathway is commonly dysregulated in cancers, providing tumors added detoxifying potential against cellular insults [141, 205, 208]. To level the playing field and protect normal tissues from IR, new therapeutic agents that enhance repair and neutralize ROS to mitigate the negative effects of radiation are needed. However, in order for these agents to be realistically efficacious, they cannot provide the same level of protection to cancerous cells. The synthetic triterpenoid CDDO-Me (oleana-1,9 (11)-dien-28-oicacid, 2-cyano-3,12-dioxo-, methyl ester; bardoxolone-methyl; RTA-402) is a multifunctional and largely nontoxic antioxidant, anti-inflammatory modulator with the ability to activate cytoprotective pathways (Fig. 2.1*B*). This orally available drug can increase the activity of Nrf2/ARE in the low nanomolar range, inducing antioxidant and anti-inflammatory pathways (**Figure 2.3**) [83, 125]. As the concentration of CDDO-Me increases into the micromolar range, it can induce differentiation and inhibit cell proliferation, eventually leading to cell death via apoptosis through the NFκβ pathway [128]. Higher concentrations of this compound have been utilized as a chemotherapeutic against multiple cancer models—CDDO-Me has shown antitumor activity in

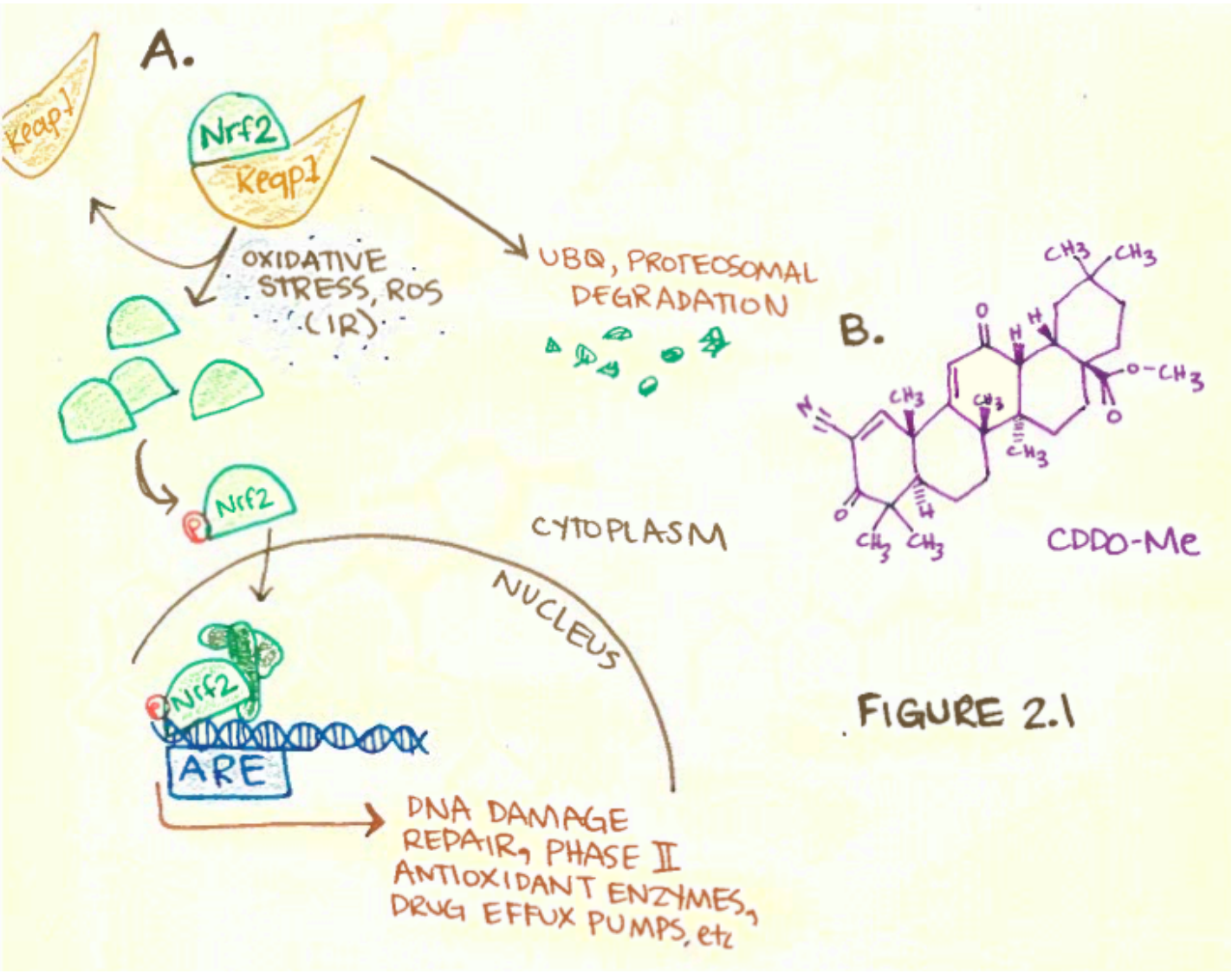

Figure 2.1: The Nrf2/ARE pathway activates cytoprotective responses.

(A) Nrf2 Pathway: Keap1 acts as a molecular oxidative sensor and marks Nrf2 for degradation. When there is an abundance of reactive species in the cells, Nrf2 accumulates in the cytoplasm, eventually undergoing various phosphorylation events to translocate to the nucleus and bind to Antioxidant Response Elements (AREs) in the genome, resulting in the transcription of multiple antioxidative and cyto-protective genes. CDDO-Me acts by facilitating the dissociation between Keap1 and Nrf2, leading to Nrf2 activation. (B) Chemical structure of CDDO-Me: Oleana-1,9(11)-dien-28-oicacid, 2-cyano-3,12-dioxo-, methyl ester (RTA-402; bardoxolone-methyl).

lymphoma patients in a phase I human trial and prevents formation of estrogen receptor-negative mammary tumors in mouse models of breast cancer [84, 124]. Additionally, the ethylamide analogue of CDDO (CDDO-Ea) can prevent cancer progression in mouse models of lung and prostate cancer [123, 230]. Additional work by the Liby and Sporn group show that CDDO compounds activate Nrf2 downstream effectors as well as other pathways in both transgenic and wildtype mouse models [122, 124, 127].

The radioprotective effects of triterpenoids have been well established. At doses that inhibit NFκβ, a CDDO analog significantly increases survival and decreases apoptosis in different tissues of lethally irradiated zebrafish embryos [40]. CDDO-Ea has been demonstrated to stabilize and activate Nrf2 in the colons of mice exposed to acute lethal doses of ionizing radiation resulting in increased survival [99]. Furthermore, CDDO-Me has been shown to be an effective radioprotector in human colonic epithelial cells [52, 99].

The purpose of the current study was to determine the radioprotective effects of CDDO-Me in normal, non-cancerous human bronchial (HBECs) and mammary (HMECs) epithelial cells as well as in human lung and breast cancer cell lines. These experiments established that while low dose CDDO-Me protected both normal HBECs and HMECs through an Nrf2-dependent mechanism, CDDO-Me provided no further induction of Nrf2 in human lung and breast cancer cells, nor did it protect these cancer cells against radiation-induced apoptosis. These results demonstrate that this orally available non-toxic radioprotector may have important medical implications for patients undergoing radiotherapy as well as individuals who might be exposed to occupational radiation.

2.2 Methods & Materials:

2.2.1 Cell Culture

Human lung - bronchial epithelial cells: Human bronchial epithelial cells (HBECs) were obtained from central lung bronchi and immortalized using ectopic expression of human telomerase reverse transcriptase (hTERT; T) and cyclin-dependent kinase 4 (CDK4; K) as described previously [171]. Experimentally transformed HBECs used in the present studies included overexpressing $KRas^{V12}$, *p53* knockdown via shRNA, and *myc* overexpression as previously described [188]. Immortalized non-cancerous HBEC 3KT, HBEC 30KT, and the experimentally transformed HBECs were cultured at 37ºC in 5% CO_2 in Keratinocyte Serum Free Media (KSFM) (Gibco) containing 50μg/mL of bovine pituitary extract and 5μg/mL of epidermal growth factor on porcine gelatin-coated tissue culture dishes (Sigma Aldrich).

Human breast - mammary epithelial cells: Human mammary epithelial cells (HME1) were immortalized by retroviral infection with hTERT and have a normal diploid karyotype (ATCC Cell Systems, Gaithsburg, MD). HMEC50 cells were originally derived from the noncancerous breast tissue of a female diagnosed with Li-Fraumeni syndrome (TP53 heterozygous) as previously described [198]. All HMECs were cultured in serum-free conditions as previously described and were mycoplasma free and DNA fingerprinted [199].

Human cancer cell lines: Non-small cell lung cancer (NSCLC) cells A549, H2009, HCC 2429, HCC 4017, H23, and HCC 15 were supplied by John Minna (Hamon Cancer Center, UT Southwestern). The breast cancer cell line MDA-MB-231 was kindly provided by Michael White (Department of Cell Biology, UT Southwestern). All cancer cell lines were cultured in basal

medium supplemented with 10% Cosmic Calf Serum (Thermo Scientific) at 37ºC in 5% CO_2. All cell lines used in the present studies were mycoplasma free (e-Myco kit, Boca Scientific) and DNA fingerprinted (PowerPlex 1.2, Promega). All cells were compared to the complete database in our own collection and to that of ATCC. All cell lines are commercially available through the ATCC Cell Systems (Gaithersburg, MD)

Human lymphocytes: Peripheral blood mononuclear cells (PBMCs) were isolated via centrifugation from the buffy coat of whole blood donated by healthy human volunteers via venipuncture. Informed consent was obtained from each donor in accordance with the Declaration of Helsinki and approved by the Institutional Review Board at UT Southwestern Medical Center (Dallas, TX). Cells were stimulated using 1μg/mL Lectin, PHA-L (EMD Biosciences) and cultured in suspension of RPMI-1640 media (Gibco) supplemented with 10% Cosmic Calf Serum (Thermo Scientific) at 37ºC in 5% CO_2.

Mouse embryonic fibroblast (MEF) cells: *Nrf2*-heterozygous (+/-) and *nrf2*-deficient (-/-) cells were the generous gift of Ralph DeBerardinis (Children's Medical Center Research Institute, UT Southwestern Medical Center, Dallas, TX) [172]. Cells were cultured in basal medium supplemented with 10% Cosmic Calf Serum (Thermo Scientific) at 37ºC in 5% CO_2.

Lung Nrf2 knockdown: Stable Nrf2 knockdown cells lines were established by infecting epithelial cells (HBEC 3KT and HME1) with a validated anti-Nrf2 shRNA expressing lentiviral vector (pGIPZ, OpenBiosystems V2LHS_238788) in the presence of 2μg/mL Polybrene (Sigma).

2.2.2 Drug Treatment and Radiation

CDDO-Me (Reata Pharmaceuticals, Irving, TX) was dissolved in DMSO. Subconfluent cell cultures were treated with 10, 50, or 150nM CDDO-Me. Experimental concentrations of CDDO-Me were determined based on cell toxicity for the different cell types (**Figure 2.2**) and used at the lowest effective dose for each tissue type-cell. Drug was administered 18 hours prior to γ radiation exposure (^{137}Cs source at 243.08 cGy/min; dosimetry provided by physicists in the Department of Radiation Oncology, University of Texas Southwestern Medical Center). Control experiments were treated with solvent only.

2.2.3 Experimental Assays

ARE-Luciferase Reporter: Cells were co-transfected with pGL4.37 [*luc2*/ARE/hygro], and pGL4.73 [*hRluc*/SV40] as a transfection expression control using 3:1 FuGENE HD according to the manufacturer's instructions (Promega). Briefly, cells were treated with drug 18 hours after luciferase transfection, and luciferase activity was measured using the Dual-Glo Luciferase Assay (Promega) after another 18 hours. Each ARE-firefly luciferase value was normalized against Renilla luciferase.

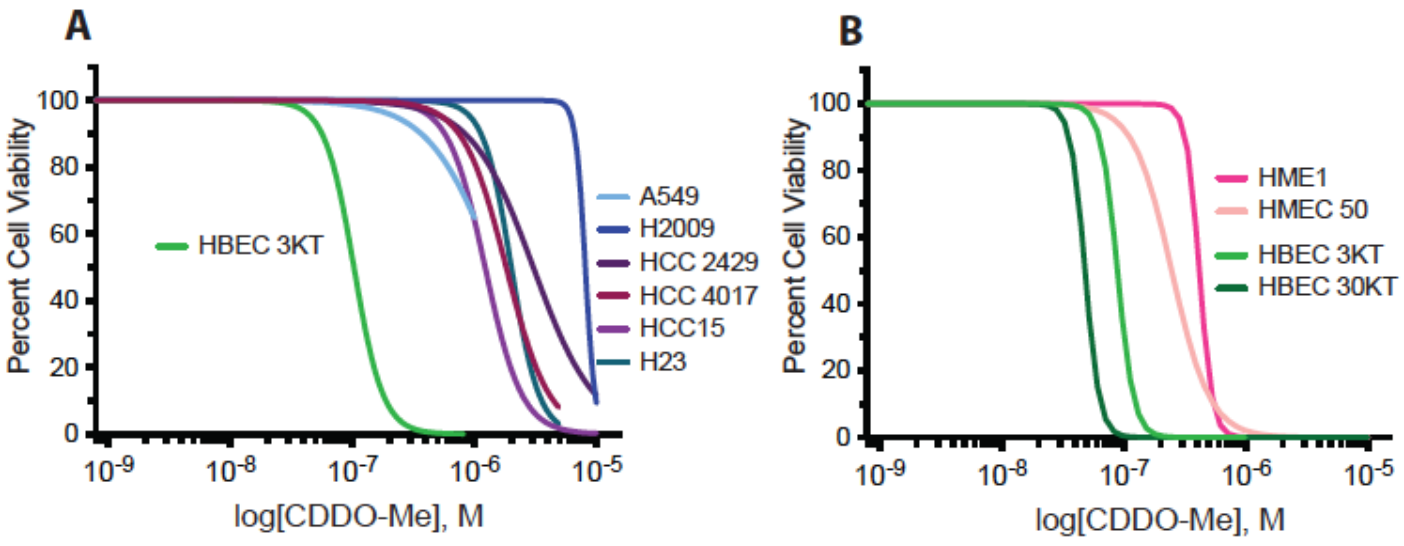

Figure 2.2

Figure 2.2: Epithelial cells are more sensitive to CDDO-Me when compared to cancer cells. Cell Titer Glo toxicity curves of various (A) NSCLCs and (B) immortalized epithelial cell lines, respectively. Cells were treated with drug and after 48-60 hours, percentage of living cells measured using Cell Titer Glo assay and normalized to untreated cells. Cancer cells can withstand higher doses (average LD_{50}=2μM), whereas epithelial cells are more sensitive to toxicity: lung (LD_{50}=70nM) and breast (average LD_{50}=250nM). Values are based off two experiments of six replicates.

Colony Formation Assay: Within 15 minutes of IR exposure, cells were trypsinized and seeded in triplicate in 10-cm dishes at clonogenic density (ranging from 100-1000 cells per dish) for colony formation assays. Ten days later, dishes were stained with a mixture of 6.0% glutaraldehyde and 0.5% crystal violet, and colonies (defined as clusters of >50 cells) were counted. Cell survival measurements were fitted using a linear quadratic equation [$SF = \exp(-\alpha D - \beta D^2)$] (SF: surviving fraction; D: radiation dose in Gy) using GraphPad Prism, and dose-modifying factors (DMF) calculated for each as a measure of radioprotection as described [158]. DMF less than 1.2 was considered the cutoff for significant protection.

Comet Assay: The alkaline comet assay (Trevigen) was used to detect DNA damage at 30 minutes post-IR according to manufacturer's instructions. Twenty random fields (200x magnification) were scanned under a fluorescence microscope. Approximately 50 cells per condition were analyzed using OpenComet software [73]. Tail moment [tail length x tail DNA %] and tail DNA % values generated by OpenComet were analyzed as a measure of DNA damage.

Western Blot Analysis: Cells were lysed in Laemmli SDS reducing buffer [50mM Tris-HCl (pH 6.8), 2% SDS, and 10% glycerol], boiled, and separated by SDS/PAGE. The following antibodies were used: anti- HO1, -PRX1, -NQO1 (1:1000; AbCam), anti- Nrf2 (1:500 Santa Cruz; 1:1000 Cell Signaling), anti-phospho-Nrf2 (1:5000; AbCam), and anti–β-actin (1:20,000; Sigma).

Proliferation Assay: MEFs were treated with 50nM CDDO-Me 18 hours prior to 10 Gy γ exposure and counted at various time intervals using an automated cell counter (TC20, Biorad) in the presence of trypan blue to assess cell viability.

Viability Assay: CDDO-Me or DMSO was added to cells at 60% confluency, and cell viability was determined 48-60 hours later with CellTiter-Glo (Promega) as per manufacturer's protocols. Reported median lethal concentration (LC_{50}) values are based on the average of two independent experiments with 6 replicates and calculated from dose-response curves generated with nonlinear regression in Prism 6 (GraphPad Software, Inc).

2.2.4 Statistical Methods

All significance values are $p<0.05$, unless otherwise stated, and were calculated using two-sided t-tests between the treatment group and its appropriate control.

2.3 Results

2.3.1 CDDO-Me induces the Nrf2 pathway in non-cancerous HBECs and HMECs, but not breast and lung cancer cell lines.

To confirm that CDDO-Me (**Figure 2.1B**) activates the Nrf2 pathway in the cells used, HBEC 3KT (Lung-3), HME1 (Breast-1), and human lymphocytes were transfected with the ARE-luciferase reporter were treated with CDDO-Me or DMSO. After 18 hours, CDDO-Me 10nM significantly increased luciferase expression in lung, and 50nM increased luciferase expression in breast ($p<0.05$, paired t-test compared to DMSO control) (**Figure 2.3A-B**). Both concentrations of CDDO-Me significantly increased luciferase expression in peripheral blood

lymphocytes ($p<0.01$, paired t-test compared to DMSO control) (**Figure 2.3C**). NSCLC cells tested, however, did not have increased ARE-luciferase after treatment with CDDO-Me (**Figure 2.3F-I**). Additionally, protein lysates collected at various times after CDDO-Me 10nM treatment of normal Lung-3 cells showed an increase of Nrf2/ARE downstream targets, including heme oxygenase (HO1), NADPH dehydrogenase quinone (NQO1), and peroxiredoxin (PRX1) (**Figure 2.3D-E**). Expression of these downstream enzymes peaks around 18 hours. For this reason, an 18-hour pre-treatment with CDDO-Me was used for all subsequent radioprotection experiments.

2.3.2 Pre-treatment with CDDO-Me decreases IR-induced DNA damage in bronchial and mammary epithelial cells as well as in PBMCs.

Alkaline comet assays were performed on lung and breast epithelial cells thirty minutes after radiation to determine if CDDO-Me protected against IR-induced DNA damage. Since many of the adverse effects of radiation occur in the blood, peripheral blood mononuclear cells (PBMCs) were assessed to determine if CDDO-Me also rescued human lymphocytes against IR-induced DNA damage. Pre-treatment with CDDO-Me protected all three non-cancerous cell types against radiation-induced DNA damage as seen by significantly decreased tail moments using the alkaline comet assay in PBMCs (**Figure 2.4C**) as well as HBEC 3KT and HME1 (**Figure 2.4A-B**) (*$p<0.05$, t-test compared to 3 Gy DMSO control). The partial protection of human lymphocytes with CDDO-Me is particularly important since significant hematological toxicities are associated with radiation therapy for lung and breast cancers [27].

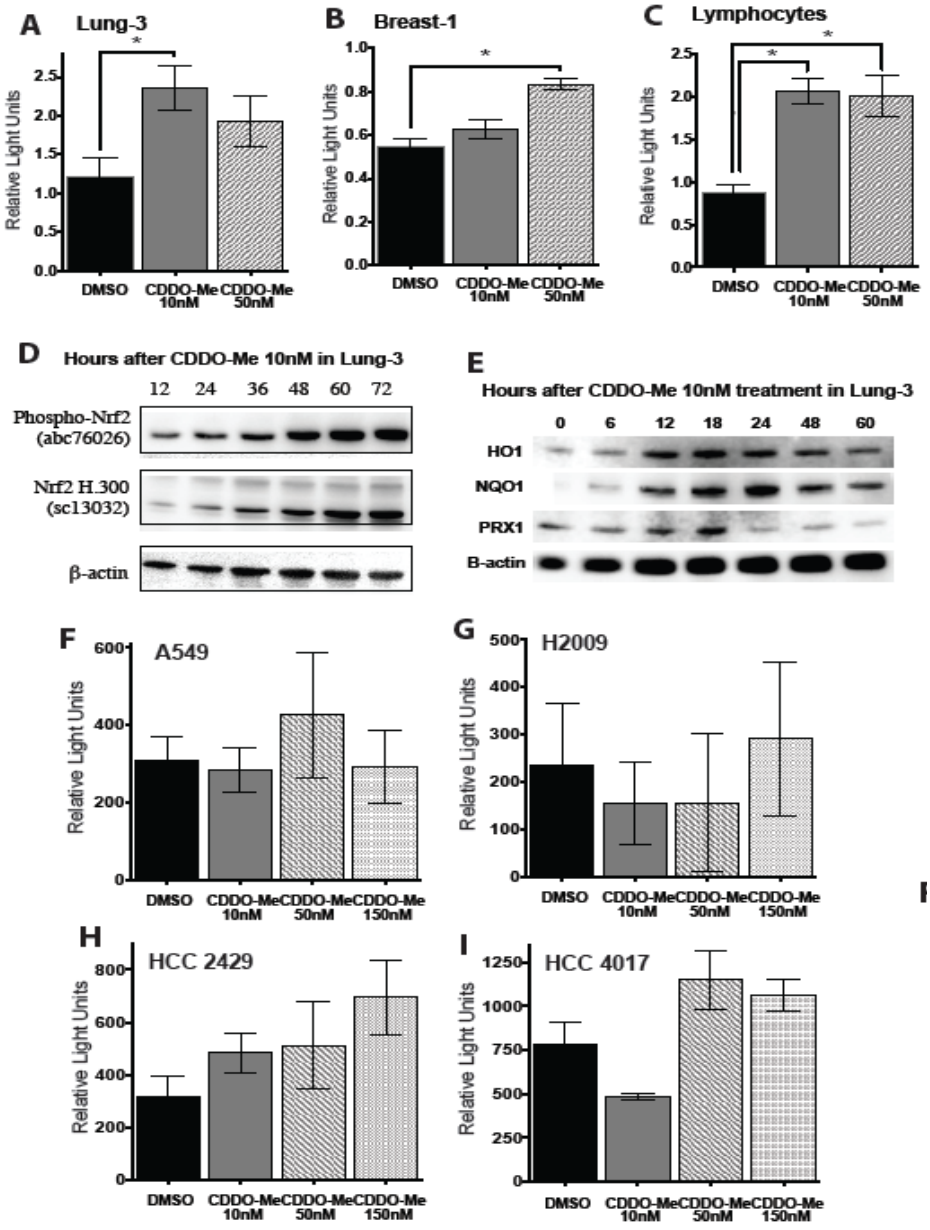

Figure 2.3: CDDO-Me activates the Nrf2 antioxidant pathway in non-cancerous cells but not NSCLCs.

(A, B, C) CDDO-Me increases expression of ARE-driven luciferase 18 hours after drug treatment in HBEC 3KT, HME1, and PBMCs, respectively. Firefly ARE-luciferase normalized to renilla control (RLU). Mean ± SEM of 6 replicates, *p<0.05 using paired t-test (between DMSO and drug). (D) Protein levels of phospho-Nrf2 (band observed at ~120kDa) and total Nrf2 (bands observed at ~68, 75kDa) after treatment with 10nM CDDO-Me in HBEC 3KT. (E) CDDO-Me 10nM activates heme oxygenase-1 (HO1, band observed at ~32kDa), NADPH dehydrogenase quinone (NQO1, band observed at ~30kDa), and peroxiredoxin (PRX1, band observed at ~20kDa), all downstream targets of Nrf2/ARE and peaking at approximately18 hours after treatment in HBEC 3KT. CDDO-Me does not affect expression of ARE-driven luciferase 18 hours after drug treatment in (F) A549, (G) H2009, (H) HCC 2429, and (I) HCC 4017. Firefly ARE-luciferase normalized to renilla control (RLU). Mean ± SEM of six replicates.

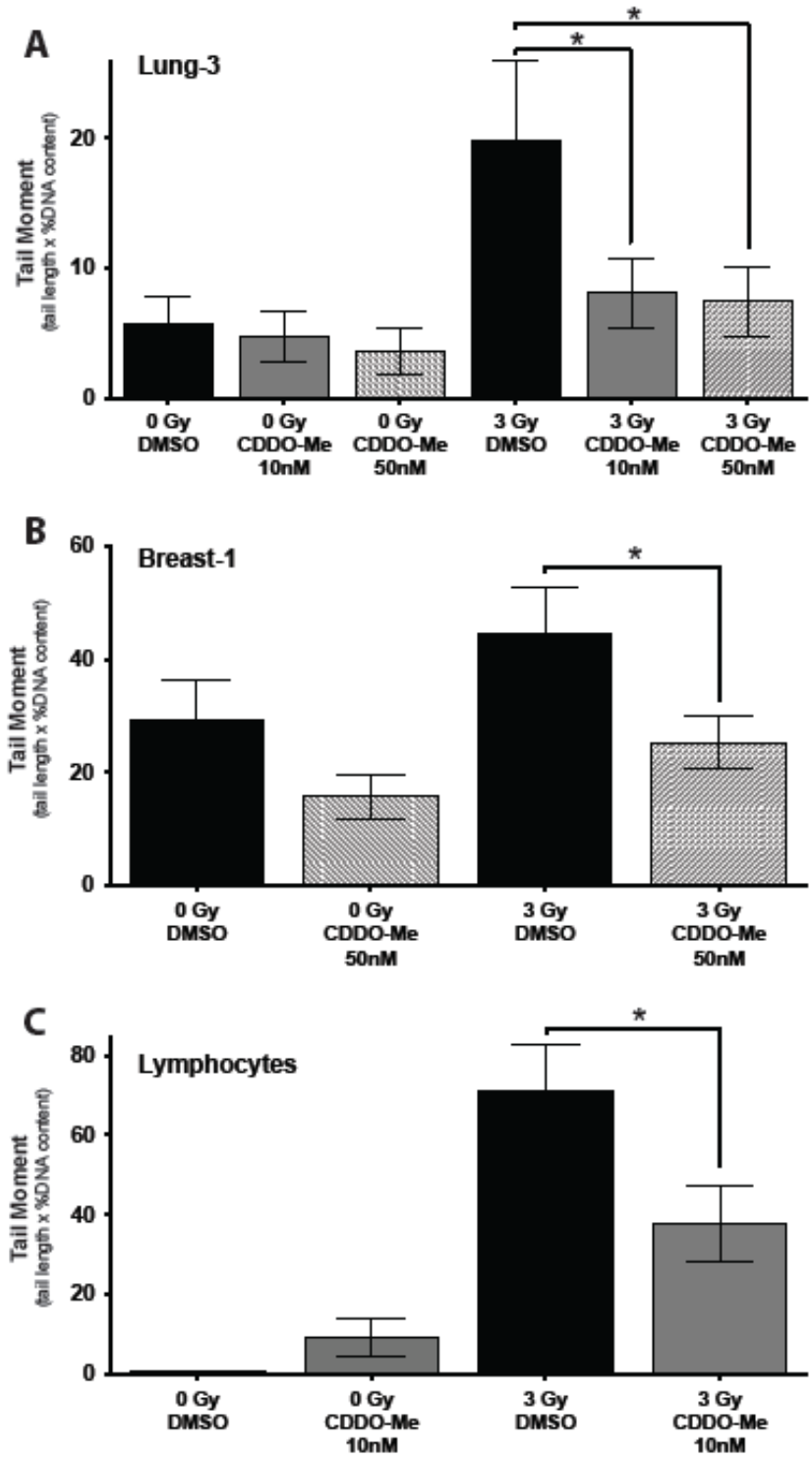

Figure 2.4

Figure 2.4: Pre-treatment with CDDO-Me decreases IR-induced DNA damage in a variety of non-cancerous cells.

CDDO-Me decreases radiation-induced DNA damage in the alkaline comet assay in bronchial and mammary epithelial cells as well as human lymphocytes. (A) HBEC 3KT, (B) HME1, and (C) PBMCs were treated with CDDO-Me 18 hours prior to IR, then mounted on slides 30 min post-IR. Data analyzed and calculated using Open Comet software [tail moment = tail length x tail DNA percentage]. Mean ± SEM of >50 cells per condition, *p<0.05 using t-test (compared to 3 Gy DMSO). **p<0.01, using T-test (compared to 0 Gy DMSO).

2.3.3 CDDO-Me is a significant radioprotective countermeasure in normal epithelia.

To determine the potential radioprotective effects of CDDO-Me, clonogenic survival assays post-IR was assessed in multiple immortalized but non-cancerous bronchial (HBEC 3KT, 30KT) and breast (HME1, HMEC 50) epithelial cells. Since epithelial cells are more sensitive to the cytotoxic effects of CDDO-Me compared to other malignant cell types (**Figure 2.2**), normal breast and lung cells were pre-treated with low nanomolar concentrations before exposure to 3 Gy radiation to determine the lowest effective radioprotective dose (10-50nM for lung, 50-150nM for breast) (**Figure 2.5A**; HBEC 30KT in **Figure 2.7F**). Both cell types, when exposed to CDDO-Me 18 hours prior to IR, had an increase in clonogenic survival when compared to DMSO treated cells (HBEC 3KT, DMF=1.32; HBEC 30KT, DMF=1.47; HME1, DMF=1.34; HMEC 50, DMF=1.28) (**Figure 2.5B-D; Figure 2.7D**). The DMFs observed with CDDO-Me are greater than most standard radioprotective agents currently used, including amifostine [9, 233]. This demonstrates that CDDO-Me is a potent radioprotective agent when given before IR in lung and breast epithelial cells.

2.3.4 Nrf2 knockdown eliminates radioprotective effects of CDDO-Me.

To confirm that Nrf2 is the mechanism through which CDDO-Me protects epithelial cells, clonogenic survival post-IR was assessed in cells stably expressing Nrf2 shRNA (shNrf2). Lung-3 cells with shNrf2 knockdown are not significantly radioprotected by CDDO-Me pretreatment (DMF=1.14) (**Figure 2.5E**), whereas cells with intact Nrf2 have increased survival when treated with CDDO-Me (**Figure 2.5D**; data for breast not shown). Nrf2 knockdown cells have decreased basal and induced expression of Nrf2 as evidenced by ARE-luciferase reporter expression when compared to an shRNA non-silencing control (*$p<0.05$, **$p<0.01$, t-test)

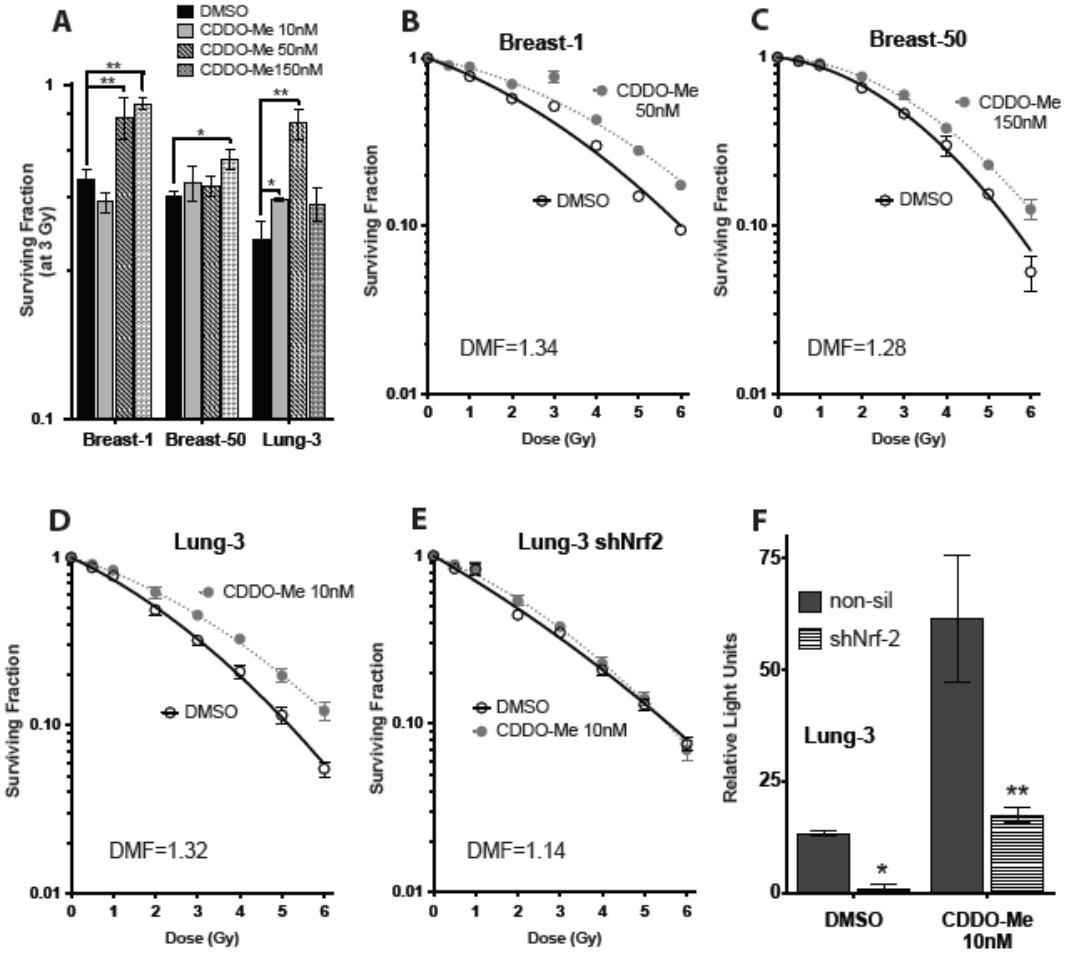

Figure 2.5

Figure 2.5: CDDO-Me is a potent radiation countermeasure in bronchial and breast epithelial cells, and Nrf2 knockdown abrogates radioprotection. (A) Normal breast and lung epithelia are radioprotected at multiple doses of CDDO-Me. Cells were treated with drug 18 hours before 3 Gy γ exposure, then seeded immediately into clonogenicity. Colonies grown for ~14 days before fixation with 6% glutaraldehyde/0.5% crystal violet stain. Mean ± SEM of four experiments seeded in triplicate, *p<0.05, **p<0.001 using t-test (compared to DMSO at 3 Gy). (B, C) HMEC and (D) HBEC cells pre-treated with 10nM CDDO-Me have a significant increase in clonogenic survival. (E) HBEC 3KT with sh-Nrf2 see no radioprotection when pre-treated with CDDO-Me. Clonogenic survivals, mean ± SEM with linear-quadratic fit curve of four experiments seeded in triplicate. (F) Nrf2 knockdown cells have a ~90% decrease of Nrf2 activity compared to non-silencing control, with diminished basal and CDDO-Me-induced ARE-luciferase activity. Mean ± SEM of six replicates, *p<0.05, **p<0.01, t-test (compared to non-silencing control).

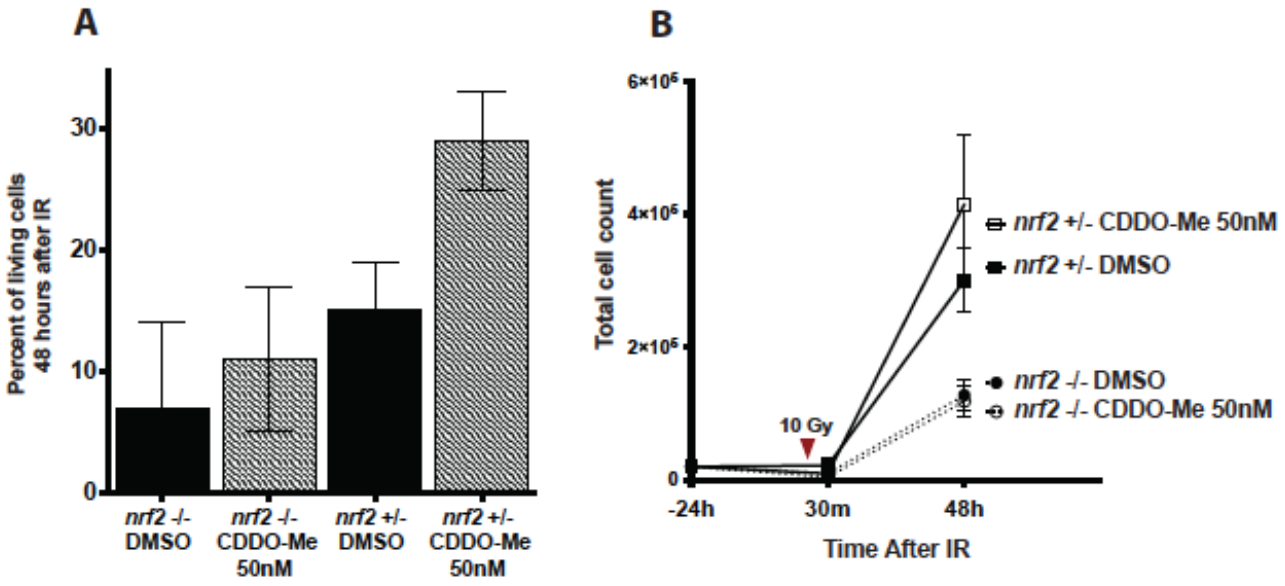

Figure 2.6

Figure 2.6: CDDO-Me protects *nrf2*-heterozygous but not *nrf2*-deficient mouse embryonic fibroblast (MEF) cells from 10 Gy radiation.

(A) Viable cells counts 48 hours post-IR show that 50nM CDDO-Me increases the number of living *nrf2* +/- MEFs approximately 2-fold compared to cells treated with DMSO, whereas *nrf2* -/- MEFs are unprotected by CDDO-Me. (B) Total number of cells after IR. Mean ± SEM of triplicates.

(**Figure 2.5F**). This indicates the Nrf2 pathway is integral to CDDO-Me radioprotection in normal epithelia.

As additional evidence that Nrf2 is necessary for CDDO-Me radioprotection, survival and viability after a sub-lethal dose of IR was assessed in *nrf2*-deficient or *nrf*-heterozygous mouse embryonic fibroblasts. Pretreatment with CDDO-Me increased the percentage of viable *nrf2* +/- cells 48 hours post-IR, but did not protect *nrf2* -/- cells (**Figure 2.6A**). Additionally, cells with deficient *nrf2* die faster compared to heterozygous cells (**Figure 2.6B**). These findings further corroborate the notion that Nrf2 is necessary for both responses to radiation as well as protection by CDDO-Me.

2.3.5 Oncogenically progressed HBECs, NSCLCs, and breast cancer cells are not protected by CDDO-Me.

In order to determine if experimentally cancer progressed human epithelial cells and cancer cell lines are also protected by CDDO-Me, clonogenic survival post-IR was assessed using an isogenic series of cell lines with progressive oncogenic manipulations. HBEC 3KT with *KRas* overexpression were still protected from radiation with CDDO-Me (Lung-3+lenti-$KRas^{V12}$, DMF=1.35) (**Figure 2.7A**). When additional changes were introduced, including *p53* knockdown and *myc* overexpression, protection from CDDO-Me was lost (Lung-3+lenti-$KRas^{V12}$+sh*p53*, DMF=0.88; Lung-3+lenti-$KRas^{V12}$+sh*p53*+*myc*, DMF=0.92) (**Figure 2.7B-C**).

To further show that CDDO-Me only protects non-malignant cells, clonogenic survivals were completed a lung cancer line (HCC 4017) that has a matched HBEC (Lung-30) derived from normal, non-cancerous tissue from the same patient. Importantly, while normal Lung-30 was protected by 10nM CDDO-Me (HBEC 30KT, DMF=1.47) (**Figure 2.7D**), the tumor cell

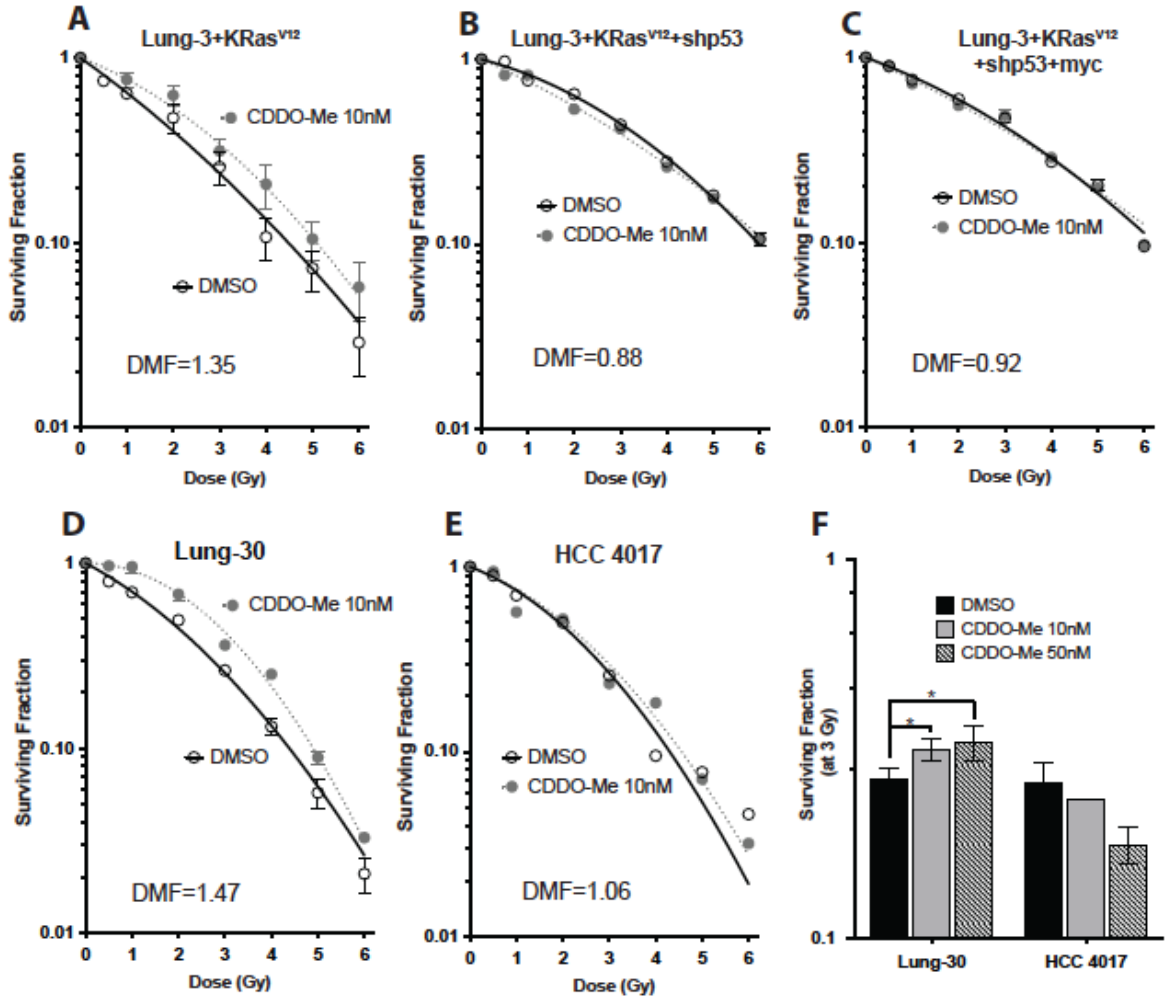

Figure 2.7

Figure 2.7: CDDO-Me radioprotection decreases with progressive oncogenic manipulations in HBECs and in a matched NSCLC line.

Isogenic oncogenic progression in HBEC 3KT. Immortalized HBECs with (A) lenti-*KRas*^{V12}, (B) lenti-*KRas*^{V12} and sh*p53* knockdown, and (C) lenti-*KRas*^{V12}, sh*p53*, and *myc* overexpression. Only lenti-*KRas*^{V12} cells are still moderately protected by CDDO-Me, but further oncogenic changes eliminate the radioprotective effects of CDDO-Me. (D) HBEC 30KT are protected by CDDO-Me. (E) HCC 4017, a NSCLC isolated from the same patient from which HBEC 30KT was derived, are unprotected by CDDO-Me. (F) Increasing concentrations to 50nM still enhances clonogenic survival of HBEC 30KT, but actually seems to decrease survival in HCC 4017 after 3 Gy radiation. Mean ± SEM of three experiments seeded in triplicate, **p<0.01, t-test (compared to DMSO at 3 Gy).

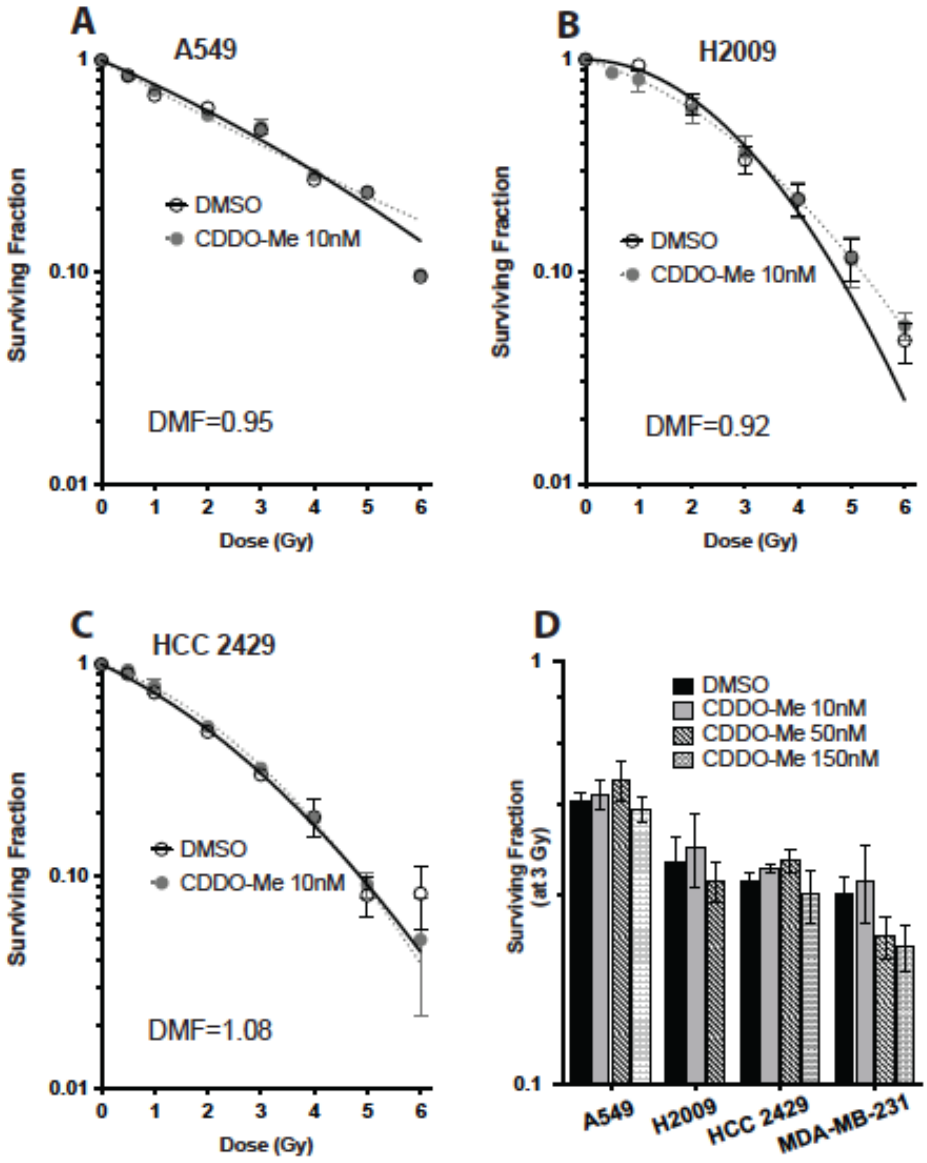

Figure 2.8

Figure 2.8: NSCLC and breast cancer cells are not protected with CDDO-Me.
Clonogenic survivals show that (A) A549, (B) H2009, and (C) HCC 2429 are not protected when pretreated with the same concentration of CDDO-Me (10nM) that protected HBEC cells. (E) Even higher concentrations of CDDO-Me are not protective of cancer cells after 3 Gy radiation, including MDA-MB-231 breast cancer line. However, 150nM CDDO-Me significantly decreases the clonogenic survival of MDA-MD-231 cells after exposure to 3 Gy radiation. Mean ± SEM of three experiments seeded in triplicate, **p<0.01, t-test (compared to DMSO at 3 Gy).

line from the same patient was not protected (HCC 4017, DMF=1.06) (**Figure 2.7E**). Furthermore, increasing the concentration to 50nM CDDO-Me decreases survival after radiation to HCC 4017 cells while still providing radioprotection to Lung-30 cells (**Figure 2.7F**). This is a promising result since CDDO-Me appears to specifically provide protection to normal, noncancerous human cells, thus supporting the use of such radioprotectors prior to radiation therapy for cancer patients.

Various other NSCLC cells and a breast cancer cell lines were tested for potential radioprotection with CDDO-Me. The basal radiosensitivity (SF_2) increases in Lung-3 (HBEC 3KT) with each additional oncogenic manipulation, indicating that these cells become more radio-resistant during the stepwise mutations that lead to cancer, whereas Lung-30's (HBEC 30KT) matched tumor line is actually more sensitive to radiation (**Table 2.1**). Since NSCLCs are heterogeneous in their radio-responsivity, a range of radio-sensitive and resistant lines were assayed (indicated by the surviving fraction of cells at 2 Gy [SF_2]), as well as NSCLCs containing a variety of different mutations (**Table 2.1**). NSCLCs pretreated with the same concentration of CDDO-Me that protected normal lung epithelial cells (10nM) were not protected from radiation, regardless of radiosensitivity or mutation status (A549, DMF=0.95; H2009, DMF=0.92; HCC2429, DMF=1.08; data for HCC 15 and H23 not shown) (**Figure 2.8A-C**). This indicates that multiple oncogenic alterations have an effect of both radiation response as well as protection by CDDO-Me.

Since cancer cell lines can generally survive in higher concentrations of CDDO-Me when compared to normal epithelial cells (**Figure 2.2**), malignant cells were treated with higher concentrations of CDDO-Me to confirm that cancer cells would not be protected at higher doses of CDDO-Me. Even concentrations up to 150nM were not sufficient to protect NSCLC,

including HCC 15 and H23 (data not shown), nor did it protect MDA-MB-231, a breast cancer cell line (**Figure 2.8D**). This demonstrates that the same low nanomolar concentrations of CDDO-Me that protect normal epithelial cells are highly unlikely to be protective in malignant cells.

Table 2.1

Cell Line	SF_2	*KRas*	*p53*	*Keap1*
HBEC 3KT	0.487	wt	wt	wt
HBEC 3KT +*KRas*^{V12}	0.474	X	wt	wt
HBEC 3KT +*KRas*^{V12}+sh*p53*	0.650	X	X	wt
HBEC 3KT +*KRas*^{V12}+sh*p53*+*myc*	0.702	X	X	wt
HBEC 30KT	0.442	wt	wt	-
HCC 4017	0.321	mut	mut (C833A)	wt
A549	0.771	mut (G34A)	wt	mut (G333C); constitutive Nrf2
H2009	0.615	mut (G35C)	mut (G818T)	wt
HCC 2429	0.514	wt	mut (G800A)	wt
HCC 15	0.484	wt	mut (A776T)	wt
H23	0.053	mut	mut	mut; Nrf2 still inducible
HME1	0.528	wt	wt	wt
HMEC 50	0.659	wt	mut	-
MDA-MB-231	0.452	mut (G38A)	mut (G839A)	wt

Table 2.1: Panel of cell radiosensitivity and mutation status.

A summary of all cell lines used in the present study. Surviving fraction of cells at 2 Gy (SF_2) is used as a metric of radio-sensitivity, with $SF_2 > 0.6$ considered a "resistant" line and $SF_2 < 0.4$ considered a "sensitive" line. Mutation status of *KRas*, *p53*, and *Keap1*/*Nrf2* is listed as either wildtype (wt) or mutated (mut) as determined by full exon sequencing [91]. There is a KEAP1 mutation in H23 cell line [166]. "X" indicates experimentally manipulated gene expression.

2.4 Discussion of CDDO-Me as a Radioprotector in the Lung

When cancer patients undergo radiation therapy, the relationship between radiation dose and tumor response generally follows a dose-response curve. Unfortunately, normal tissue damage follows an even steeper increase with increasing radiation dose [168]. Long-term effects and toxicity for the patient caused from normal tissue damage limit the total dose that can be administered, and for this reason, widening the therapeutic margin has been and remains a crucial goal in the radiation oncology field. In this study, I show that CDDO-Me selectively protects normal non-cancerous lung and breast epithelial cells while leaving tumor cells unprotected against radiation, resulting in a potentially higher therapeutic window for current standards of care radiotherapy.

In order for a radioprotector to be classified as such, or to be used with conventional radiotherapeutic doses, it is critical that the agent be able to be administered in optimal dosing, have low toxicity, and most importantly, not protect tumor cells. The current standard for acute radiation exposure is amifostine, a hydrophilic phosphorothioate compound that does not readily cross cell membranes, must be converted to an active metabolite, and can only be administered intravenously [9]. The radioprotection amifostine provides varies greatly depending on the oxygen content and tissue type, with lung protection factors being amongst the lowest (DMF approximately 1.2). In addition, amifostine has high cytotoxic activity against normal cells and has serious side effects such as hypotension and peripheral neuropathies (refer to **Section 1.9**) [9]. In contrast, I found that CDDO-Me is much more effective in protecting both normal lung and breast epithelial cells (average DMF of 1.35). Since CDDO-Me is orally available with a low toxicity profile, this makes it a more attractive option as a radioprotector, especially when only given short term.

Not only is CDDO-Me a potent radioprotective countermeasure in epithelial cells, but it can significantly protect human lymphocytes from radiation-induced DNA damage. This is a particularly promising result considering that damage to the hematopoietic system is often one of the main dose-limiting toxicities of radiation therapy, with anemia, bleeding, and infections being common [27]. Furthermore, the long-term negative consequences of radiation include development of secondary leukemias and lymphomas later in life [137]. Since I demonstrate that CDDO-Me has radioprotective effects against human blood lymphocytes, this is one more added benefit of CDDO-Me that may help protect individuals exposed to radiation (such as astronauts on long-term space missions and first responders to nuclear accidents).

Since Nrf2 is necessary for CDDO-Me to exert its protective effects on epithelial cells, it is necessary to point out that even cells with Nrf2 knockdown have a small amount of Nrf2 activity, and these cells are still induced by CDDO-Me. Similar effects have been observed in other studies [99], but since there is never a 100% decrease of Nrf2 with shRNA knockdowns, there may be residual Nrf2 even in the sh-Nrf2 cells. Since the Nrf2 protein is extremely difficult to assay directly, the exact quantification of knockdown level is determined either through quantitative RT-PCR or Western Blot of downstream markers (~60% knockdown, data not shown), or using a reporter, such as the ARE-luciferase (~90% knockdown, shown in **Figure 2.5F**). Since there is still some Nrf2 leftover in these cells, this may partially explain why the Nrf2/ARE pathway is still partially inducible by CDDO-Me in knockdown cells, but this induction may not be sufficient to exert a protective effect. To confirm the importance of the Nrf2 signaling pathway in the radioprotection observed, I demonstrated that mouse cells with complete *nrf2*-deficiency are unprotected by CDDO-Me. It is important to point out that CDDO-Me is likely activating other additional compensatory pathways.

When radiation exposure produces large amounts of reactive species in cells, Nrf2/ARE is not the only pathway activated. Radiation has been shown to stabilize hypoxia inducible factor (HIF-1α) by activating p38 MAPK and resulting in the decreased half-life of its E3 specific ligase, protein von Hippel-Lindau [100]. There have been reports that amifostine induces hypoxia inducible factor alpha (HIF-1α) in both cell culture and mouse tissues [105]. Thus, reactive species produced by radiation may mimic and affect multiple pathways simultaneously, including the Nrf2/ARE and HIF/HRE pathways.

Although CDDO-Me is a potent radioprotector for normal, non-cancerous cells, it did not protect any of the cancer cells tested in these studies. Interestingly, c-myc has been identified as an Nrf2-interacting protein [120], but a single mutation is unlikely responsible for loss of CDDO-Me effects. This is clearly demonstrated with the experimentally manipulated gene expression in the isogenic HBEC system—immortalized HBECs with lenti-*KRas*^{V12} and sh*p53* knockdown are not protected regardless of whether or not the cells have *myc* overexpression. Additionally, some of the NSCLC cells with intact *KRas* or *p53* yet are not protected by CDDO-Me, indicating that multiple oncogenic changes are required to confer resistance to CDDO-Me radioprotection.

There are published reports showing that higher doses of CDDO-Me and other triterpenoids (above 1μM) can inhibit cancer cell growth and induce cancer cell death in a multitude of cancer types [195, 230]. The flip side, however, is that these higher doses also inhibit the growth and affect the viability of normal cells (**Figure 2.2**). In the nanomolar range used in these experiments (up to 150nM), I did not observe any decreases in proliferation or increased cell death in NSCLC cell lines in the absence of radiation treatment that would be expected at higher concentrations. While these studies do not show any significant chemo-

preventative effects of CDDO-Me in the lung, there are indications that slightly higher doses (>150nM) of CDDO-Me may act as a radiosensitizer in some lung and breast cancer cells. Most promisingly, I did not observe any radioprotective effects in cancer cells, even when the doses were increased.

The original phase II clinical trial using CDDO-Me for treatment of diabetic kidney disease used doses ranging from 25-150mg daily [156]. While these doses are not toxic as a one-time treatment, they have the potential to accumulate over time as almost all patients experienced some side effects over the course of fifty-two weeks [156]. However, our present series of experiments utilized low nanomolar concentrations of CDDO-Me as a one-time treatment, allowing patients to conceivably be treated for a short period before radiation exposure and minimizing potential long-term toxicities.

CDDO-Me, and other compounds in the same triterpenoid family, have been shown to have chemoprotective properties in addition to radioprotective properties [126]. Many chemotherapeutic drugs used for lung cancer, such as paclitaxel and carboplatin, induce DNA damage and produce ROS; these effects can be detrimental to healthy non-cancerous cells. Damage to rapidly dividing cells (bone marrow, gastrointestinal tract, and skin) often results in radiation-induced toxicities. For this reason, the use of CDDO-Me could be expanded as a potentially effective chemoprotective agent. Ideally, CDDO-Me can be given short-term to cancer patients undergoing radiation or chemotherapy to increase the therapeutic margin, resulting in better outcomes and less toxicity.

CHAPTER THREE

CHARACTERIZATION OF POTENTIALLY NEW RADIOPROTECTIVE AGENTS

3.1 Introduction to Alternative Radioprotectors

The development of novel radiation countermeasures requires screening new compounds that may have mechanisms that differ from those classically described.

RTA-408

A newer formulation of synthetic triterpenoid, RTA-408, was developed by Reata Pharmaceuticals (Irving, TX) for use in IR-induced skin dermatitis, an important and common side effect of patients undergoing radiation treatment. RTA-408, a sister compound of CDDO-Me (RTA-402), acts through the same Nrf2/ARE pathways to activate cytoprotective enzymes (refer to **Figure 2.1A**). All chemical structures of new RTA formulations were kept proprietary.

Treatment with RTA-408 is hypothesized to protect normal skin, but not cancer cells, from radiation-induced dermatitis. In order to test this, the effect of RTA-408 on irradiated breast and lung cancer cell lines was evaluated. Initial experiments conducted by Reata investigators demonstrated that in cell lines with low basal Nrf2 activity, antioxidant anti-inflammatory modulator (AIM) treatment with RTA-408 caused robust increases in NQO1 transcript levels, whereas cells with high basal Nrf2 activity, there was no further induction by AIM treatment. Since most breast cancer lines evaluated have a partially activated Nrf2 state compared to normal breast cell lines, I determined if RTA-408 affects the sensitivity of cancer cells to IR-induced damage and cell death.

Yel002

In 2012, the Schiestl group (Departments of Radiation Oncology, Pathology, & Environmental Health Sciences; University of California Los Angeles) proposed two novel protective therapies against radiation: Yel-001 and Yel-002 (**Figure 3.1A**). These small organic molecules had a reported hematopoietic DMF of 1.15 and were uncovered in the yeast DEL high throughput assay [178]. This assay measures the sensitivity of IR-induced DNA deletions throughout phases of the cell cycle and is efficient for measuring intrachromosomal recombination events when six kilobases or more of genomic DNA is deleted [86]. Furthermore, IR is a potent inducer of DNA deletion events, and antioxidant/radioprotective treatments can protect proliferating yeast cells from radiation-induced DNA deletions using the DEL assay [74, 75, 109, 206]. Originally a plate-based assay, the DEL principle was adapted into a high-throughput screen format and utilized to screen thousands of biologically active compounds, thus leading to the identification of Yel-001 and Yel-002. Interestingly, Yel-001 and Yel-002 had already been shown to protect against radiation-induced DSBs when added up to an hour after exposure to radioactive iodine (^{131}I) [81].

Schiestl and colleagues observed that adding either Yel001 or Yel002 to irradiated cultures reduced cell death and genomic instability in the yeast DEL plate-based assay [179]. When tested *in vivo*, Yel-002 increased survival of mice when administered at both 1 and 24 hours after IR (DMF of 1.15); this corresponded to an average of a 25% reduction in lethality *in vivo* following a lethal dose (8 Gy) of IR with the first therapeutic injection administered 24 hours post exposure followed by injections at 48, 72, 96, and 120 hours. Additionally, treatment with Yel compounds reduced IR-induced leukemia rates, as well as spontaneous leukemia rates in non-irradiated animals, and post-IR treatment with Yel-002 accelerated the recovery of the

hematopoietic system [179]. The authors did not observe any toxicity of these compounds at the doses used.

Although the exact mechanisms of action of the Yel compounds are currently unknown, there are some suggestions of increased DNA repair or genome stabilization with reduction in senescence pathways [81, 179]. Since CDDO-Me, and most other radioprotective agents, are less effective as a radiation mitigators in HBECs, Yel compounds may have potential since they show early promise: they are highly effective when administered up to twenty-four hours after radiation exposure and appear to have a low toxicity profile.

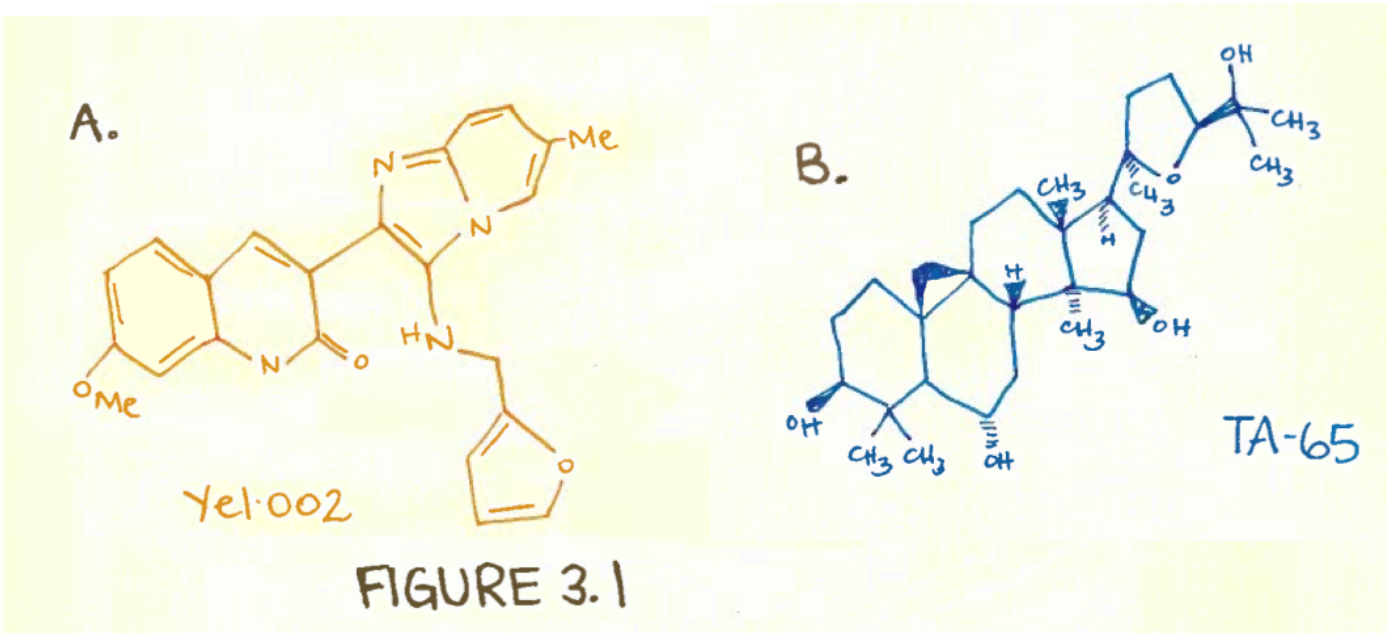

Figure 3.1: Chemical Structures of Yel-002 and TA-65

TA-65

The small molecule telomerase activator TA-65 (cycloastragenol) isolated from *astragalus membranaceus* was suggested to have protective effects against IR-induced DNA damage (**Figure 3.1B**). Telomerase, the enzyme that binds and extends DNA ends of chromosomes, TA-65 administration for up to twelve months lengthened critically short telomeres and remodeled proportions of circulating leukocytes in human subjects [80, 142]. Other studies using TA-65 showed this molecule reduced DNA damage associated with telomere shortening as well as protected against oxidative stress-induced DNA damage [13, 229]. Based on these data, Predrag Slijepcevic and Gordana Joksic (Brunel University, London, United Kingdom; Vinca Institute, Belgrade, Serbia) proposed that TA-65 may have protective effects against IR-induced DNA damage. They tested irradiated human lymphocytes treated with TA-65 in the micronucleus assay—a measure of chromosomal breakage induced in mitotic cells after metaphase [56]. Slijepcevic and Joksic's data suggest that TA-65 is radioprotective in human lymphocytes at both 1 Gy and 4 Gy [163]. Since CDDO-Me was able to protect human lymphocytes against IR-induced damage (refer to **Section 2.3**), I wanted to replicate their results with TA-65 as well as determine if TA-65 was a valid radioprotector in epithelial cells. Furthermore, since TA-65 seemed to act through alternative mechanisms from traditional radioprotectors, I sought to determine if TA-65 possessed any antioxidative properties.

3.2 Methods & Materials:

3.2.1 Cell Culture

Human lung - bronchial epithelial cells: HBECs were obtained from central lung bronchi and immortalized using ectopic expression of hTERT and cyclin-dependent kinase 4 (refer to **Section**

2.2.1) [171]. No experimentally transformed HBECs were used in these studies. HBEC 3KTs were cultured at 37ºC in 5% CO_2 in Keratinocyte Serum Free Media (KSFM) (Gibco) containing 50μg/mL of bovine pituitary extract and 5μg/mL of epidermal growth factor on porcine gelatin-coated tissue culture dishes (Sigma Aldrich).

Lung Nrf2 knockdown: Stable Nrf2 knockdown cells lines were established by infecting epithelial cells (HBEC 3KT) with a validated anti-Nrf2 shRNA expressing lentiviral vector (pGIPZ, OpenBiosystems V2LHS_238788) in the presence of 2 μg/mL Polybrene (Sigma).

Human breast - mammary epithelial cells: Human mammary epithelial cells (HME1) were immortalized by retroviral infection with hTERT and have a normal diploid karyotype (ATCC Cell Systems, Gaithsburg, MD). HMEC50 cells were originally derived from the noncancerous breast tissue of a female diagnosed with Li-Fraumeni syndrome (TP53 heterozygous) as previously described [198]. MCF-10A and MCF-12A (ATCC Cell Systems, provided by Reata Pharmaceuticals) were grown in Mammary Epithelial Cell Growth Media (Lonza). All mammary cells were cultured in serum-free conditions as previously described and were mycoplasma free and DNA fingerprinted [199].

Human cancer cell lines: Breast cancer cell lines SK-BR-3, MDA-MB-453, MCF-7, BT-474, BT-549, MDA-MB-231 were provided by Reata Pharmaceuticals (originally ordered from ATCC Cell Systems) and grown in Dulbecco's Modified Eagle Media (DMEM; Gibco) supplemented with 10% fetal bovine serum (Gibco) at 37ºC in 5% CO_2. The lung cancer line

NCI-H460 (Reata Pharmaceuticals) was used as a positive control and was grown using RPMI-1640 media (Gibco) supplemented with 10% fetal bovine serum (Gibco) at 37ºC in 5% CO_2. Non-small cell lung cancer (NSCLC) cells A549, H2009, HCC 2429, HCC 4017, H23, and HCC 15 were supplied by John Minna (Hamon Cancer Center, UT Southwestern Medical Center, Dallas, TX). All NSCLC cell lines were cultured in basal medium supplemented with 10% Cosmic Calf Serum (Thermo Scientific) at 37ºC in 5% CO_2. All cell lines used in the present studies were mycoplasma free (e-Myco kit, Boca Scientific) and DNA fingerprinted (PowerPlex 1.2, Promega). All cell lines used are commercially available through the ATCC Cell Systems (Gaithersburg, MD)

Human lymphocytes: Peripheral blood mononuclear cells (PBMCs) were isolated via centrifugation from the buffy coat of whole blood donated by healthy human volunteers via venipuncture. Informed consent was obtained from each donor in accordance with the Declaration of Helsinki and approved by the Institutional Review Board at UT Southwestern Medical Center (Dallas, TX). Cells were stimulated using 1ug/mL lectin, PHA-L (EMD Biosciences) and cultured in suspension of RPMI-1640 media (Gibco) supplemented with 10% Cosmic Calf Serum (Thermo Scientific) at 37ºC in 5% CO_2.

3.2.2 Drug Treatment and Radiation

RTA-408 (Reata Pharmaceuticals, Irving, TX) was dissolved in DMSO. Subconfluent cell cultures were treated with 50 or 150 nM RTA-408. Yel-002 (Robert Schiestl, University of California Los Angeles) was dissolved in 70% ethanol and used at final concentrations of 50 nM and 100 nM. TA-65 was dissolved in DMSO and used at concentrations of 10 nM, 100 nM, and

1 μM. Experimental concentrations of Yel-005 and TA-65 were determined based on cell toxicity for different cell types (**Figure 3.2A-B**) and used at the lowest effective dose. Drug was administered 18 hours prior to γ exposure (^{137}Cs source at 243.08 cGy/min, dosimetry provided by physicists in the Department of Radiation Oncology; University of Texas Southwestern Medical Center). Control experiments were treated with solvent only.

3.2.3 Experimental Assays

ARE-Luciferase Reporter: Cells were co-transfected with pGL4.37 [*luc2*/ARE/hygro], and pGL4.73 [*hRluc*/SV40] as a transfection expression control using 3:1 FuGENE HD according to the manufacturer's instructions (Promega). Briefly, cells were treated with drug 18 hours after luciferase transfection, and luciferase activity was measured using Dual-Glo Luciferase Assay (Promega) after another 18 hours. Each ARE-firefly luciferase value was normalized against Renilla luciferase.

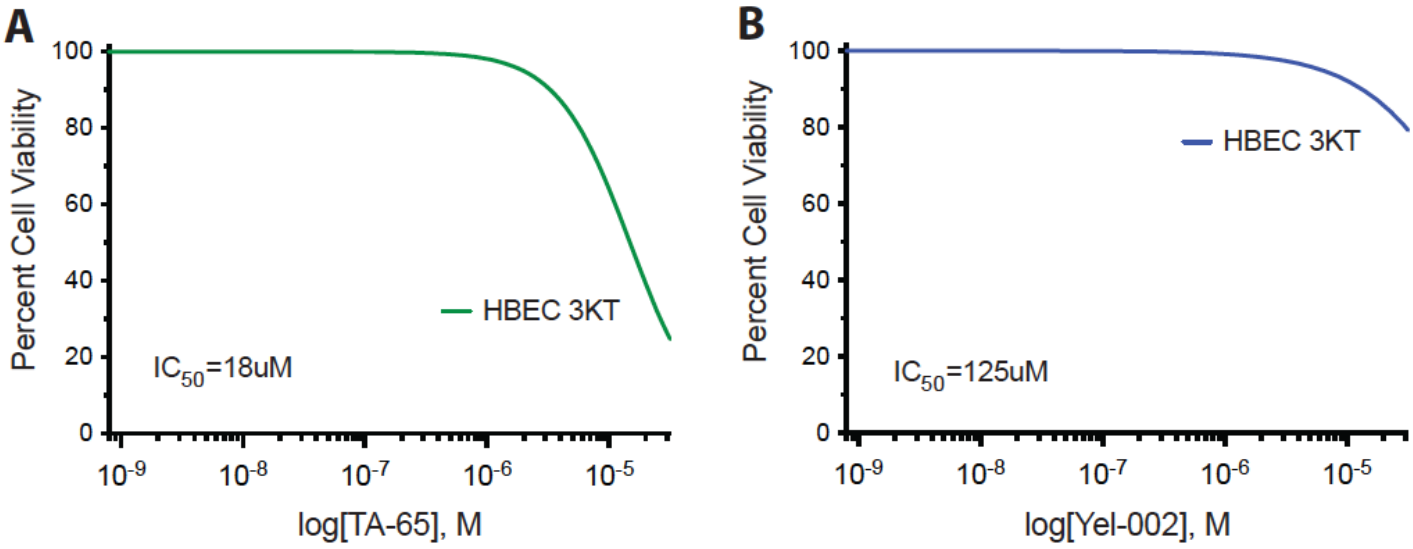

Figure 3.2

Figure 3.2: Toxicity of TA-65 and Yel-002 on HBECs.

Cell Titer Glo toxicity curves of HBEC 3KT with (A) TA-65 and (B) Yel-002, respectively. Cells were treated with drug and after 48-60 hours, percentage of living cells measured using Cell Titer Glo assay and normalized to untreated cells. In lung epithelial cells, TA-65 has an average LD_{50} of 18μM, and Yel-002 LD_{50} of 125μM. Values are based off two experiments of six replicates.

Colony Formation Assay: Immediately following IR exposure, cells were trypsinized and seeded in triplicate in 10-cm dishes at clonogenic density (ranging from 100-1000 cells per dish) for colony formation assays. Ten days later, dishes were stained with a mixture of 6.0% glutaraldehyde and 0.5% crystal violet, and colonies (defined as clusters of >50 cells) were counted. Cell survival measurements were fitted using a linear quadratic equation [$SF = \exp(-\alpha D - \beta D^2)$] (SF: surviving fraction; D: radiation dose in Gy) using GraphPad Prism, and dose-modifying factors (DMF) calculated for each as a measure of radioprotection as described [158]. DMF less than 1.2 was considered the cutoff for significant protection.

Comet Assay: Alkaline comet assay (Trevigen) to detect DNA damage at 30 minutes post-IR was performed according to manufacturer's instructions. Twenty fields (200x magnification) were scanned continuously under a fluorescence microscope. Approximately 50 cells per condition were analyzed using OpenComet software [73]. Tail moment [tail length x tail DNA %] and tail DNA % values generated by OpenComet were analyzed as a measure of DNA damage.

Western Blot Analysis: Cells were lysed in Laemmli SDS reducing buffer [50 mM Tris-HCl (pH 6.8), 2% SDS, and 10% glycerol], boiled, and separated by SDS/PAGE. The following antibodies were used: anti- HO1, -PRX1, -NQO1, -GST1 (1:1000; AbCam), anti- Nrf2 (1:500 Santa Cruz; 1:1000 Cell Signaling), anti-phospho-Nrf2 (1:5000; AbCam), and anti–β-actin (1:20,000; Sigma).

Viability Assay: CDDO-Me or DMSO was added to cells at 60% confluency, and cell viability was determined 48-60 hours later with CellTiter-Glo (Promega) as per manufacturer's protocols. Reported median lethal concentration (LC_{50}) values are based on the average of two experiments with 6 replicates and calculated from dose-response curves generated with nonlinear regression in GraphPad Prism 6 (GraphPad Software, Inc).

3.2.4 Statistical Methods

All significance values are $p<0.05$, unless otherwise stated, and were calculated using two-sided t-tests between the treatment group and its appropriate control.

3.3 Results

3.3.1 RTA-408 protects some, but not all, breast cancer cell lines.

To determine if RTA-408 has radioprotective effects in human breast cancer cells, clonogenic survival assays were performed to determine protection after irradiation. Based on the characterizations of Nrf2 inducibility performed by Reata, cell lines were grouped into two "profiles;" Profile 1 exhibited linear induction of NQO1 levels with increasing doses of RTA-408, whereas induction of NQO1 levels in Profile 2 cells seemed to plateau (**Table 3.1**). RTA-408 50nM significantly protected SK-BR-3 and MCF-7 (DMF=1.37; DMF=1.47) (**Figure 3.3A-B**). However, RTA-408 was not a significant radioprotector in BT-549 or MDA-MB-231 (**Figure 3.3C**). In normal breast epithelial cells, RTA-408 was only protective for MCF-10A (DMF=1.24), whereas MCF-12A was unprotected by similar doses of RTA-408 (**Figure 3.3D**). RTA-408 did not protect the constitutively active NSCLC cell line NCI-H460 against radiation (**Figure 3.3D**). Some experiments compared RTA-408 side by side with CDDO-Me (RTA-402),

showing that both compounds have seemingly similar patterns of protection (**Figure 3.3C-D**). Furthermore, based on the induction profiles summarized in **Table 3.1**, the cell lines protected by RTA-408 did not follow a specific pattern of Nrf2 induction.

Table 3.1

Cell Line	P_{ef}	SF_3	NQO1 induction (Profile)
MCF-10A	0.89	0.545	✔
MCF-12A	0.33	0.879	✔
HME1	0.60	0.518	✔
HMEC 50	0.55	0.512	✔
SK-BR-3	0.02	0.484	✔ (1)
MDA-MB-453	0.19		✔ (1)
BT-474	0.19		✔ (1)
MCF-7	0.22	0.361	2
BT-549	0.52	0.388	2
MDA-MB-231	0.15	0.254	2
NCI-H460*	0.05	0.241	**Constitutive Nrf2**

Table 3.1: Panel of breast cancer cell radiosensitivity and NQO1 induciblity profiles. A summary of the cell lines used in the present study. NCI-H460 is a constitutively expressing Nrf2 lung cancer cell line (Keap1 mutant) used as a positive control. Plating efficiency (P_{ef}); surviving fraction of cells at 3 Gy (SF_2) is used as a metric of radio-sensitivity. NQO1 inducibility data is summarized from qPCR experiments conducted by Reata Pharmaceuticals. Breast cancer lines have higher basal NQO1 levels compared to normal breast lines. Normal breast cells have low basal Nrf2 activity with strong induction of NQO1. Profile 1 cells (SK-BR-3, MDA-MB-453, BT-474) have a robust increase in NQO1 mRNA when treated with RTA-408 or other AIMs. Profile 2 cells (MCF-7, BT-549) have higher basal activity, so treatment with RTA-408 results in a plateau and there is no further induction of NQO1.

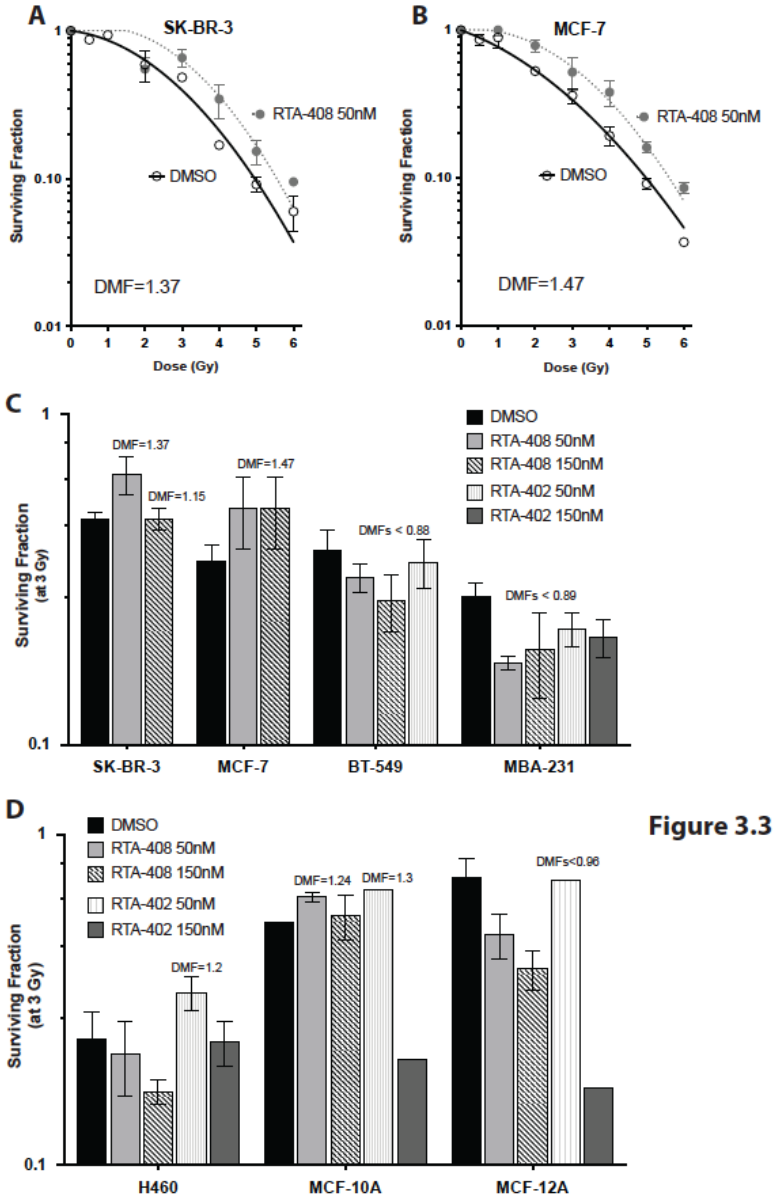

Figure 3.3

Figure 3.3: RTA-408 protects some, but not all, breast cell lines.

Clonogenic survival assays of (A) SK-BR-3 and (B) MCF-7 are radioprotected when pretreated with RTA-408. Clonogenic survivals, mean ± SEM with linear-quadratic fit curve of three experiments seeded in triplicate. (C) RTA-408 does not protect the cancer lines BT-549 or MD-MBA-231 after 3 Gy γ exposure, even at increased drug concentrations. (D) RTA-408 does not protect all normal breast epithelial cell lines. MCF-10A is protected, whereas MCF-12A is not. Radioprotection in (C, D) was compared to RTA-402 (also known as CDDO-Me, see **Chapter 2**). Cells were treated with drug 18 hours before 3 Gy γ exposure, then seeded immediately into clonogenicity. Colonies grown for ~14 days before fixation with 6% glutaraldehyde/0.5% crystal violet stain. Mean ± SEM of four experiments seeded in triplicate.

3.3.2 Yel-002 is not an effective mitigator or radioprotective countermeasure in HBECs.

To determine Yel-002's radioprotective effects, HBEC 3KTs were treated with either 50 or 100nM Yel-002 at various times prior to and after exposure to IR. Yel-002 did not protect cells against radiation when applied four hours after exposure (+4) (**Figure 3.4A**). Furthermore, Yel-002 did not provide significant protection when given at 18 hours prior to IR (DMF=1.05), and neither dose was sufficient at both one and four hours after irradiation (**Figure 3.4B**). This indicates that Yel-002 is an insufficient mitigator and countermeasure for HBECs, indicating that the reported radioprotection by others is likely to be cell and tissue dependent.

3.3.3 TA-65 activates the Nrf2 pathway in HBEC, but not lymphocytes.

Since TA-65 is not a traditional AIM, I wanted to determine if TA-65 was able to activate Nrf2/ARE in the cells already tested with other AIMS. HBEC 3KT (Lung-3) and human lymphocytes were first transfected with the ARE-luciferase reporter and then treated with TA-65 or DMSO. After 18 hours, TA-65 100nM and 1μM significantly increased luciferase expression in lung HBECs ($p<0.05$, paired t-test compared to DMSO control) (**Figure 3.5A**). The induction of Nrf2/ARE thus appears to be dependent on Nrf2 activity, since there was significantly decreased induction of ARE-luciferase in HBEC 3KT with Nrf2 knockdown compared to controls ($p<0.01$, paired t-test compared to non-silencing control) (**Figure 3.5B**). However, TA-65 did not significantly increase ARE-luciferase expression in peripheral blood lymphocytes (**Figure 3.5C**). Additionally, protein lysates collected at various times after TA65 100nM treatment of human lymphocytes showed no increases in Nrf2/ARE downstream targets, including NQO1, HO1, glutathione S-transferase (GST1), Nrf2, and phospho-Nrf2 (**Figure 3.5B**).

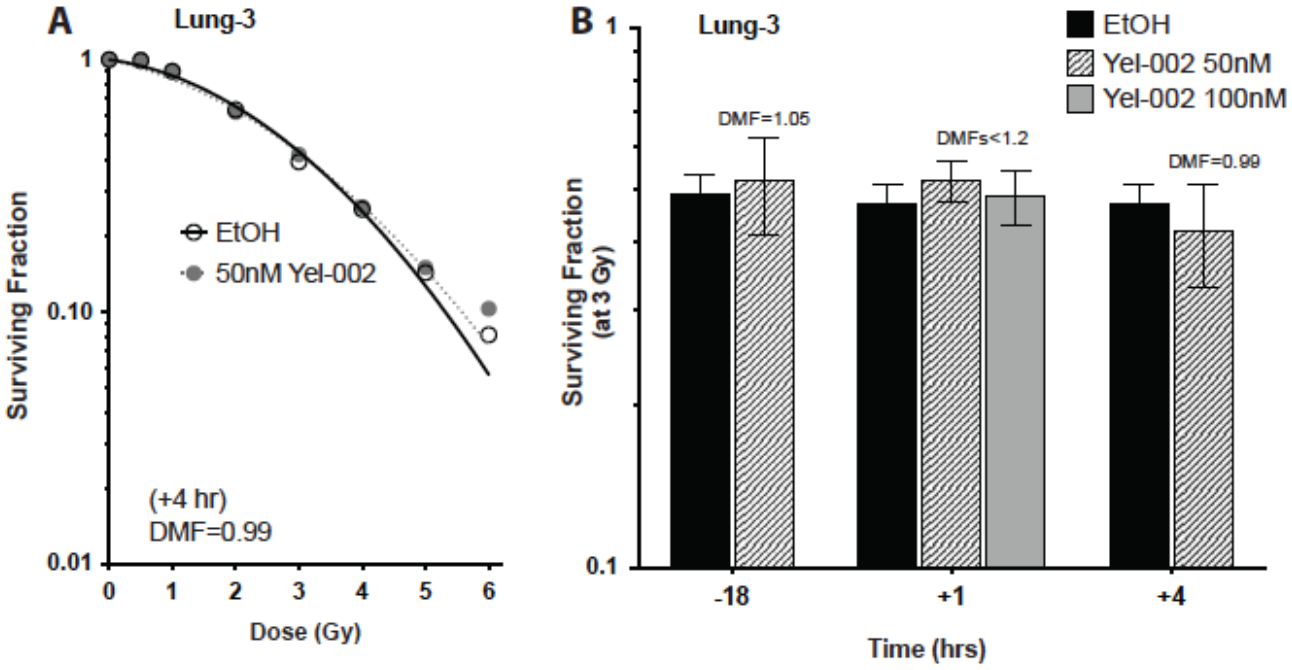

Figure 3.4

Figure 3.4: Yel-002 is an ineffective radiation mitigator and countermeasure in HBECs. (A) Clonogenic survival for HBEC 3KT treated with Yel-002 50nM four hours after IR exposure. (B) Yel-002 applied 18 hours prior to IR (-18), one hour after (+1), and four hours after (+4) is not protective of HBECs after 3 Gy γ exposure. Mean ± SEM of three experiments seeded in triplicate.

3.3.4 TA-65 is not an effective radioprotective countermeasure in HBECs.

To determine if TA-65 is a radioprotector, HBEC 3KTs were treated with either 100nM or 1μM TA-65 at various times (-18, +1). TA-65 does not protect lung epithelial cells against radiation when applied as a countermeasure 18 hours prior to γ exposure, nor is it effective as a mitigator when applied one hour after IR (**Figure 3.6A**).

3.3.5 TA-65 does not prevent IR-induced DNA damage in lymphocytes.

Alkaline comet assays were performed human lymphocytes thirty minutes after radiation to determine if TA-65 protected against IR-induced DNA damage. Since many of the adverse effects of radiation occur in the blood, PBMCs were assessed to determine if TA-65 also rescued human lymphocytes against IR-induced DNA damage. I found that pre-treatment with TA-65 does not significantly protect PBMCs against radiation-induced DNA damage, although radiation significantly increases tail moments using the alkaline comet assay in PBMCs (**Figure 3.6B**).

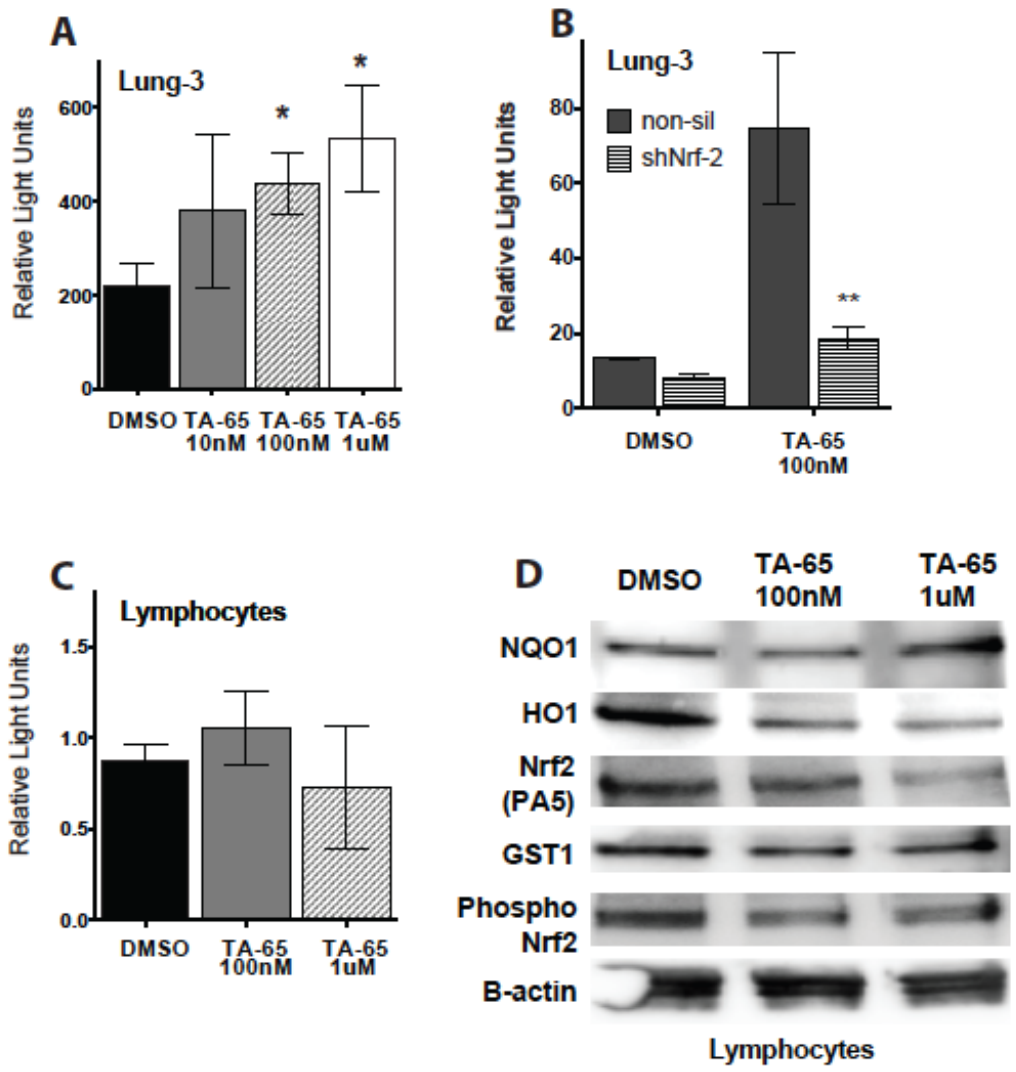

Figure 3.5

Figure 3.5: Pre-treatment with TA-65 activates Nrf2/ARE in HBECs, but not lymphocytes. (A) TA-65 increases expression of ARE-driven luciferase 18 hours after drug treatment in HBEC 3KT. Firefly ARE-luciferase normalized to renilla control (RLU). Mean ± SEM of 6 replicates, *p<0.05 using paired t-test (between DMSO and drug). (C) TA-65 does not affect expression of ARE-driven luciferase 18 hours after drug treatment in PBMCs. Firefly ARE-luciferase normalized to renilla control (RLU). Mean ± SEM of six replicates. (D) Protein levels of NADPH dehydrogenase quinone (NQO1, band observed at ~30kDa), heme oxygenase-1 (HO1, band observed at ~32kDa), total Nrf2 (bands observed at ~68, 75kDa), glutathione S-transferase (GST1, band observed at ~28kDa), and phosphor-Nrf2 (band observed at ~120kDa) after treatment with 100nM and 1μM TA-65 in PBMCs.

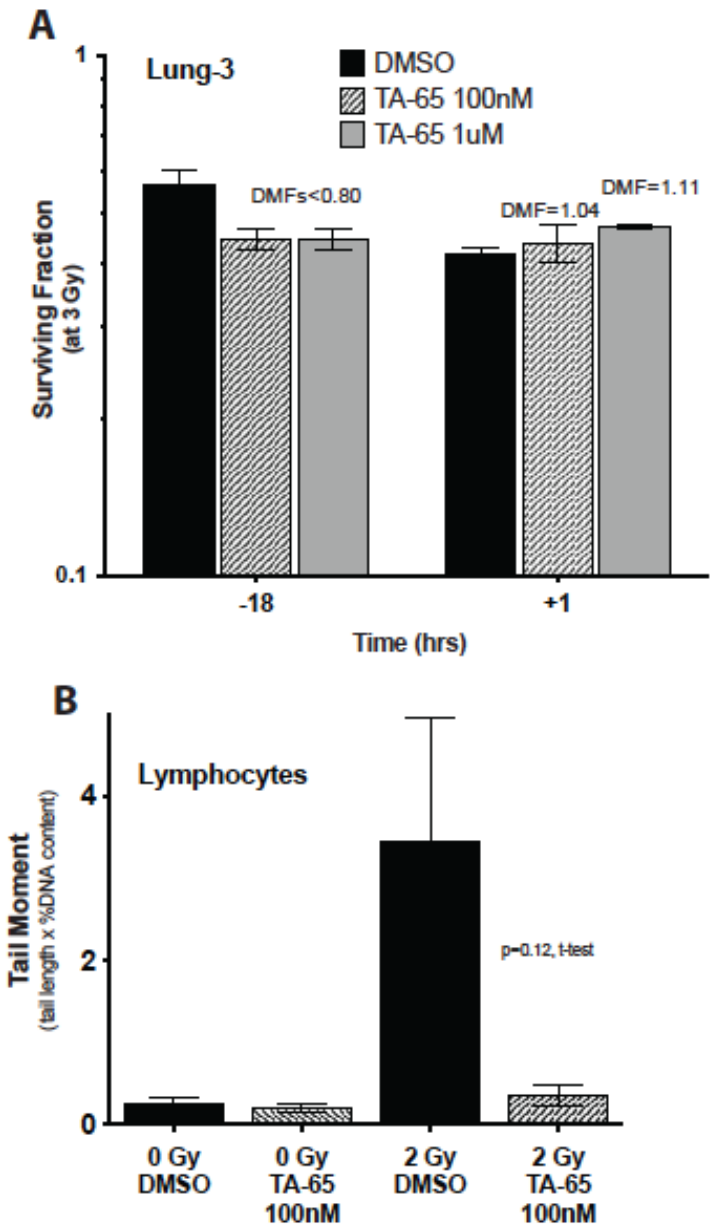

Figure 3.6

Figure 3.6: Pre-treatment with TA-65 does not protect HBECS or decrease IR-induced DNA damage in lymphocytes.

(A) Clonogenic survival for HBEC 3KT treated with TA-65 at 18 hours prior to IR (-18) or one hour after (+1) 3 Gy γ exposure. Mean ± SEM of three experiments seeded in triplicate. (B) PBMCs were treated with TA-65 18 hours prior to IR, then mounted on slides 30 min post-IR. Data analyzed and calculated using Open Comet software [tail moment = tail length x tail DNA percentage]. Mean ± SEM of >50 cells per condition, (ns compared to 2 Gy DMSO).

Discussion of Alternative Radioprotectors

The three compounds RTA-408, Yel-002, and TA-65 were predicted to protect normal epithelial cells, but the present data do not support the utility of these drugs as radioprotectors compared to CDDO-Me.

While RTA-408 is a potent AIM, it is also able to protect some cancerous cell lines. This protection is independent of basal Nrf2 pathway induction profiles, as cells from both profiles were protected by RTA-408 (**Table 3.1, Figure 3.3**). In contrast, two other cancer cell lines were unprotected by this compound, and therefore it is important to determine what differences allow for protection by RTA-408. Another unexpected result is that RTA-408 did not protect all normal breast cells. Since RTA-408 protection did not depend on Nrf2 activation state of the cells, these contradictory data will make RTA-408 difficult to implement as a radioprotector, given its tumor-protective effects.

While Yel-002 held promise, current studies were unable to demonstrate any radioprotection in the lung; Yel-002 was also an ineffective mitigator in colonic epithelial cells (personal communications with Sang Bum Kim, UT Southwestern Medical Center, Dallas, TX). Studies showing Yel-002 protected against DNA DSBs in thyroid cell cultures used radioisotopes of iodine, which mainly emit β radiation through β decay of the nucleus; only about ten percent of its energy and dose is released as γ radiation [81]. Furthermore, initial studies by Schiestl and Rivina based the utility of Yel-002 on the DEL assay in yeast, which can only detect DNA deletions and chromosomal rearrangements larger than six kilobases [75]. However, indirect actions of IR, such as ROS generation and subsequent cellular injury, cause the majority of IR-induced damage (refer to **Figure 1.5**); the DEL assay may not be specific enough to detect smaller or subtler events.

In experiments with TA-65, Slijepcevic and Joksic used the micronuclei assay, which is not as sensitive to all types of damage caused by IR (oxidative damage, etc). Furthermore, different cell types may respond differently to IR, and since blood cells perform unique functions compared to epithelial lung cells, it is possible that PBMCs and HBECs will not see the same protection.

CHAPTER FOUR

ORGANOTYPIC CULTURE IN THREE DIMENSIONS PREVENTS RADIATION-INDUCED TRANSFORMATION

4.1 Introduction to 3D Culture

The diversity and range of radiation types are also a concern for United States National Aeronautics and Space Administration (NASA) and astronauts on long-term space missions. While exposure to damaging radiation on earth is limited due to the protective atmosphere and only low energy EM radiation, space radiation includes high-LET radiation fields; radiation-induced carcinogenesis is a primary limitation. Exposure to galactic cosmic radiation composed of high-energy protons and HZE nuclei as well as solar particle events (SPE) can occur unexpectedly and have the capacity to penetrate engineered shielding [38, 50]. Based on recommendations from the National Council of Radiation Protection and Measurement (NCRP), NASA limits astronauts' lifetime risk of radiation-induced death to a three percent increase [36]. Since there is clear evidence that exposure to radiation poses a significant risk of increased carcinogenesis, this study focuses on understanding lung cancer risk associated with radiation exposure.

Our ability to accurately assess cancer risks, especially in the lung, is limited by a lack of good *in vitro* models. Most prediction models of radiation-induced cancers are based on data from atomic bomb survivors and studies performed in mice or with cells cultured in monolayer (2D) culture. As the scientific community has matured since the inception of growing human cells in a laboratory almost seventy years ago, it has established that human cells grown on plastic dishes with artificial medium in the lab do not necessarily behave the same as they do

when tested in live organisms or whole tissues [193]. Extracellular matrix, mesenchymal cells such as fibroblasts, endothelial, smooth muscle cells, and other influences such as immune factors are all lost when cells are grown in 2D. However, cell growth, polarity and structural organization, signaling, and some stromal epithelial interactions can be modeled in three-dimensional (3D; also referred to as organotypic or "like an organ") culture models and is considered to be a more accurate model of the *in vivo* microenvironment [117].

In order to better simulate physiological architecture and lung organ function *ex vivo*, certain 3D culture models have been established using HBECs with interactions from stromal fibroblasts [11, 59, 62, 153]. When grown under differing 3D conditions, HBECs are able to differentiate into multiple airway cells types [44, 225, 240]. More recent studies have demonstrated that when HBECs are seeded on top of Matrigel®, overlaying lung fibroblasts, the HBECs form web-like aggregates that over a few day branch and bud (**Figure 4.1C**)—a structure resembling the saccular phase of lung development (refer to **Figure 1.3**) [93].

Since HBECs grown in 3D culture appear to be in a more differentiated state and form higher order structures that are more indicative of native lung physiology as compared to HBECs grown in 2D culture, I tested if these 3D cultured human cells may be a more accurate model for assessing the effects of radiation on cancer progression and transformation. I believe that that radiation risk assessments have been overestimating cancer progression and hypothesize that the effects of irradiation in 3D culture alters radiation-induced transformation or subsequent repair pathways differently when compared to radiation in standard 2D culture. I tested 3D culture models of radiation-induced carcinogenesis and predicted cell transformation assays would be more similar to animal models as compared to 2D *in vitro* culture models.

4.2 Methods & Materials

4.2.1 Cell Culture

Human lung bronchial cells: HBECs were obtained from central lung bronchi and immortalized using ectopic expression of hTERT and cyclin-dependent kinase 4 (refer to **Section 2.2.1**) [171]. The experimentally transformed HBEC used in the present study included overexpressing *KRas*^{V12} and *p53* knockdown via shRNA [188]. Immortalized HBEC 3KT+*KRas*^{v12}+sh*p53* were cultured at 37ºC in 5% CO_2 in KSFM (Gibco) containing 50 μg/mL of bovine pituitary extract and 5 μg/mL of epidermal growth factor on porcine gelatin-coated tissue culture dishes (Sigma Aldrich).

Primary lung fibroblasts: IMR90 cells, derived from normal lung tissues (ATCC) were cultured in basal media supplemented with 10% Cosmic Calf Serum (Thermo Scientific) at 37ºC in 5% CO_2 and 2% O_2.

Organotypic Culture: 3D cultures were performed as previously described [93, 117]. Briefly, a feeder layer of 250k IMR90 fibroblasts was seeded in a 24-well plate 48 hours prior to seeding HBECs. Growth factor-reduced, phenol-red free Matrigel® (BD Biosciences) was layered on top of the fibroblasts (undiluted, 170 μL/well) and allowed to solidify at 37ºC. 300k HBEC 3KT+*KRas*^{v12}+sh*p53* were seeded on top of the solidified Matrigel®, cultured in Air Liquid Interface (ALI) media [225]. Cultures were grown at 37ºC in 5% CO_2 for 5 days and supplemented with media changes containing 10% Matrigel® every other day (see **Figure 4.1C**). Within 12 hours after IR, 3D structures were dissociated from Matrigel® cultures using cell recovery solution (Corning), trypsinized, and cultured alongside 2D cultures until they formed a

true monolayer—within 3 population doublings (PD). All assays were performed on experimental cells after dissociating and passaging in 2D culture, no more than 10 PD after IR (unless otherwise specified). Full experimental design is illustrated in **Figure 4.1D**.

4.2.2 Radiation

Gamma (γ) radiation exposures used a ^{137}Cs source at 243.08 cGy/min (Department of Radiation Oncology, University of Texas Southwestern Medical Center). Charged particle radiation experiments (iron, proton) were performed at the NASA Space Radiation Laboratory (Upton, NY). Cultures were exposed to 0.25 Gy ^{56}Fe at 600 MeV/nucleon, or to 0.5, 1, or 2 Gy $^{+}$H at 150 MeV/nucleon.

4.2.3 Experimental Assays

Anchorage Independent Soft Agar Assay: For soft agar assays, 8,000 viable cells were suspended and plated in 0.33% Difco Noble agar (BD Biosciences) in KSFM in six replicates in 12-well plates, layered over a 0.5% agar base. The number of macroscopically visible colonies (0.5 mm) was counted up to 25 days later with imaging at 0.63× using the Zeiss Axiovert 100M and quantification using ImageJ. Each experiment was repeated 3-4 times, with cells seeded between 3-10 PD after IR.

Matrigel™ Invasion Assay: For Matrigel™ invasion assays, 8,000 viable cells were suspended in KSFM and seeded into the top chamber of 24-well invasion chambers (8-μm pore; BD Biosciences). KSFM supplemented with 5% Cosmic Calf Serum (Thermo Scientific) as a chemoattractant was used in the bottom chamber. Cells were allowed to migrate for 18 hours,

then processed per manufacturer's protocol. Hoechst 33342 (Sigma) was used to stain nuclei for imaging at 20× using the Zeiss Axiovert 200M and quantification using ImageJ. Each experiment was repeated 3 times, with cells seeded between 5-10 PD after IR.

Proliferation Assay: To determine growth curves, 4,000 cells were cultured in triplicate in 6-well plates, and then trypsinized and counted every two days using a TC20™ Automated Cell Counter (Bio-Rad). Cells were seeded within 3 PD after IR.

Live/Dead Cell Assay: To determine cell viability and cytotoxicity within 4 hours after IR (on undissociated, untrypsinized cells), cells were stained with 2μM calcein AM and 4μM EthD-1 using the Live/Dead® kit (Invitrogen) as per manufacturer's instructions.

Colony Formation Assay: Cells were seeded in triplicate in 10-cm dishes at clonogenic density (100 cells per dish) for colony formation assays. Ten days later, dishes were stained with a mixture of 6.0% glutaraldehyde and 0.5% crystal violet, and colonies (defined as clusters of >50 cells) were counted. Cells were seeded within 4 PD after IR.

4.2.4 Immunofluorescence Staining

For 3D immunofluorescence analysis of 3D Matrigel cultures, aggregated budding structures were washed, fixed with 4% paraformaldehyde, paraffin embedded, and sectioned as previously described [93]. Briefly, two percent agarose was poured directly into the wells containing fixed 3D structures, allowed to cool and solidify, and then the plugs containing the 3D HBEC structures were placed in histology cassettes in 10% normal buffered formalin and processed,

embedded, and 5μm thick sections were cut for immunofluorescence analysis. The sections were de-paraffinized through three different xylenes, rehydrated in a series of ethanol and washed in de-ionized water for 5 min. Following heat induced antigen retrieval, sections were blocked at RT with 10% goat serum albumin (Zymed) in PBS containing 1% bovine serum albumin (Sigma Aldrich) and 0.025% Triton X-100 (Sigma Aldrich) for 2 hours. Sections were rinsed with PBS and incubated with primary antibodies overnight at 4 ºC in a humidified chamber. Antibodies used were tested for immunofluorescence analysis of paraffin-embedded samples. The sections were incubated with Alexa Fluor 488 goat anti-rabbit (Invitrogen; A-11008) or Alexa Fluor 488 goat anti-mouse (Invitrogen; A-11001) at a dilution of 1:500 for an hour at RT in a dark humidified chamber. Sections were then washed three times with PBS and mounted with Vecta Shield mounting medium with DAPI (Vector Labs) cover-slipped, and imaged (Axiovert 200M fluorescence microscope). Each staining was performed on multiple sections in triplicates.

4.2.5 Gene Expression Analysis

Microarray: RNA from each experimental condition (of 2 Gy γ exposure), as well as undissociated 3D structures, was collected using an RNeasy Plus mini kit (Qiagen). Biotin labeled cDNA was prepared using Illumina TotalPrep kit (Ambion), and quality of total RNA and biotinylated cDNA checked using the Experion system (Biorad). HT12v4 Beadchip hybridization was performed following Illumina standard protocol (Ambion). Briefly, 750ng of biotin labeled cDNA was hybridized to the chip overnight at 58 ºC, followed by washing and staining. HT12v4 Beadchips were scanned on the Illumina HiScan scanner and data analyzed with Illumina Beadstudio software.

Quantitative Reverse Transcription PCR: RNA was extracted from 2D and dissociated 3D cultures using an RNeasy Plus kit (Qiagen) following the manufacturer's instructions. RNA was quantified using a Nanodrop, and 1 μg of total RNA was reverse transcribed with the iScript™ first-strand cDNA synthesis kit (BioRad) using an optimized combination of random hexamers and oligo-dT. Following cDNA synthesis, quantitative PCR was set up using SsoFast™ EvaGreen® supermix (Biorad) with optimized cycling conditions for LightCycler 480II (Roche).

Based on preliminary analysis of microarray data, the following genes were selected as being either up- or downregulated between 2D and 3D: Jun proto-oncogene (JUN), sirtuin 2 (SIRT2), Ras-related GTP binding protein (RAB6A), and CDC-like kinase 1 (CLK1), MYC, ADAM metallopeptidase with thrombospondin type 1 motif 6 (ADAMTS6), and BMI polycomb ring finger oncogene (BMI1). Housekeeping genes used were glucuronidase beta (GUSB), heat shock protein 90kDa alpha class B member 1 (HSP90AB1), and hypoxanthine phosphoribosyltransferase 1(HPRT1).

Primer (F=forward, R=reverse) sequences are as follows: JUN-F: TCCAAGTGCCGAAAAAGGAAG, JUN-R: CGAGTTCTGAGCTTTCAAGGT; SIRT2-F: CACGCAGAACATAGATACCCTG, SIRT2-R: CAGTGTGATGTGTAGAAGGTGC; RAB6A-F: CTTGGAGGATCGAACAGTACGA; RAB6A-R: AGCTAGGAATCAAGCTCCTGAA; CLK1-F: AGAGACCATGAAAGCCGGTAT, CLK1-R: CATGTGAACGACGATGTGAAGT; MYC-F: TCCCTCCACTCGGAAGGAC, MYC-R: CTGGTGCATTTTCGGTTGTTG; ADAMTS6-F: CCCTTCAACAACGACATCTGT, ADAMTS6-R: CCGTTCAATGCTCACTGATCT; BMI1-F: CGTGTATTGTTCGTTACCTGGA, BMI1-R: TTCAGTAGTGGTCTGGTCTTGT.

Housekeeping genes primers are: GUSB-F: CTCATTTGGAATTTTGCCGATT, GUSB-R: CCGAGTGAAGATCCCCTTTTTA; HPRT1-F: TGACACTGGCAAAACAATGCA, HPRT1-R: GGTCCTTTTCACCAGCAAGCT; HSP90AB1-F: CCAAAAAGCACCTGGAGATCA, HSP90AB1-R: TGTCGGCCTCAGCCTTCT.

4.2.6 Statistical Methods

All analyses were performed using R version 3.0.1 and Bioconductor version 2.13 [67, 215]. Data were screened for outliers using the lumi package, and processed using non-parametric background subtraction and median normalization using the MBCB package [48, 242]. Probes in which any sample had a detection p-value > 0.05 were eliminated, resulting in 14,754 probes (**Table 4.1**). The expression profile for the DNA damage response genes listed in Table 2 in Asaithamby, *et al* (2011) were compared in the unirradiated samples, and heatmaps were generated using pheatmap package with dendrograms using average clustering with Euclidean distance for both samples probes [10, 102] . Hierarchal clustering after normalization (**Figure 4.9A**) shows a drastically divergent expression profile for 3D samples collected in 3D, so they were excluded from further analysis.

After removing the 3D samples, the detection p-value was re-evaluated for the remaining twelve samples, and 16,442 probes ($p<0.05$) were used in all subsequent analysis (**Table 4.1**). Significant gene sets were determined between two groups using t-tests and Benjamini–Hochberg procedure to control the false discovery rate (FDR<0.05) implemented with the multitest package, with fold change calculated using samr [108, 167]. For each gene list, up- and down- regulated genes were analyzed separately using Qiagen's Ingenuity® Pathway Analysis (IPA®, QIAGEN Redwood City, www.qiagen.com/ingenuity). The 2D0 vs 3D0 and 2D2 vs 3D2

comparisons were re-analyzed using both limma and the more conservative eBayes statistic with fold change calculation as the difference of log-intensities (**Appendices A-B**) [207]. Overlapping genes were removed from each resulting significant genes list and imported into IPA with up- and down- regulated genes analyzed separately (**Table 4.1**). Complete lists of genes with significant expression changes, separated by analysis and comparison, can be found in the **Appendix** section.

Table 4.1

Analysis	Significant probes	Up-regulated	Down-regulated
2D0 v 3D0	2,301	1,813	488
2D2 v 3D2	603	267	336
2D0 v 2D2	831	682	149
3D0 v 3D2	3,357	2,857	500

	Significant probes w no overlap	Up-regulated	Down-regulated
Limma 2D0 v 3D0	533	291	242
Limma 2D2 v 3D2	857	513	344

Table 4.1: Number of probes with significant expression changes from each comparison.

4.3 Results

4.3.1 Cells irradiated in 3D form fewer and smaller colonies in soft agar compared to cells irradiated in 2D.

To determine the ability of cells to grow in an anchorage-independent manner, irradiated cells were seeded into the soft agar assay between 3 and 10 PDs after IR (**Figure 4.1D**). HBEC 3KT+*KRas*^{v12}+sh*p53* have a basal soft agar transformation frequency of approximately nine per 10,000 cells, regardless of their initial growth in 2D or 3D, as seen in the unirradiated controls for each group. When exposed to increasing doses of γ exposure, up to 2 Gy, there is a significant increase in the number of colonies of 2D-irradiated cells (t-test comparing 0 Gy to 2 Gy; $p<0.05$) (**Figure 4.2A**). However, 3D-irradiated cells formed significantly fewer colonies compared to their 2D-irradiated counterparts (t-test; *$p<0.05$, **$p<0.01$) (**Figure 4.2A**). Additionally, the size of these 3D colonies was smaller on average than 2D colonies (t-test; *$p<0.05$, **$p<0.01$) (**Figure 4.2B**). This pattern also held true with protons at 2 Gy at 150 MeV/n (t-test; *$p<0.05$) (**Figure 4.2C**), although colony sizes were not significantly different (**Figure 4.2D**). The most robust transformation event seen was in 2D with iron at 0.25 Gy at 600Mev/n, with cells forming significantly more colonies than unirradiated control cells (t-test comparing 0 Gy to 2 Gy; $p<0.001$) (**Figure 4.2E**). Consistent with the proton and γ exposure, cells exposed to iron while in 3D culture formed significantly fewer (t-test; ***$p<0.001$) (**Figure 4.2E**) and smaller (t-test; **$p<0.01$) (**Figure 4.2F**) colonies than 2D-irradiated cells, with their values matching those of the unirradiated control cells. The difference in the number and magnitude of these colonies can be visualized in **Figures 4.3C-F**. These results indicate that with a variety of radiation types, 3D culture reduces IR-induced increase in anchorage independent colony growth of HBEC 3KT+*KRas*^{v12}+sh*p53*.

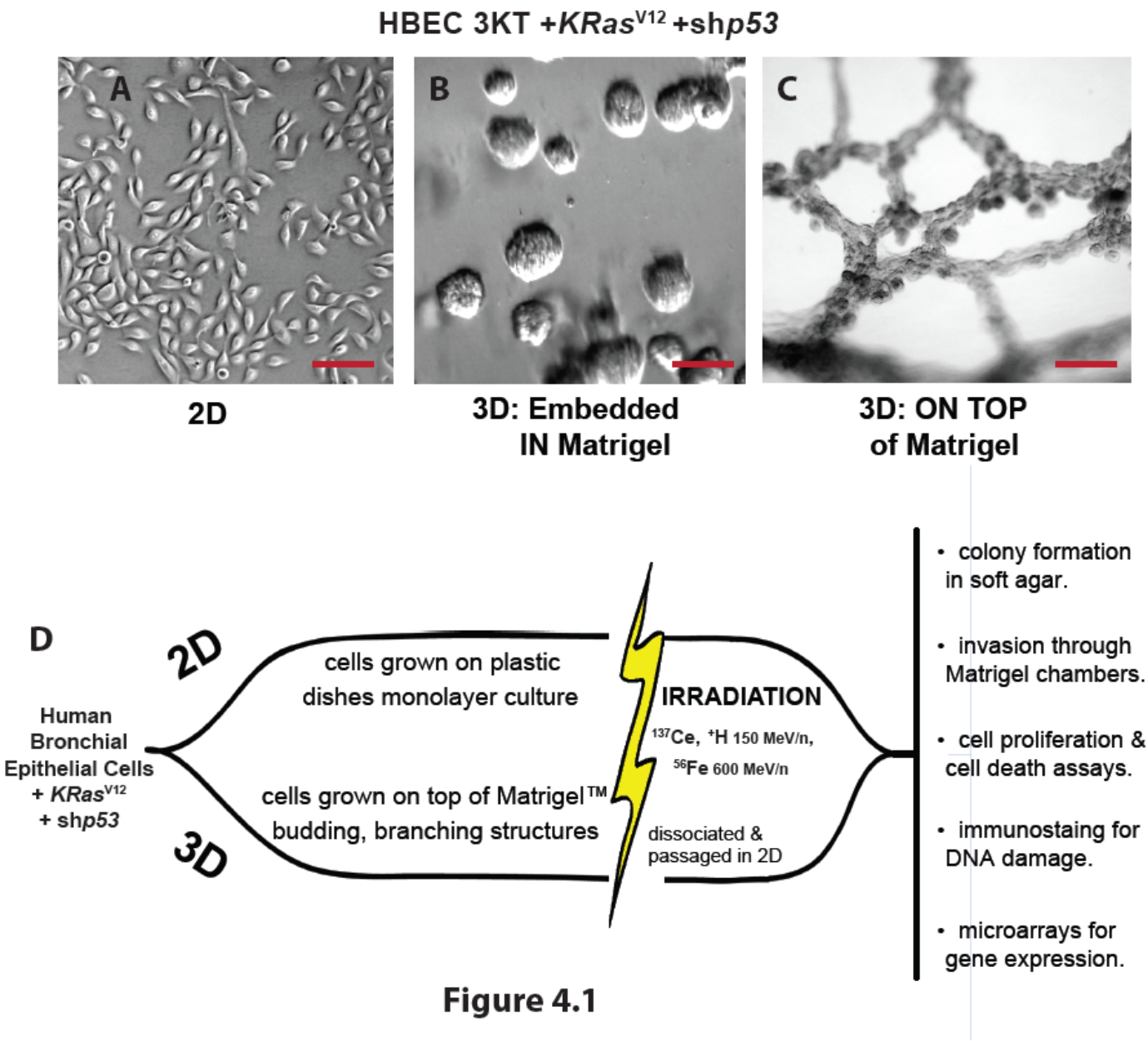

Figure 4.1: Timeline and design of experimental conditions.

HBEC 3KT+*KRas*^{v12}+sh*p53* cells grown in (A) 2D in KSFM (B) 3D embedded in a 90:10 Matrigel:ALI suspension with underlying fibroblast feeder layer (C) 3D on top of Matrigel® with underlying fibroblast feeder later. Scale bars represent (A) 100μm and (B, C) 50μm. (D) Schematic of experimental design. HBECs were grown either in 2D or 3D on top conditions. Once 3D cells formed branching structures (5 days), both culture conditions were exposed to different types of radiation. Different experimental endpoints are listed.

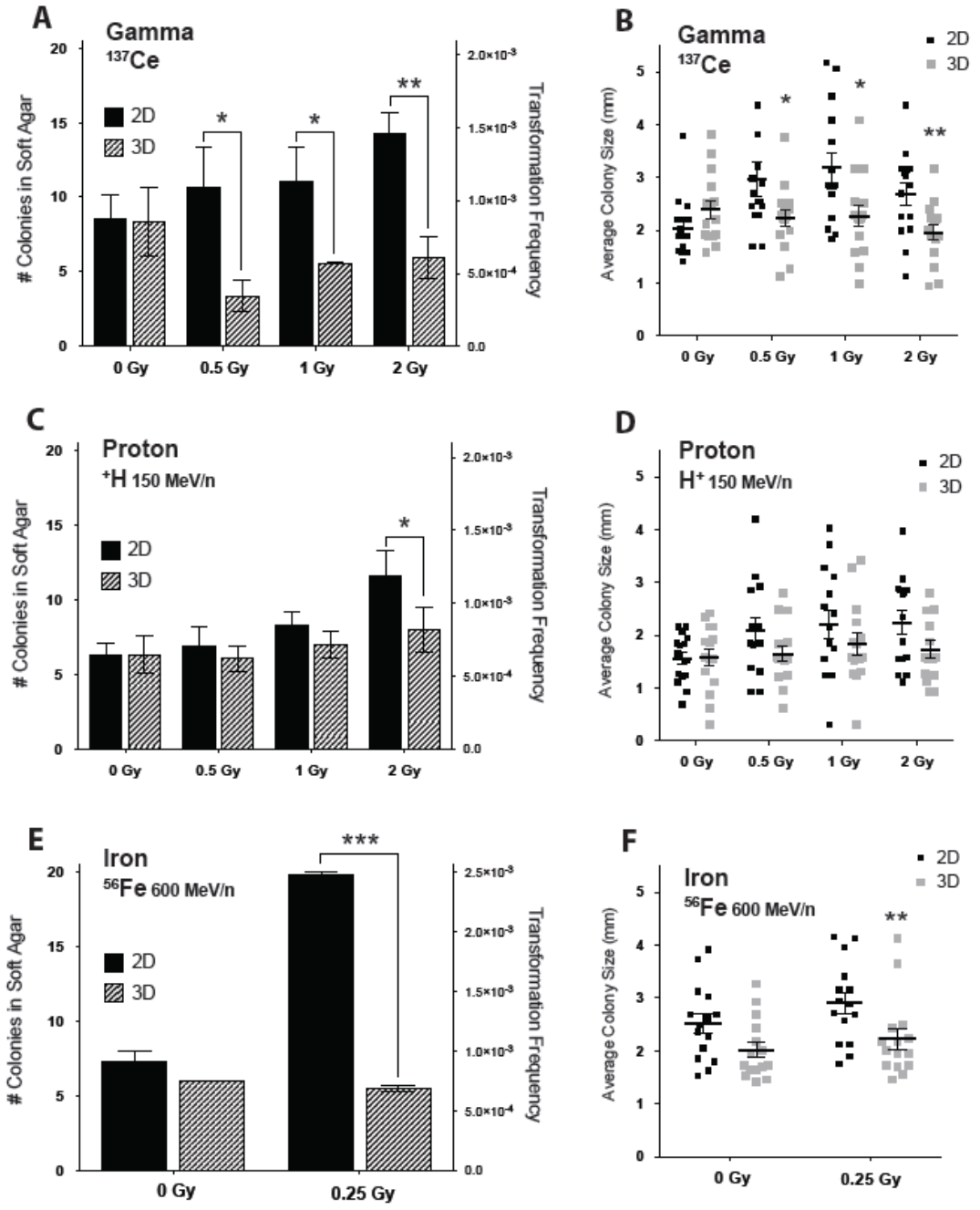

Figure 4.2

Figure 4.2: Number and size of soft agar colonies of cells within 10 PD after IR exposure. Anchorage independent colony growth after irradiation with (A, B) γ (C, D) proton, and (E, F) iron shows 3D-irradiated cells for fewer and smaller colonies than 2D-irradiated cells. Mean ± SEM, *p<0.05, **p<0.01, ***p<0.0001.

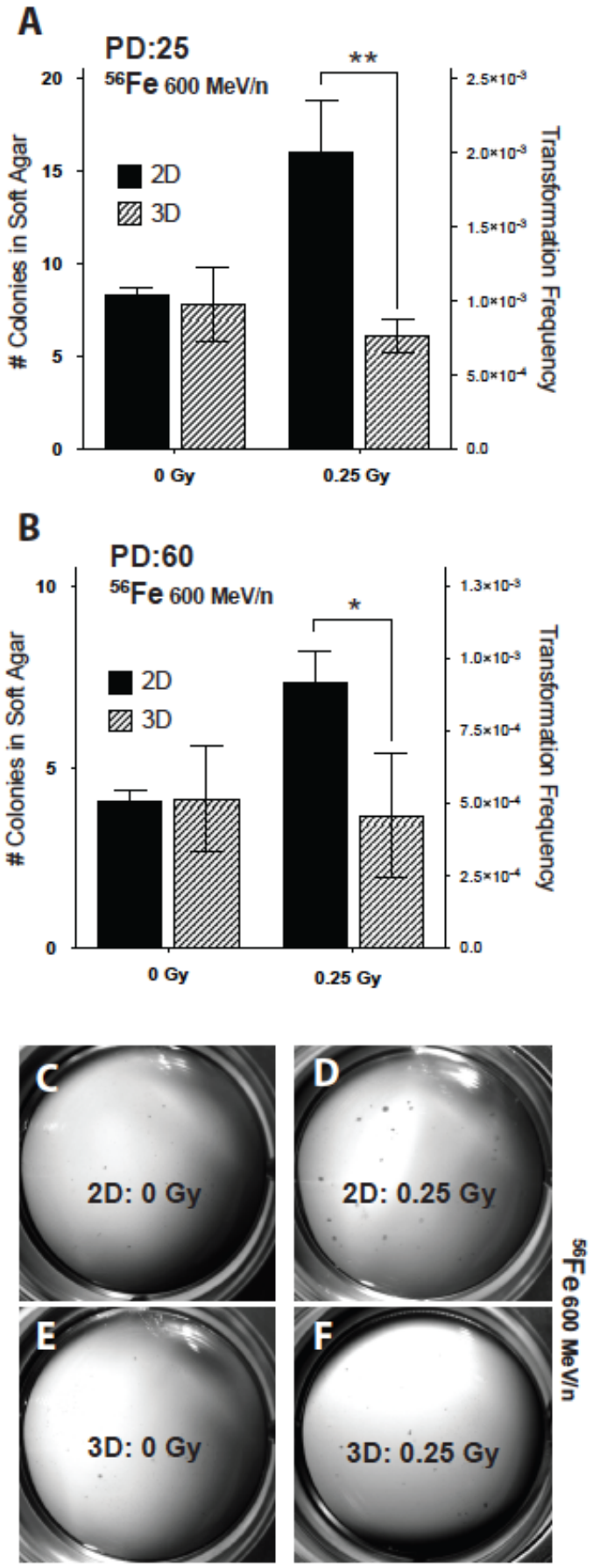

Figure 4.3: Soft agar colonies after long-term culture after ^{56}Fe exposure. Number of colonies after (A) 25 PDs, and (B) 60 PDs after IR shows that 3D-irradiated cells still have no increase in anchorage independent growth when compared to 2D-irradiated cells. Mean ± SEM, *p<0.05, **p<0.01. (C-F) Representative images of soft agar colonies. The colonies in panel (D) from 2D with 0.25 Gy are the largest and most numerous.

Figure 4.3

4.3.2 Protection from transformation by 3D culture persists up to 60 population doublings after exposure to heavy ions.

To determine the long-term effects of radiation and 3D culture on transformation, HBECs were propagated in culture for up to four months after iron irradiation. After a month, 3D-irradiated cells still show no signs of increased colony formation at 25 PDs (**Figure 4.3A**) or at 60 PDs (**Figure 4.3B**). While 2D-irradiated cells form significantly more colonies than 3D-irradiated cells, the magnitude of these differences diminishes with time (t-test; $^{**}p<0.01$, $^{*}p<0.05$) (**Figure 4.3A-B**). These data show that transformation occurs immediately after IR—there is no latent period where cells must undergo selection.

4.3.3 Transformation of 2D-irradiated cells is due neither to population differences, nor to proliferation/differentiation status.

In order to rule out assorted culture method artifacts, variations of 2D and 3D cultures were irradiated with 2 Gy γ then assayed in soft agar. To rule out that the transformation seen in 2D (**Figure 4.2A**) is simply due to a subset of more progressed cells within the population, four separate clonal populations of HBEC 3KT+*KRas*^{v12}+sh*p53* (provided by Claudia Schafer; Department of Cell Biology; University of Texas Southwestern Medical Center) were isolated and exposed to 2 Gy γ in 2D. Two of the four clones (#3, #4) formed significantly more colonies after IR (t-test; $^{*}p<0.05$) (**Figure 4.4A**). However, two clones did not have an statistically significant increase in anchorage independent growth after IR exposure (#17, #30), although there was a trend of increased colonies after IR. These two clones also seemed to have a higher unirradiated basal transformation frequency, indicating perhaps that IR did not have as significant of an effect on these cells (**Figure 4.4A**).

To ensure that the process of 3D culture itself did not eliminate a subset of cells which may have been primed to transform when grown in 3D, and that the dissociation/trypsinization process itself did not select out any population of potentially transformed cells, HBECs were grown on top of 3D Matrigel® culture (exactly like **Figure 4.1D**), and were only irradiated after being dissociated from 3D culture and re-forming a 2D monolayer (**Figure 4.1A**). These 3D to 2D cells transform at the same frequency as other 2D-irradiated cells (t-test; ***$p<0.001$) (**Figure 4.4B**), indicating that the conditions at the time of IR are what matter, and that HBECs can transition from 3D to 2D without losing their oncogenic potential—importantly, the process of growing cells in 3D culture does not select against or kill off certain cell types that may be more transformed within the population.

Cells grown in 2D in KSFM grow in a log-phase fashion, with a majority of the cells in an active stage of the cell cycle, whereas cells in 3D are mostly differentiated with downregulated replicative activity due to certain growth factors in the ALI media—only approximately twenty percent of cells in the culture (located in the buds) actively divide. To assure that neither media nor confluency of cells at the time of IR has an effect on transformation, 2D cells were grown in ALI media to full confluency, then irradiated (**Figure 4.4D**). These cells still exhibited increased colony formation in soft agar after IR (t-test; *$p<0.05$) (**Figure 4.4E**), indicating that neither the differentiation media used for 3D culture, nor the confluency of the cells was responsible for the 3D transformation effect.

There are multiple methods of growing HBECs in 3D culture, and depending on the specific conditions, the cells will form different types of 3D structures (ie branching/budding webs when grown on top of Matrigel vs. cysts when embedded in Matrigel) (**Figure 4.1B-C**). To show that the 3D environment as a whole, with differentiated structures, can be protected,

HBECs embedded in a 90:10 Matrigel®:ALI suspension on top of a fibroblast feeder layer were irradiated (**Figure 4.4F**). This alternate version of 3D culture still prevented the increase in radiation-induced anchorage independent growth at 2 Gy (t-test; no difference between unirradiated and 2 Gy) (**Figure 4.4G**). This pattern of protection followed the same trend at 0.5 Gy and 1 Gy for cells on top of Matrigel (data not shown). Furthermore, to show that the entire 3D culture environment is crucial, HBECs were grown on top of 3D Matrigel® without using an underlying fibroblast feeder layer. Although the Matrigel® and media are sufficient to induce the web-like organization of HBECs, the cells do not form more complex 3D structures over time, with a decrease in extensive branching and budding. Although when irradiated under these conditions there is no significant increase in colony formation, there is a trend of increased colony growth after 2 Gy of γ exposure (**Figure 4.4C**), indicating that each of the 3D culture conditions (media, Matrigel®, fibroblast feeder layer, etc) may synergize when combined to provide the optimal conditions and signaling for the 3D environmental protection against IR.

4.3.4 3D-irradiated cells are less invasive than 2D-irradiated cells.

To assess the ability of cells to invade through a layer of Matrigel™ basement membrane matrix, γ and iron irradiated HBEC 3KT+*KRas*^{v12}+sh*p53* were placed in Matrigel™ invasion chambers. 3D cells exposed to γ had significantly fewer invading cells than 2D-irradiated cells (t-test; *$p<0.05$) (**Figure 4.5A**). Iron-irradiated 3D cells showed the same pattern of decreased invasion (t-test; **$p<0.01$) (**Figure 4.5B**). These results show that cells irradiated under 3D conditions have reduced invasive properties compared to cells irradiated in 2D culture.

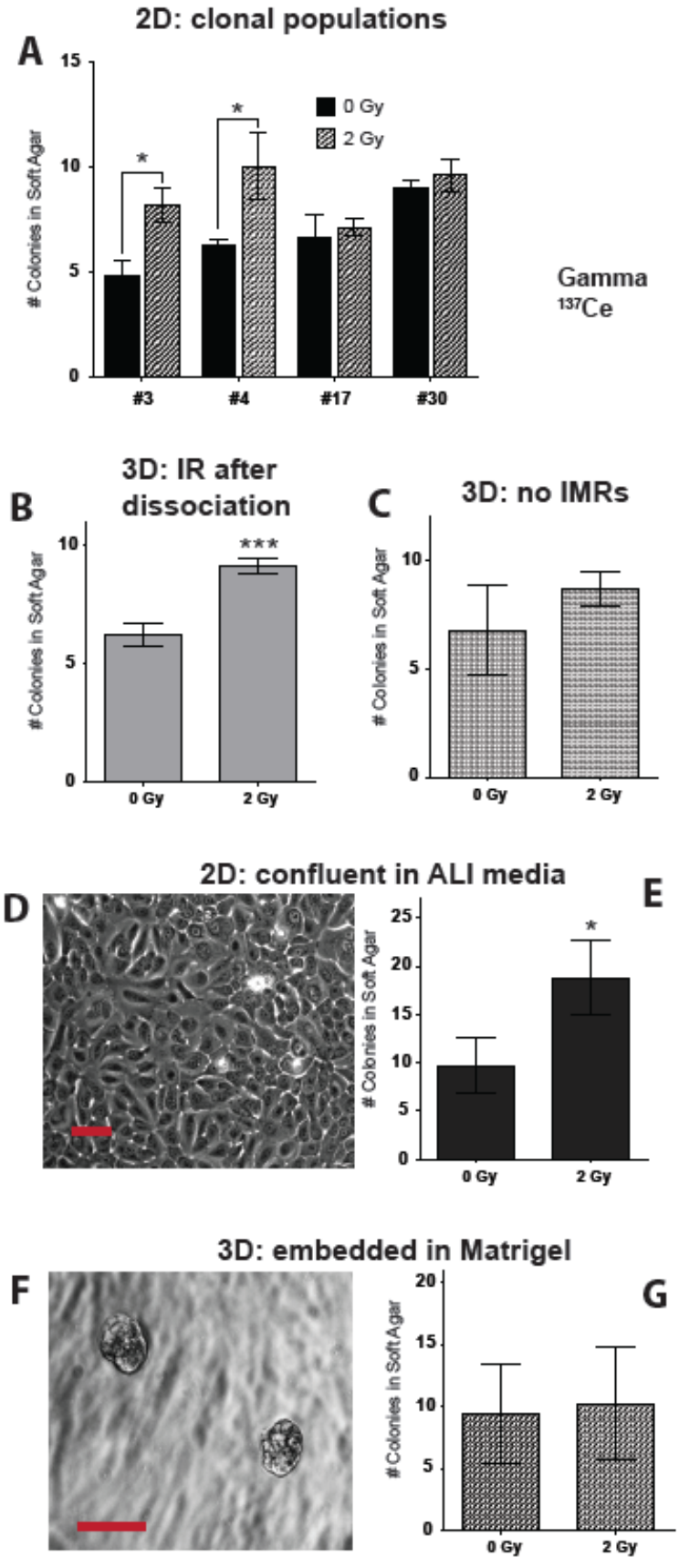

Figure 4.4: Alternative and intermediate culture conditions recapitulate soft agar phenotype. Various permutations of 2D and 3D cultures were irradiated with 2 Gy of γ. (A) Four different clonal populations of HBEC 3KT+*KRas*^{v12}+sh*p53* were exposed to 2 Gy of γ. Mean ± SEM, *p<0.05. (B) HBECs were grown on top of 3D Matrigel® culture (exactly like Figure 1C), and were only irradiated AFTER being dissociated from 3D culture and forming a 2D monolayer again. Mean ± SEM, *p<0.05. (C) HBECs were grown on top of 3D Matrigel® WITHOUT using any fibroblast feeder layer. (D) HBECs were grown to confluency in the same ALI media used for 3D culture, then irradiated. Scale bar represents 50μm. (E) These cells still had increased growth in soft agar after IR. Mean ± SEM, *p<0.05. (F) HBECs were embedded in a 90:10 Matrigel®:ALI suspension on top of a fibroblast feeder layer. Scale bar represents 50μm. (G) This alternate version of 3D culture still prevents the increase in radiation-induced anchorage independent growth. Mean ± SEM.

Figure 4.4

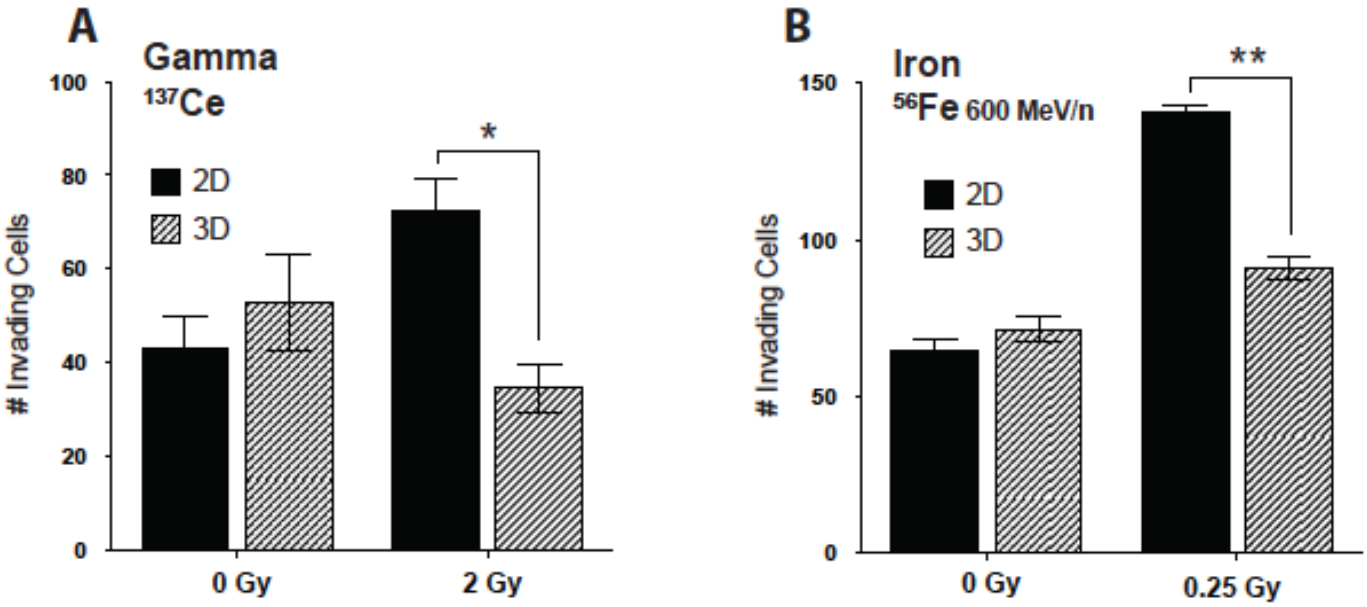

Figure 4.5

Figure 4.5: Invasion through Matrigel™ chambers within 10 PD after IR exposure.

The average number of invading cells per field after irradiation with (A) 2 Gy γ or (B) 0.25 Gy iron (600 MeV/n). Only 2D-irradiated cells have increased numbers of invading cells. Mean ± SEM, *p<0.05, **p<0.01.

4.3.5 Culture conditions do not affect proliferation rates or cell death after IR exposure.

Cells exposed to all three types of IR showed similar growth curves within 3 PDs after IR, regardless of culture conditions (**Figure 4.6A-C**). Additionally, there was no difference in the ability of cells to survive after either γ or iron exposure in the colony formation assay, regardless of culture conditions (**Figure 4.7**). Finally, cells do not show increased numbers of dead cells 90 minutes after IR in either 2D or 3D conditions (**Figure 4.8**). This indicates that cells in both culture conditions grow at similar rates, even after IR, and so the fact that 2D-irradiated cells are more transformed is not a result of differences in irradiated populations from selective killing, nor is it due to faster growth rates.

4.3.6 Cells in 2D and 3D upregulate different pathways after IR.

Irradiated cells from both 2D and 3D conditions were analysed for transcriptional differences. Cluster dendrogram using all gene probes shows a large separation between cells in 3D ("3D") and all 2D grown cells (including 3D cultures after dissociation, notated with either 0 or 2 for radiation doses) (**Figure 4.9A**). This indicates that cells undergo many transcriptional changes within 3 doublings after dissociation from 3D cultures, with expression patterns more similar to cells in 2D. This culture difference influences cell expression more than radiation. The disparity between 3D cells in 3D and 3D cells after dissociation is also demonstrated with the heat map in **Figure 4.9B**. Other groups have described decreases in DNA repair pathways and slower repair kinetics after IR in 3D culture [10]. Our experimental data shows a similar trend of downregulated DNA repair genes in 3D when compared to either 2D or 3D dissociated cultures, using the same list of genes reported by Asaithamby, *et al* (**Figure 4.9B**) [10].

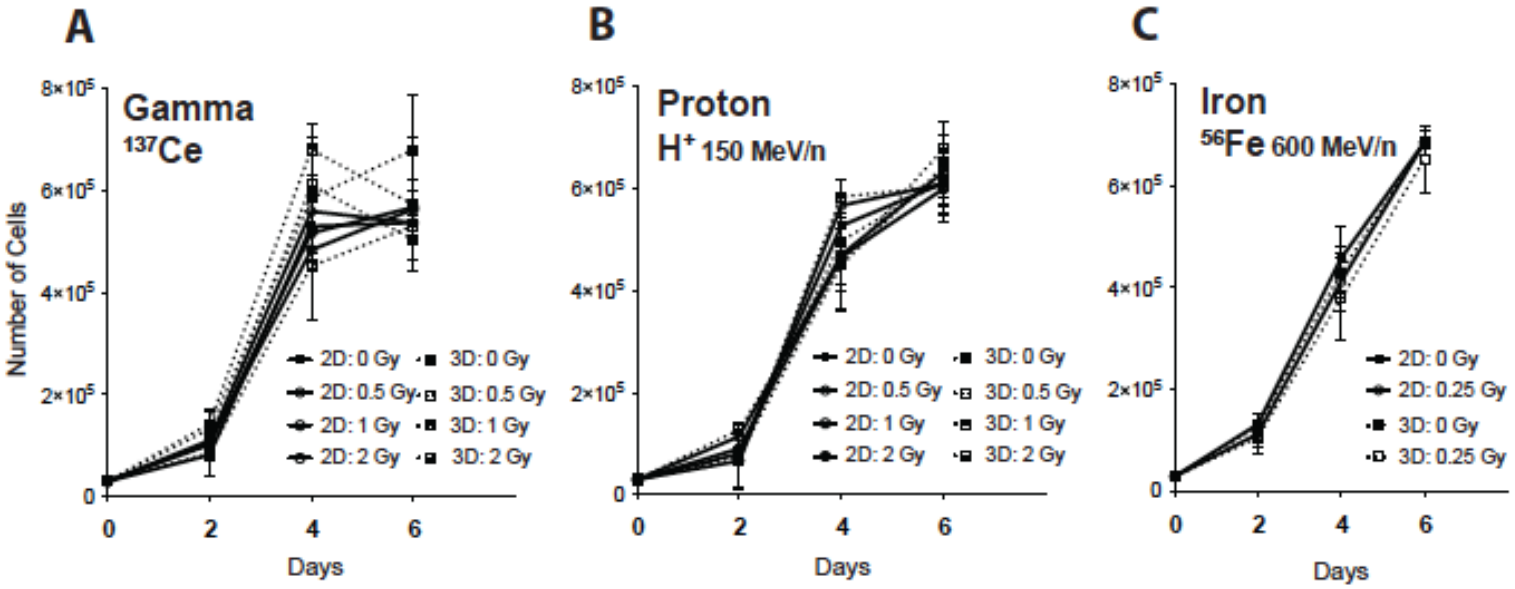

Figure 4.6

Figure 4.6: Cell growth curves within 3 PD after IR exposure.

Cells irradiated with (A) γ (B) proton, and (C) iron all have similar growth and proliferation patterns, regardless of cell culture conditions at the time of IR. Mean ± SEM.

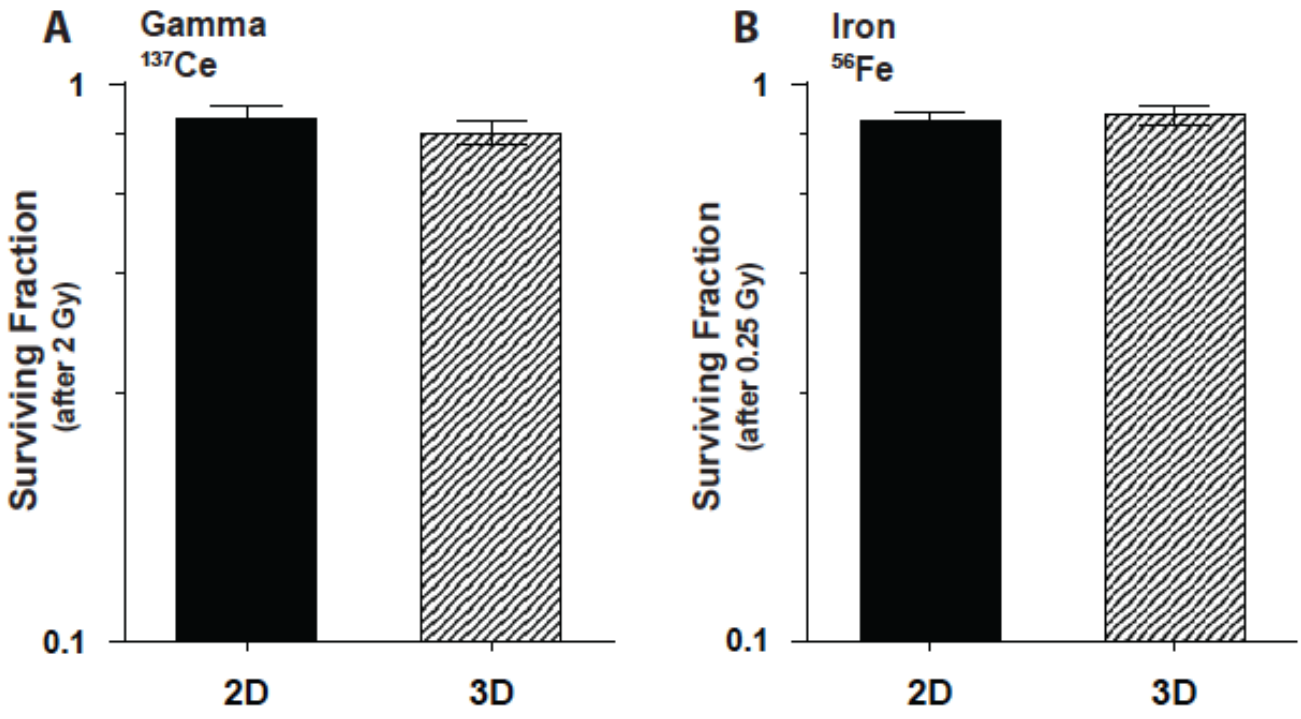

Figure 4.7

Figure 4.7: Colony formation assay of cells within 5 PD after IR.

There is no difference in the ability of cells to survive and replicate after irradiation. Mean ± SEM of the surviving fraction of cells after (A) 2 Gy γ and (B) 0.25 Gy iron (600 MeV/n).

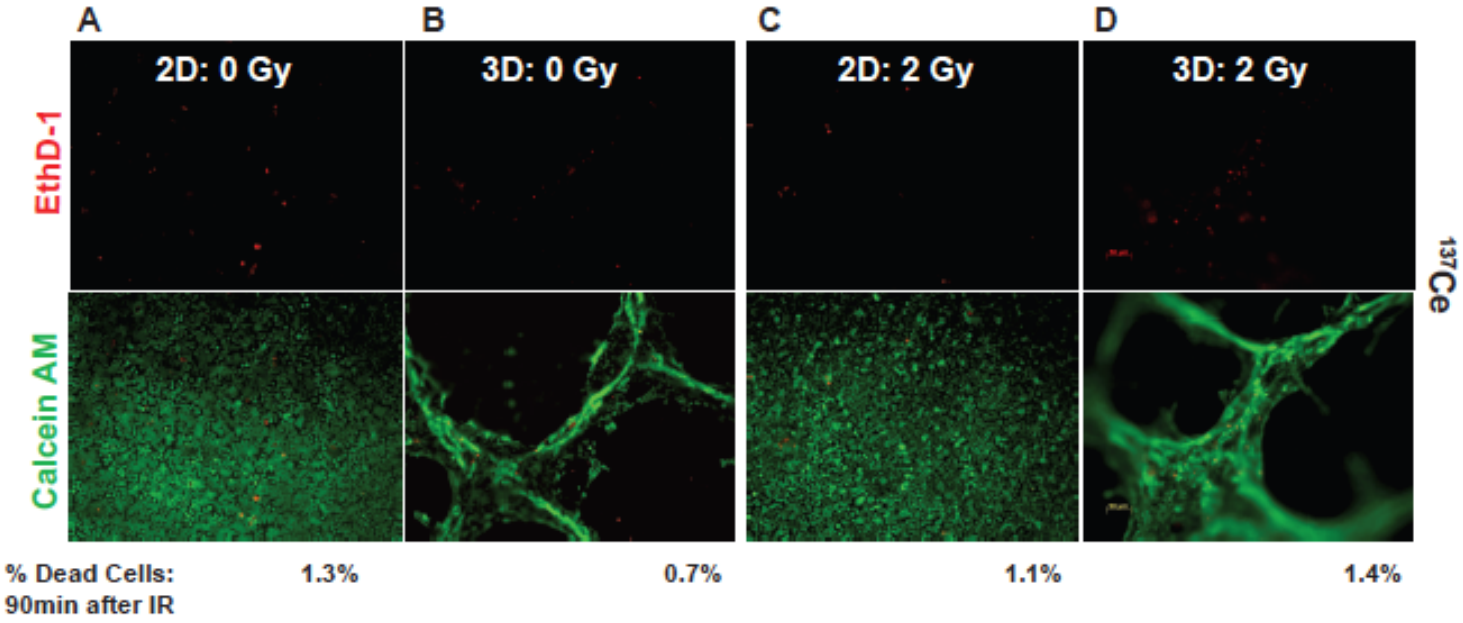

Figure 4.8

Figure 4.8: Dead cells in 2D and 3D cultures 90 minutes after IR.

Staining of γ-irradiated cultures with ethidium D1 and calcein AM 90 minutes after IR shows no difference in the number of dead (EthD1, red) cells compared to total cells between (A) unirradiated 2D and (B) unirradiated 3D cultures. Irradiated cultures (C) 2D with 2 Gy (D) 3D with 2 Gy also show no increased numbers of dying cells. Green cells indicate living cells (calcein AM).

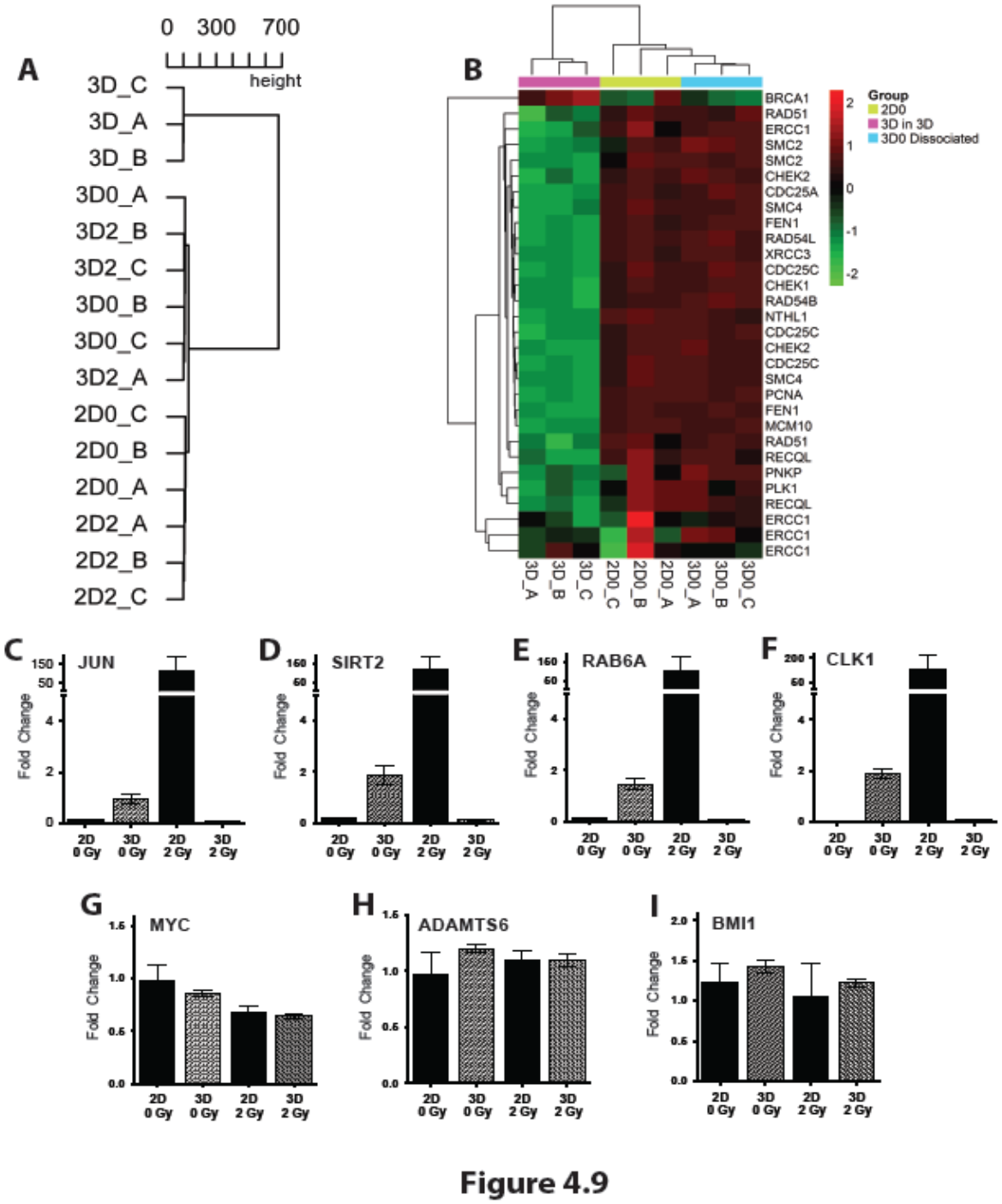

Figure 4.9

Figure 4.9: Transcriptional changes between cells in 2D and 3D culture.

(A) Cluster dendrogram shows hierarchical clustering of all groups. RNA collected from 3D cells in 3D are vastly different from cells in 2D as well as 3D cells after dissociation. (B) Heatmap showing expression of DNA repair genes, which are downregulated in 3D compared to 2D. (C-I) qPCR used to validate initial microarray findings shows relative mRNA levels of each gene normalized to housekeeping controls. Mean ± SEM.

Although pathway analysis and mapping is still ongoing, a group of genes was chosen preliminarily based on large fold changes in expression predicted by microarray analysis (full lists of genes can be found in **Appendices A-B**). After removing genes that were expressed in both 2D and 3D groups, differences between cells exposed to 2 Gy γ in 2D culture ("2D2") and 3D cultures after dissociation ("3D2") showed that Jun, SIRT2, RAB6A, and CLK1 are all robustly increased in 2D culture after γ exposure, but not in 3D cells (**Figure 4.9C-F**). However, there were no differences in Myc, ADAMTS6, or BMI1, despite predicted changes based on microarray (**Figure 4.9G-I**). These validation experiments will form the basis for ongoing pathway anaylsis and mapping with IPA®.

4.4 Discussion of 3D Culture and Radiation

In this study, I show that irradiation of human airway cells in 3D culture, instead of traditional 2D culture, reduces the frequency of progression toward malignant phenotypes. I demonstrate that irradiating cells in traditional 2D culture significantly increases cancer progression phenotypes, but 3D culture results in extensive transcriptional changes, which may mitigate this radiation-induced transformation.

Since the methods for 2D and 3D cultures are so vastly different, it was important to exclude any confounding effects that may have been due purely to technical culture method differences (experimental setup, reagents, timing, etc). For this reason, the data presented in **Figure 4.4** is crucial for validating that 3D culture prevents IR-induced transformation. I show that two variations of 3D culture (HBECs seeded on top of as well as embedded within Matrigel®) both prevent the negative transformative effects of IR, and also that fibroblasts are necessary to exert the full effect.

The process of growing cells in 3D brought up the possibility that a sub-population of cells could have been excluded or selected against when taken out of 2D and placed on top of Matrigel®. Due to natural heterogeneity in cell culture populations, these cells may have been more aggressive or transformed initially, but unable to participate in forming 3D structures and therefore selected out of the culture. Additionally, 3D cultures had to undergo a more stringent trypsinization process during dissociation to remove structures from the Matrigel and allow for the formation a monolayer culture quickly again in 2D; this process had the potential to kill off certain 3D cell populations, thus excluding cells transformed by IR when seeded into the soft agar assay. It is important to note that if this were true, one would expect for the unirradiated basal transformation rate between 2D and 3D grown cells to be different. However, in every experiment in this study, the number of colonies formed after 0 Gy was comparable in 2D and 3D. HBECs can transition from 2D to 3D and back again to 2D without losing their oncogenic potential (**Figure 4.4B**). Furthermore, cells grown in either 2D or 3D conditions grow at comparable rates, even after IR exposure (**Figure 4.6**). I am confident that no cells were selected out of the 3D irradiated populations, and that the transformation rates between 2D and 3D cultures are indeed comparing similar cell populations, without specific selection against 3D cells.

This study is still in progress, and I will determine if culture conditions affect the ability of cells to survive and replicate after IR. Ongoing experiments include measuring DNA synthesis immediately after IR (on undissociated 3D cells) via incorporation of the nucleoside analogue EdU (5-ethynyl-2'-deoxyuridine) using a Click-iT® EdU Imaging Kit (Invitrogen) are currently underway. Additionally, immunohistochemical stains for cleaved caspases, gamma-H2AX, ROS,

and other markers can confirm and extend our existing data regarding the differences between irradiated 2D and 3D cells.

The mechanistic differences between 2D and 3D irradiated cells is also still under examination. Multiple groups have shown that DNA damage is repaired more slowly in 3D culture due to chromatin organization [1, 10]. After organotypic skin cultures are irradiated, they show fewer DNA damage foci compared to 2D cells. This may be attributed to differences in intracellular signaling and cell differentiation [1]. These patterns are also recapitulated in the current study, with DNA damage repair pathways downregulated in 3D compared to 2D cells (**Figure 4.9B**). These differences between 2D and 3D are most likely due to changes in chromatin structure, and therefore changes in DNA damage may be more difficult to see. Importantly, there are blatant changes when 3D cells are dissociated and returned to 2D culture conditions. However, 3D cells are assayed for malignant phenotypes after being dissociated from 3D structures, and still they exhibit decreased transformation, even though there is no apparent loss of cells due to differing culture conditions. Therefore it is important to separate out changes due to changing culture conditions versus cancer progression changes that occur between 2D and dissociated 3D cultures.

Many of our confirmed upregulated genes in 2D irradiated cells (such as Jun and RAB6A) can function as oncogenes, leading to increases in invasive and malignant phenotypes; both Jun and RAB6A are upregulated in multiple types of cancers [51, 145]. However, SIRT2 has been demonstrated as a tumor suppressor through its role in regulating mitosis and genome integrity [97]. These seemingly contradictory clues about transcriptional changes need to be followed up with genetic manipulation studies to determine what specific pathways are responsible for differences in IR-transformation of 2D and 3D cells.

These results are the first to show that cell culture conditions are fundamental for cellular responses to radiation and can affect cancer progression. If 3D culture is more a biologically representative model than 2D culture, then perhaps current studies assessing transformation and radiation may be overestimating radiation risks using standard 2D culture methods. Ideally, expanding the utility of these improved 3D culture can more accurately model cell-based biology, allowing us to better understand the biological consequences of radiation.

CHAPTER FIVE

DISCUSSION & CONCLUSIONS

Radiation exposure has many detrimental biological effects, and with the incidence of cancers remaining high, it is crucial to understand underlying mechanisms of cellular protection against transformation and cell death. Many epidemiological studies have illustrated the lung's exquisite susceptibility to the carcinogenic effects of radiation [45, 131, 165]. Developing more biologically representative methods of tissue culture in 3D can provide better insight to cellular responses by modeling microenvironmental factors. Furthermore, characterizing protective chemical agents and their effects on both normal and cancerous cell populations allows for potential treatments and development/implementation of protective countermeasures for human subjects.

The development of the HBEC 3KT line has been an important reagent in evaluating the effects of radiation exposure on lung cancer progression; by manipulating and adding certain oncogenic factors, these cells can gradually transform toward lung cancer [171, 188]. Since their development, many investigations have shown that carcinogenesis in the HBEC system depends not only on intrinsic genetic factors, but also extrinsic factors such as serum levels in media and presence of ECM proteins [44, 93, 187].

In this body of work, I have shown that certain antioxidant, anti-inflammatory modulators (AIMs), including the triterpenoids CDDO, can selectively protect normal epithelial cells against the negative effects of IR. Although CDDO-Me is ineffective when administered after radiation as a mitigator in HBECs (data not shown), other work has demonstrated that CDDO may be able

to protect colonic epithelial cells when administered within an hour post-IR [99]. So far its use in lung and breast is limited as a countermeasure in that it must be given prior to IR exposure, and therefore would only be useful in controlled radiological settings (*ie*. radiation therapy, occupational exposure), whereas it may not be especially useful during disasters or radiological emergencies (*ie*. terrorism, nuclear accidents). This is true for most all of the drug therapies developed in the past fifty years—free radical scavengers that only render protection against initial DNA and cell damage when administered prior to, but not after radiation exposure. However, first responders may be protected if there is sufficient time to administer CDDO prior to IR exposure. It is still necessary to address the amount of lead-time for countermeasure protection—while eighteen to forty-eight hours provides significant radioprotection, shorter time frames have not been investigated with CDDO.

I have also demonstrated that irradiating cells in traditional 2D culture significantly increases cancer progression phenotypes, but 3D culture results in extensive transcriptional changes, which reduce radiation-induced transformation. Ongoing studies will focus on dissecting the differences between 2D and 3D culture and understanding the specific cellular mechanisms resulting in 3D protection against transformation. Determining how intrinsic and extrinsic factors coordinate to regulate lung epithlia is important for the interpretation of radiation effects on the lung as a whole. If regulation of cells *in vitro* differs from that *in vivo*, then any observed effect may not directly translate to biological situations in the body. For example, radiation exposure should affect the lung microenvironment and epithelium simultaneously. This could lead to a dysregulated stromal compartment that promotes a permissive environment for carcinogenesis to occur; dysregulated microenvironment may also synergize with existing or radiation-induced genetic alteration in the epithelium. On the other

hand, external influences may assist cells after injury, activating different transcriptional programs than in cells *in vitro*.

Since its discovery cancer has remained a mysterious entity. In 1937, *Fortune* magazine published a report entitled "Cancer: The Great Darkness:"

> The startling fact is that no new principle of treatment, whether for cure or prevention, has been introduced […] the methods of treatment have become more efficient and more humane. Crude surgery without anesthesia or asepsis has been replaced by modern painless surgery with its exquisite technical refinement. Biting caustics that ate into the flesh of past generations of cancer patients have been obsolesced by radiation with X-ray and radium […] but the fact remains that the cancer "cure" still includes only two principles—the removal and destruction of diseased tissue. No other means have been proved. [61]

Although much advancement has been made over the past century, knowledge of molecular genetics has not fully translated into effective treatments, nor has it explained why some treatments succeed and others fail. Cells acquire mutations and grow without normal regulatory control, acquiring more mutations along the way to eventually form a tumor with invasive and metastatic properties. These tumors are then treated with IR or chemotherapies to kill cells and possibly prevent them from migrating throughout the body—the best case in these scenarios would be to kill the cells carrying mutated genes. This creates a sharp disconnect between the mechanism driving cancer versus the proposed therapy. IR and traditional chemotherapy do not "fix" the mutated genes; they are non-specific and cannot selectively affect

mutated cancer cells. Instead of placing a band-aid over the wound, we must find ways to connect the mechanistic explanation of this illness with medical interventions.

Appendices

Appendix A: Genes with significant expression changes after removal of overlapping probes (limma) comparing 2D versus dissociated 3D HBECs with no irradiation.

Gene Symbol	Log Fold Change
LOC643272	1.026
DBN1	1.007
LOC653107	0.868
ZDHHC13	0.863
MIR221	0.853
CAPRIN2	0.847
WSB1	0.779
MATR3	0.776
MIRLET7D	0.761
ITSN1	0.754
HS.493947	0.739
GJB3	0.725
TAGLN3	0.713
VNN1	0.711
LTBP4	0.706
GAGE4	0.703
SPRY4	0.700
GOLGA8B	0.692
NET1	0.690
DVL1	0.681
CAPRIN2	0.677
ID1	0.673
LOC100133803	0.661
PLAA	0.657
CSF3	0.656
CTPS2	0.653
PCTK1	0.643
CSF3	0.641
EHF	0.629
SNORD94	0.629
PLCG1	0.627
FAM108B1	0.622
BNC1	0.616
RGNEF	0.611
C10ORF46	0.609

Gene Symbol	Log Fold Change
AMPH	0.603
IL1RL1	0.601
EIF3CL	0.593
KIAA0261	0.591
NET1	0.590
CPEB2	0.589
ANGPTL4	0.589
LOC100130623	0.588
HIP1R	0.581
PKP3	0.579
LOC650909	0.579
NAV3	0.575
CD274	0.572
ATRN	0.568
SLC38A1	0.558
HBEGF	0.550
EFTUD1	0.545
NPIP	0.545
HS.551128	0.545
GPR3	0.541
MTSS1	0.540
GTF2IP1	0.539
SERPINB2	0.539
MGC5139	0.536
LOC652388	0.535
KLF10	0.534
SERPINE1	0.533
LOC200030	0.530
COBRA1	0.529
FOS	0.524
LAMB3	0.520
CDK5R1	0.520
AKAP12	0.518
KLF10	0.515
OSMR	0.514

Gene Symbol	Log Fold Change
TRIML2	0.512
HERC3	0.511
SHC1	0.508
LOC100129982	0.502
IL1RL1	0.500
ETS1	0.499
DUSP6	0.499
ILF3	0.497
TGFA	0.494
AP2B1	0.493
ANGPTL4	0.488
AP2B1	0.486
TSC22D2	0.485
SLC25A24	0.480
ACIN1	0.480
SNX30	0.479
CASC4	0.477
SNORA18	0.476
MSN	0.476
SEC24B	0.474
LOC399959	0.473
SS18L1	0.465
RPS6KA3	0.465
TP73L	0.464
SGK1	0.464
SPRY4	0.463
SMTN	0.462
DVL3	0.460
ZCCHC3	0.456
LAMC2	0.453
MOBKL2B	0.452
AMMECR1L	0.452
SLC4A7	0.451
SPTBN1	0.450
RALGAPB	0.449

Gene Symbol	Log Fold Change
LOC92755	0.448
DHX9	0.445
ASAM	0.444
TJP1	0.444
LRP11	0.440
ATP2A2	0.438
ZC3H12A	0.437
ZNF697	0.437
JAK1	0.436
CLIP4	0.431
BAT2	0.430
MATR3	0.428
PTPRM	0.426
MCL1	0.426
SOX7	0.425
XPOT	0.423
HERPUD1	0.423
PHKA2	0.423
TAGLN3	0.422
CAPRIN1	0.422
RYK	0.419
ADIPOR1	0.418
KIAA2010	0.417
BNC1	0.416
HS.558212	0.416
SPAG9	0.416
SMAD3	0.415
ZFC3H1	0.415
TRIB1	0.414
CDKN2B	0.414
SLC39A6	0.411
PABPN1	0.409
SMG7	0.409
LOC652688	0.407
CSRNP2	0.405
SIAH2	0.404
STX6	0.404
CHD7	0.403
FLNB	0.402
ATP5I	0.394
FHOD1	0.394

Gene Symbol	Log Fold Change
KIF5B	0.392
PTPRA	0.392
HK2	0.392
G6PD	0.391
LAMB1	0.388
SGK1	0.387
BCOR	0.385
NRD1	0.384
SH2B3	0.384
C16ORF52	0.383
TRIM5	0.381
ACSS2	0.381
TGM2	0.380
HERPUD1	0.380
CTGF	0.379
ASAP1	0.378
CYB5D1	0.378
NCOR2	0.376
FNBP4	0.376
KDELR3	0.376
ENO2	0.374
GDI1	0.373
BNC1	0.373
CD44	0.371
TNKS1BP1	0.371
LAMC2	0.371
SOX9	0.370
MYEOV	0.368
ASAP2	0.367
KIAA1539	0.367
KPNA6	0.367
SDHA	0.367
INO80C	0.366
MICALL1	0.365
MTMR3	0.365
RERE	0.362
LOC653820	0.362
UBQLN1	0.361
SNRK	0.361
NCOR2	0.361
G3BP2	0.361

Gene Symbol	Log Fold Change
POLM	0.360
SDCBP2	0.360
TINAGL1	0.359
ITGB1	0.358
TRIM44	0.357
CSNK2A1	0.356
RBL2	0.355
PKP1	0.355
ACSS2	0.355
TNFAIP1	0.354
SPIRE1	0.354
DUSP5	0.352
CCND2	0.351
JOSD1	0.350
DDEF2	0.350
MTSS1	0.349
PITPNM1	0.347
TUBB	0.344
CSNK1D	0.344
HMGA1	0.342
PIAS3	0.342
CDCP1	0.341
IL13RA2	0.341
ZNF275	0.341
DGKA	0.340
PTPRE	0.340
ASAP1	0.340
HNRPK	0.339
EXOSC10	0.339
NUP153	0.333
TPX2	0.332
TJP1	0.331
LOC652846	0.324
EIF4B	0.323
IL1A	0.323
LOC728188	0.322
VPS33B	0.322
ARF4	0.321
FNTA	0.321
LAMA3	0.320
LSM12	0.319

Gene Symbol	Log Fold Change
SURF4	0.316
IQCB1	0.316
MORF4L2	0.314
BAT2D1	0.314
RPS6KA4	0.314
IWS1	0.313
FOSL1	0.312
CREB3L2	0.311
SH3KBP1	0.308
RBM15	0.307
NPC1	0.305
FUBP3	0.303
RAB5C	0.301
CAV2	0.300
DCAF7	0.297
MGEA5	0.297
RAP2A	0.296
ACTB	0.294
MAPKAPK2	0.293
FADS1	0.289
ANKRD57	0.284
GSS	0.282
LOC647000	0.281
IL1B	0.281
GJB3	0.280
UFM1	0.279
SRXN1	0.278
PTMS	0.276
ACTR1B	0.275
COMMD6	0.273
BAIAP2L1	0.271
ERRFI1	0.271
CDK5RAP1	0.268
LARP1	0.268
SLC20A1	0.267
EFHD2	0.263
DERL1	0.261
FKBP1A	0.257
HDGF	0.257
SFN	0.256
LTBR	0.255

Gene Symbol	Log Fold Change
LOC642489	0.252
DCTD	0.252
PCBP2	0.251
TNFRSF6B	0.250
C19ORF22	0.247
ACTG1	0.243
LAMA3	0.242
CALM1	0.241
RBM12	0.239
SRC	0.238
C11ORF10	0.237
MED24	0.235
SYPL1	0.221
YWHAZ	0.210
LOC641814	0.174
EDF1	-0.191
PRDX5	-0.205
ROBLD3	-0.222
KDELR1	-0.227
TMEM111	-0.228
MRPS22	-0.229
DCTPP1	-0.234
ATP6AP1	-0.236
SF3B5	-0.238
YIF1A	-0.240
MRPS12	-0.244
NDUFS3	-0.245
BUD31	-0.250
PHPT1	-0.250
EFNA1	-0.254
COPS3	-0.257
SF3A2	-0.257
LOC644511	-0.261
COPS5	-0.261
SNRPC	-0.264
LOC649447	-0.265
KRT8	-0.266
COMMD4	-0.268
AK3L1	-0.268
NT5C3	-0.270
ANAPC11	-0.270

Gene Symbol	Log Fold Change
SEPX1	-0.273
C8ORF55	-0.273
UROS	-0.274
SUMF2	-0.275
LOC100128196	-0.278
RFXANK	-0.278
NMRAL1	-0.279
SNRPN	-0.279
MRPS26	-0.280
LOC390557	-0.282
CIAPIN1	-0.283
HSBP1	-0.284
NOP56	-0.289
UBXN2A	-0.289
HINT2	-0.292
RPP40	-0.294
SDHAF2	-0.295
TRIAP1	-0.295
NIP7	-0.297
SLC2A1	-0.298
BOLA3	-0.299
SDF2	-0.299
ATL3	-0.299
SKP2	-0.301
DNAJC8	-0.301
MGMT	-0.301
DCXR	-0.309
BCAS4	-0.309
H2AFJ	-0.310
RNASEH2A	-0.310
HOXB7	-0.312
C7ORF59	-0.312
LOC643856	-0.312
LOC648390	-0.312
SIL1	-0.313
TMEM160	-0.313
RHBDD2	-0.313
C10ORF116	-0.314
NDUFA9	-0.320
DNTTIP1	-0.321
EDF1	-0.323

Gene Symbol	Log Fold Change
ORC5L	-0.324
TEX264	-0.325
UBE2L6	-0.325
SNRPB	-0.325
ZYX	-0.326
C20ORF27	-0.326
ACTR10	-0.327
NDUFS7	-0.328
TSNAX	-0.328
LYRM4	-0.328
PEX16	-0.329
DHRS7B	-0.329
STAP2	-0.329
TPD52L1	-0.332
PQBP1	-0.333
LOC100130562	-0.333
CD320	-0.333
CMBL	-0.333
C7ORF49	-0.339
PDIA6	-0.341
UBXN4	-0.342
PMVK	-0.343
KIAA0114	-0.344
KLHDC4	-0.344
S100A9	-0.347
RHBDD2	-0.348
GNPTG	-0.350
RPL14L	-0.350
UBAC2	-0.351
TP53I13	-0.352
BOLA3	-0.352
MRPS18B	-0.355
BIRC5	-0.356
NR2C2AP	-0.356
ARL6IP4	-0.356
DGCR6	-0.358
CHCHD3	-0.360
TMSL3	-0.362
TARBP2	-0.365
COMT	-0.366
C7ORF10	-0.367

Gene Symbol	Log Fold Change
CDC42	-0.368
TINF2	-0.368
ACOT9	-0.368
LOC643438	-0.370
RAD51AP1	-0.371
PLLP	-0.372
DHCR24	-0.374
LOC729992	-0.376
BCL7B	-0.376
COMMD9	-0.378
LOC729774	-0.378
ZNHIT1	-0.378
MRPL27	-0.379
ISG15	-0.379
LOC388556	-0.379
ITPA	-0.383
LOC387703	-0.383
NUDT16L1	-0.385
C16ORF13	-0.385
SCARNA10	-0.388
MRPS11	-0.388
ATP6V0E2	-0.389
SNAP47	-0.389
ARD1A	-0.391
CWF19L1	-0.392
COPE	-0.394
LOC91561	-0.397
LEPROT	-0.399
UBIAD1	-0.399
NT5C3	-0.402
WBP1	-0.404
KLHDC8B	-0.404
KCNN4	-0.405
HS.535360	-0.409
PSMB8	-0.412
GANAB	-0.418
ASPSCR1	-0.421
PAQR7	-0.422
ABHD14A	-0.424
SNRPC	-0.427
NINJ1	-0.431

Gene Symbol	Log Fold Change
CBR1	-0.436
ANKRD22	-0.436
HAX1	-0.438
MSL3L1	-0.439
SLC22A18AS	-0.444
GCHFR	-0.444
RPAP2	-0.445
SLC35F2	-0.449
TMBIM1	-0.450
TCP1	-0.455
ARID4B	-0.456
LOC100131471	-0.461
SAR1A	-0.462
C7ORF68	-0.464
C14ORF142	-0.464
TCF7	-0.466
XAF1	-0.467
PINX1	-0.467
C4ORF48	-0.471
DDX49	-0.472
HIST2H2AA3	-0.474
DGCR6L	-0.475
CHP	-0.476
C9ORF23	-0.478
ECE2	-0.480
RER1	-0.481
LOC644214	-0.481
ECSIT	-0.486
OIP5	-0.487
LOC100128056	-0.487
DSCC1	-0.489
TTC8	-0.491
LOC100130071	-0.493
AYP1P1	-0.498
LOC100129566	-0.499
RMI1	-0.502
CCDC101	-0.502
DENND2A	-0.504
PRNPIP	-0.506
FAM114A2	-0.506
GSTO2	-0.511

Gene Symbol	Log Fold Change
TAF5L	-0.518
C2ORF79	-0.521
KRT15	-0.522
MANBAL	-0.522
FBXO32	-0.522
NCRNA00094	-0.524
ZC3H5	-0.538
C11ORF83	-0.539
HAX1	-0.541
AFMID	-0.543
PYCARD	-0.545
CARD14	-0.547
SF3B3	-0.553
DBP	-0.556
LOC100128627	-0.567
ORMDL2	-0.569
LOC100129297	-0.575
RGL1	-0.588
HIST2H2AA4	-0.588
C22ORF27	-0.603
LOC729157	-0.604
GOLGA7	-0.607
SGCB	-0.622
PXMP4	-0.623

Gene Symbol	Log Fold Change
IFIT3	-0.635
IL7R	-0.665
HS.543956	-0.667
PRPF40A	-0.668
MAP1D	-0.669
HS.542027	-0.672
DENND2D	-0.685
FBXO16	-0.691
LOC100133565	-0.700
HS.580169	-0.700
HS.542579	-0.701
LOC100132428	-0.730
HS.325396	-0.741
TFF3	-0.750
FBXO32	-0.770
IFIT1	-0.778
LOC100133692	-0.838
LOC100131970	-0.842
TSPAN1	-0.877
B3GNT1	-0.906
SOX2	-0.928
SOX2	-1.073

Appendix B: Genes with significant expression changes after removal of overlapping probes (limma) comparing 2D versus dissociated 3D HBECs after 2 Gy.

Gene Symbol	Log Fold Change
TXNL1	1.167
LOC441550	1.027
HSPE1	1.014
SNORA32	1.000
LOC654350	0.978
SNORD80	0.946
PDCD10	0.943
C3ORF14	0.940
LOC440063	0.933
RNF39	0.917
LOC646949	0.911
GNG10	0.889
TSC22D1	0.880
FABP5	0.860
MRPL47	0.842
LOC441073	0.835
AGR2	0.833
ZNF280D	0.832
CROP	0.832
LOC100129657	0.830
ACPT	0.826
ATF4	0.822
LOC729009	0.817
SNORD49A	0.815
CLK1	0.813
LOC100128291	0.799
PODXL2	0.787
ZNF22	0.778
B3GNT5	0.772
KRCC1	0.763
LOC388122	0.761
FZD6	0.760
CSTF3	0.760
LOC641848	0.753
TCEA1	0.753
LOC643911	0.753
GOLT1B	0.749

Gene Symbol	Log Fold Change
LOC652541	0.747
RPL9	0.735
TXNDC9	0.734
LOC100131672	0.733
PMS2L2	0.724
GOLGA6B	0.721
DCAF6	0.718
LOC729236	0.715
TP53INP1	0.715
LOC648822	0.706
LOC390183	0.704
LOC649555	0.698
LOC100130932	0.697
FLJ22639	0.693
HS.363510	0.692
C11ORF73	0.692
LOC440991	0.692
ARL17P1	0.691
LSM6	0.687
LOC100129237	0.687
HS.314414	0.686
RNPC3	0.684
NIPAL2	0.683
RTN4	0.680
LOC730029	0.680
LOC100128060	0.675
UFM1	0.674
LOC653631	0.671
CENPQ	0.671
ARRDC4	0.670
ANKRA2	0.669
BUB3	0.669
SCG5	0.669
LOC100131205	0.666
LOC100128440	0.662
ZNF404	0.660
LOC728602	0.659

Gene Symbol	Log Fold Change
RTN3	0.657
LOC100128337	0.656
BZW1	0.655
LOC100129067	0.650
C9ORF85	0.648
LOC729686	0.645
ALS2CR8	0.644
LOC645968	0.644
C6ORF120	0.642
HS.405877	0.642
LOC440145	0.641
CXADR	0.638
LOC100132547	0.635
PERP	0.635
TRA1P2	0.634
LOC100128060	0.633
LOC391370	0.633
C9ORF163	0.630
SFRS11	0.630
LOC727821	0.629
FLJ43681	0.628
CDC2	0.628
TMEM167A	0.627
CCDC90B	0.627
FAM162A	0.623
NNMT	0.623
LOC100129759	0.622
SLPI	0.622
NDUFB9	0.622
TCN1	0.613
FBXO38	0.612
KLRC3	0.610
P704P	0.610
CHPT1	0.609
C6ORF173	0.609
LOC392285	0.608
ASPH	0.608

Gene Symbol	Log Fold Change
TFPI	0.606
LOC100128689	0.606
NAP1L1	0.606
SOAT1	0.604
APIP	0.604
LOC100134504	0.603
HLA-F	0.602
PMS2	0.602
GAGE12F	0.599
LOC100129742	0.599
LOC642502	0.597
LOC100130154	0.595
LOC100131526	0.593
RPL23	0.593
ISCA1	0.592
NACAP1	0.587
ACAT2	0.587
STAT5B	0.587
LOC390735	0.586
ODF2L	0.585
GTPBP2	0.584
LOC341965	0.583
LOC641768	0.581
C20ORF108	0.580
COMMD10	0.580
LOC729208	0.579
C1QL1	0.578
PTGES3	0.578
LOC644615	0.578
LOC730052	0.577
LOC100132673	0.577
LOC653773	0.574
POLR2J3	0.574
SFRS18	0.574
RBM7	0.573
MRPL48	0.571
MCTS1	0.571
LOC286512	0.570
C7ORF28B	0.568
LOC649946	0.567
SCD5	0.564

Gene Symbol	Log Fold Change
PPP4R4	0.562
HNRNPA2B1	0.560
SNORD36A	0.556
DDX17	0.555
DNAJC25-GNG10	0.549
LOC100133277	0.549
OSTC	0.547
LOC100131323	0.545
C2ORF76	0.544
TSPAN13	0.541
MGC12965	0.540
EIF3M	0.538
LOC727865	0.538
LOC441484	0.538
LOC729255	0.538
LOC728484	0.536
ELF3	0.535
YWHAG	0.534
HS.569175	0.534
RRAS2	0.533
LOC100132199	0.531
LOC642989	0.531
LOC645630	0.530
AIG1	0.527
MYC	0.525
UBLCP1	0.524
LOC727984	0.522
LOC100128086	0.520
LOC645157	0.520
LOC729342	0.519
LOC730278	0.518
PMEPA1	0.517
LOC100132139	0.516
LOC729500	0.514
LOC442232	0.513
MND1	0.511
LOC728026	0.510
FAM92A1	0.510
ZNHIT3	0.505
LOC730255	0.505

Gene Symbol	Log Fold Change
SUB1	0.499
LOC644877	0.499
PNN	0.498
LOC653702	0.497
LOC100131672	0.497
AHSA2	0.497
LOC158160	0.496
NCRNA00081	0.495
LOC100129866	0.495
HNRPA1L-2	0.494
LOC641849	0.493
ATAD1	0.492
LOC100129685	0.492
TCEAL8	0.491
SF3B14	0.491
ALDH3B2	0.490
LOC100132992	0.488
EAPP	0.488
ITGB3BP	0.487
LOC100130892	0.487
LOC646527	0.485
MBIP	0.484
C12ORF60	0.483
VKORC1	0.481
RPL7	0.479
CSTF3	0.478
LOC391532	0.477
ETS1	0.475
HAT1	0.474
LOC100132918	0.474
LOC653566	0.473
LOC648210	0.472
COX7B	0.471
LOC729500	0.471
CPOX	0.470
ZFAND6	0.470
BET1	0.468
LOC401537	0.468
NOP56	0.467
C6ORF160	0.466
HNRPC	0.466

Gene Symbol	Log Fold Change
LOC391833	0.464
LOC100131609	0.464
FKBP3	0.461
STX7	0.460
SNRPN	0.459
C4ORF41	0.459
C5ORF44	0.458
ARMCX6	0.458
CDC42SE2	0.456
SMNDC1	0.455
LOC647037	0.455
SIP1	0.454
PPP2R3C	0.454
CD58	0.453
FABP5L2	0.453
C13ORF27	0.452
LOC653071	0.452
FTHL12	0.451
LOC493869	0.450
LOC645691	0.449
HIGD1A	0.449
HIF1A	0.446
MMP28	0.446
LOC653778	0.446
LOC100132291	0.443
IFT52	0.443
LOC389156	0.442
PCNA	0.441
C8ORF59	0.441
LOC646785	0.440
LOC100132457	0.438
CCT6P1	0.437
LOC439953	0.437
SCOC	0.437
PRKAB2	0.437
LOC100129086	0.436
LOC388076	0.436
ARL4A	0.435
SFRS12	0.433
UQCRH	0.430
PRKAR1A	0.429

Gene Symbol	Log Fold Change
SYTL1	0.427
LOC645693	0.426
LOC389787	0.426
ATP5C1	0.426
LOC100133012	0.422
LOC100132863	0.421
FRG1	0.420
TCP1	0.420
B2M	0.419
HSPC157	0.418
LOC653147	0.418
LOC729646	0.418
LOC401640	0.417
LOC440595	0.416
POP4	0.416
C18ORF10	0.415
CNIH4	0.415
LOC100129118	0.414
LIMCH1	0.414
EI24	0.412
MRPS33	0.411
SAR1B	0.411
LOC728732	0.411
COMMD10	0.410
UNC119B	0.410
LOC653658	0.409
ZNF83	0.408
LOC647030	0.408
GNG10	0.408
LOC100131261	0.407
HMMR	0.405
ALG5	0.405
CMPK1	0.405
NAE1	0.404
CCDC104	0.404
DYNLRB1	0.403
P4HA1	0.403
ATF4	0.403
LOC644029	0.403
40800.000	0.402
LOC728244	0.400

Gene Symbol	Log Fold Change
LOC440928	0.399
RPS26L	0.397
LOC654244	0.397
C1ORF41	0.396
ABCG1	0.396
LOC389156	0.394
NIPSNAP3A	0.392
LOC642975	0.391
PSMA3	0.390
LOC645138	0.389
F3	0.388
LOC731640	0.388
CD9	0.387
LOC100129599	0.386
LOC647150	0.385
TIAL1	0.384
MTPN	0.384
EEF1AL7	0.384
SLC35D2	0.383
LOC100132795	0.382
LOC727865	0.382
LOC730324	0.380
PDIA3P	0.379
LOC651149	0.379
PTTG3P	0.378
CRIPT	0.376
LOC100130511	0.376
HNRPDL	0.375
UBE2Q2	0.375
RPL39L	0.374
PGAM4	0.374
SLC25A40	0.373
LOC389662	0.372
MRPS33	0.371
DBI	0.370
LOC440731	0.370
TSC22D3	0.370
MED7	0.369
KLHDC2	0.369
TCEAL8	0.368
PPA2	0.367

Gene Symbol	Log Fold Change
LOC100131387	0.367
LOC647081	0.365
NIPAL4	0.365
ABHD3	0.364
TMEM189-UBE2V1	0.363
LOC100131905	0.363
SIP1	0.361
LOC644790	0.361
TSC22D1	0.361
SUMF2	0.360
DSTN	0.360
C9ORF46	0.359
NDUFA4	0.359
CHMP5	0.358
C14ORF109	0.357
NUP54	0.355
LOC644799	0.355
YEATS4	0.355
LOC645715	0.354
NDUFAB1	0.353
ACYP2	0.352
LOC642590	0.352
ZC3H15	0.351
IDI1	0.351
RAP2C	0.351
LOC100127918	0.350
CYCSL1	0.350
STARD3NL	0.347
TUSC1	0.347
LOC641844	0.346
TXNDC5	0.346
OSTC	0.345
C8ORF40	0.344
C3ORF23	0.344
LOC389672	0.343
PSMA6	0.338
CITED4	0.338
SEC11C	0.338
LOC645094	0.338
MGC87895	0.338

Gene Symbol	Log Fold Change
STEAP1	0.335
MAP2K1IP1	0.335
LYRM5	0.334
LOC387825	0.334
LOC100128410	0.334
LOC220433	0.333
C6ORF115	0.333
SPTLC1	0.333
SELK	0.332
MAP7	0.331
MRPL42	0.330
LOC728672	0.327
RBX1	0.327
GGH	0.327
SNHG5	0.324
CSTA	0.321
LOC728739	0.321
CKMT1B	0.320
HS.363526	0.320
ATP1B3	0.320
B2M	0.319
LOC651894	0.317
RYK	0.317
MTX2	0.316
LOC100128266	0.315
LOC151579	0.315
TIPRL	0.315
CLDND1	0.315
CCDC23	0.315
RPL13L	0.314
LOC100130308	0.314
CHMP5	0.312
C17ORF95	0.311
LOC442454	0.310
LMF2	0.310
LOC728782	0.308
TMEM219	0.307
RPS27L	0.307
LOC388654	0.306
GTF2H5	0.304
F2RL1	0.303

Gene Symbol	Log Fold Change
C14ORF109	0.302
LOC646849	0.302
PSMA3	0.300
LOC729362	0.300
ANKRA2	0.300
UBE2E3	0.300
STX8	0.299
TGIF1	0.297
CRTAP	0.296
PPIA	0.296
MGST1	0.296
LOC124512	0.294
ZC3H11B	0.292
PIGF	0.291
RAB5A	0.291
CNIH	0.290
TRAK2	0.290
LOC390354	0.290
DYNLT1	0.288
ZBED5	0.288
TPST2	0.288
TMEM49	0.287
LOC391126	0.287
LOC391656	0.286
TGIF1	0.286
UNC50	0.283
LOC729926	0.281
COPS8	0.279
MGST2	0.276
ANLN	0.275
RAB9A	0.275
YWHAE	0.274
UBE2V2	0.272
LOC401397	0.272
CDKN3	0.271
LOC100128936	0.269
C14ORF166	0.268
TMEM14B	0.266
MRPL13	0.265
LOC646819	0.263
ATP5F1	0.261

Gene Symbol	Log Fold Change
LOC653566	0.258
LEPROTL1	0.258
PDCD10	0.257
TSC22D1	0.255
GGCT	0.253
C11ORF1	0.252
PFN2	0.248
FAM108C1	0.246
LOC441073	0.241
UBE2A	0.240
LOC100131940	0.230
NDUFS4	0.228
TOMM20	0.228
VPS29	0.225
COX7A2	0.222
KDELR2	0.222
MANBAL	0.217
RPS24	0.216
RPLP0	0.214
TRMT5	0.213
S100A11	0.212
HBXIP	0.212
CALM2	0.194
GTPBP4	-0.199
MRPL37	-0.215
PLSCR3	-0.216
ATIC	-0.219
PIN1	-0.221
PHF5A	-0.221
SLC16A3	-0.228
CUTA	-0.229
SERINC3	-0.229
LOC401115	-0.229
PLOD2	-0.232
SEC13	-0.233
RASIP1	-0.234
PARL	-0.234
HAS3	-0.235
BCKDK	-0.235
MAPKAPK3	-0.237
LOC389168	-0.241

Gene Symbol	Log Fold Change
LAD1	-0.244
CAMK2N1	-0.245
MKNK2	-0.248
VIL2	-0.249
PSMD2	-0.252
KRT18P13	-0.252
MAPK13	-0.254
NT5DC3	-0.255
APEX2	-0.258
PLOD3	-0.259
RNH1	-0.266
RBM10	-0.267
EWSR1	-0.268
CCDC86	-0.268
NFKBIA	-0.271
SNX27	-0.274
CDK6	-0.275
HPS6	-0.278
ACTR1A	-0.283
ASH2L	-0.283
GRSF1	-0.283
POLR1E	-0.285
CCND3	-0.286
MUL1	-0.286
PTBP1	-0.288
PRPF4	-0.290
HSPH1	-0.290
DNMT1	-0.291
SRRM1	-0.291
PIK3R2	-0.291
BRMS1	-0.292
ADD1	-0.293
LYAR	-0.294
CASP2	-0.294
LRRFIP2	-0.294
PRDM4	-0.297
PTPLAD1	-0.298
PLEKHB2	-0.298
ZNF787	-0.299
EIF6	-0.299
MTHFS	-0.299

Gene Symbol	Log Fold Change
NUDC	-0.302
ACTN1	-0.303
RANGAP1	-0.303
EIF4A1	-0.303
PAK1IP1	-0.304
BANP	-0.305
NFKB1	-0.305
NOTCH1	-0.306
E4F1	-0.306
METTL13	-0.307
TAF15	-0.309
RHPN2	-0.309
RNMT	-0.310
XPO4	-0.310
AKIRIN1	-0.312
RBM28	-0.312
MCM7	-0.313
HS.370359	-0.315
DDRGK1	-0.315
CCNY	-0.316
FAM46B	-0.317
NTHL1	-0.317
PPM1G	-0.319
FKBP4	-0.320
CTSB	-0.323
RBM14	-0.324
CDC20	-0.324
MACF1	-0.324
HS.27048	-0.328
FBXO21	-0.328
NVL	-0.328
XRCC6	-0.330
TNPO3	-0.330
LOC340260	-0.331
CCDC51	-0.331
ZBTB43	-0.332
GSK3B	-0.333
UGCG	-0.333
GEMIN4	-0.334
FLJ10374	-0.335
PARP4	-0.337

Gene Symbol	Log Fold Change
C11ORF2	-0.339
WWP2	-0.339
RAI14	-0.340
FEN1	-0.340
SMARCA4	-0.343
PARP1	-0.343
NOL6	-0.344
SYNJ2BP	-0.344
PKP4	-0.344
COL17A1	-0.348
ZC3HAV1	-0.348
FASTKD5	-0.350
HNRPM	-0.352
YY1	-0.352
SPNS1	-0.353
C16ORF35	-0.353
ISG20L2	-0.354
FRYL	-0.355
EIF4G1	-0.356
PCNX	-0.356
LRWD1	-0.358
COBLL1	-0.358
PTPRF	-0.358
RNF121	-0.360
ATG10	-0.362
COG2	-0.363
C1ORF163	-0.363
MYO5C	-0.364
PLEKHA1	-0.364
DDX27	-0.366
LAS1L	-0.366
CCNF	-0.366
NCLN	-0.366
DNM1L	-0.366
NFIB	-0.367
EIF2AK4	-0.368
CFLAR	-0.368
USP14	-0.369
XPO5	-0.370
C1ORF71	-0.371
RPL8	-0.372

Gene Symbol	Log Fold Change
GNB5	-0.377
PAK4	-0.379
PDSS2	-0.380
PDPK1	-0.383
NUP62	-0.384
UBN1	-0.384
SLC9A1	-0.384
LOC723972	-0.385
CEP350	-0.386
EVI5	-0.387
COL4A1	-0.387
R3HCC1	-0.388
SLC20A2	-0.389
ABCF1	-0.391
SQSTM1	-0.392
FBXW4	-0.392
ZNF593	-0.392
BBX	-0.393
KIAA0355	-0.394
ATF5	-0.394
AHNAK	-0.396
TYW1B	-0.397
DOCK5	-0.399
SLC25A22	-0.402
IL27RA	-0.403
AHNAK2	-0.406
LOC100008588	-0.407
SNTB2	-0.407
PCDH7	-0.408
MED16	-0.408
LOC729535	-0.408
KAT5	-0.408
TCEB3	-0.409
PCYOX1	-0.414
FICD	-0.414
DNM1L	-0.414
DDX19A	-0.415
NUCKS1	-0.419
INO80D	-0.421
MBP	-0.423
PLEKHF1	-0.424

Gene Symbol	Log Fold Change
PRKDC	-0.425
SASH1	-0.426
EP400	-0.428
NBPF10	-0.428
ASCC2	-0.429
C21ORF57	-0.431
HNRNPL	-0.432
ATRIP	-0.432
TNFRSF10A	-0.433
LOC730316	-0.433
SDSL	-0.435
LOC644422	-0.437
SNTB2	-0.437
CCDC102A	-0.438
FAT1	-0.440
USP9X	-0.440
XPNPEP3	-0.441
FAT1	-0.444
C17ORF53	-0.444
CHD8	-0.445
PIAS4	-0.445
CRTC3	-0.448
GCN1L1	-0.449
ZNF142	-0.450
UBR4	-0.455
NACC2	-0.455
TDG	-0.458
TRIM13	-0.460
GMPPB	-0.460
ASXL2	-0.461
SBF1	-0.464
PXMP4	-0.466
DHX37	-0.467
DNAJB12	-0.468
SF3B1	-0.469
CDT1	-0.472
L2HGDH	-0.479
LOC653103	-0.482
APCDD1L	-0.483
ZZEF1	-0.484
AP1B1	-0.487

Gene Symbol	Log Fold Change
DFFA	-0.488
RASAL2	-0.488
BANP	-0.492
TLN1	-0.494
C14ORF102	-0.496
UBE2O	-0.498
UPF1	-0.501
USP24	-0.504
ITPRIPL2	-0.505
AKAP13	-0.505
TNPO1	-0.506
C21ORF70	-0.516
JARID1A	-0.519
FEM1B	-0.526
NAT10	-0.529
TRRAP	-0.533
DYNC1H1	-0.535
ZNF148	-0.538
DYRK2	-0.539
RNF113A	-0.540
SCAMP3	-0.544
PAPD5	-0.545
LOC645233	-0.547
KCTD12	-0.550
HIRIP3	-0.551
IGF2R	-0.553
EIF2C2	-0.559
CHAF1A	-0.559
EHD1	-0.561
COL4A3BP	-0.563
POLR3A	-0.566
CCDC21	-0.566
FBN2	-0.569
FYTTD1	-0.573
PRKAR2A	-0.575
LIMS1	-0.589
LOC644422	-0.590
SNHG9	-0.595
DIS3L	-0.596

Gene Symbol	Log Fold Change
LOC100134098	-0.603
HNRNPUL2	-0.603
HS.482960	-0.603
PDP2	-0.603
HM13	-0.604
RFC2	-0.604
MYCBP2	-0.606
RRBP1	-0.607
ZBTB40	-0.609
RAB35	-0.611
ZNF320	-0.615
TNRC6B	-0.622
INCENP	-0.622
CUEDC1	-0.625
B3GNTL1	-0.626
SRGAP1	-0.631
ZNF594	-0.633
LOC100129269	-0.634
LRAP	-0.635
LOC440345	-0.655
RPPH1	-0.661
LOC648509	-0.667
GNL3L	-0.671
LOC642033	-0.673
HS.163752	-0.673
C14ORF78	-0.683
LOC100134584	-0.694
LOC100133402	-0.695
ALKBH8	-0.695
NDUFS1	-0.696
HS.555252	-0.702
LOC100132774	-0.706
ZFHX3	-0.715
AAK1	-0.717
LOC646697	-0.724
GNB4	-0.725
SF1	-0.725
DLC1	-0.726
TOP3A	-0.743
HS.580797	-0.749

Gene Symbol	Log Fold Change
EYA4	-0.768
C9ORF38	-0.773
FAM129A	-0.777
HS.184721	-0.777
LATS2	-0.799
LOC652330	-0.801
LOC727987	-0.809
SLIT2	-0.809
C3ORF34	-0.818
UHMK1	-0.830
PHAX	-0.831
HS.572444	-0.832
RNU1F1	-0.845
TRQ1	-0.847
ZMAT3	-0.853
HIPK2	-0.866
TNFAIP8L1	-0.899
RNU1-3	-0.905
RNU1A3	-0.927
RNU1G2	-0.939
MIR886	-1.034
RNU4ATAC	-1.053
LOC100130516	-1.077
VTRNA1-1	-1.108
TRK1	-1.116
RNU1-5	-1.183
TDP1	-1.316
LOC100130835	-1.355
MIR1974	-1.570
RNY1	-1.702
SNORD13	-1.778
BCYRN1	-1.779
HS.579631	-1.965
HS.543887	-2.090

Bibliography

1. Acheva, A., et al., *Mechanisms of DNA damage response to targeted irradiation in organotypic 3D skin cultures*. PLoS One, 2014. **9**(2): p. e86092.
2. Adamson, I.Y. and D.H. Bowden, *The type 2 cell as progenitor of alveolar epithelial regeneration. A cytodynamic study in mice after exposure to oxygen*. Lab Invest, 1974. **30**(1): p. 35-42.
3. Administration, F.a.D., *Ethyol® (amifostine) for injection*, U.S.D.o.H.H. Services, Editor. 1999.
4. Administration, F.a.D., *Palifermin (Keratinocyte Growth Factor)*, U.S.D.o.H.H. Services, Editor. 2004.
5. Ahmad, I.U., et al., *Soy isoflavones in conjunction with radiation therapy in patients with prostate cancer*. Nutr Cancer, 2010. **62**(7): p. 996-1000.
6. Alberg, A.J., et al., *Epidemiology of lung cancer: ACCP evidence-based clinical practice guidelines (2nd edition)*. Chest, 2007. **132**(3 Suppl): p. 29S-55S.
7. Alok, A., J.S. Adhikari, and N.K. Chaudhury, *Radioprotective role of clinical drug diclofenac sodium*. Mutat Res, 2013. **755**(2): p. 156-62.
8. Amati, B., *Integrating Myc and TGF-beta signalling in cell-cycle control*. Nat Cell Biol, 2001. **3**(5): p. E112-3.
9. Andreassen, C.N., C. Grau, and J.C. Lindegaard, *Chemical radioprotection: a critical review of amifostine as a cytoprotector in radiotherapy*. Semin Radiat Oncol, 2003. **13**(1): p. 62-72.
10. Asaithamby, A., et al., *Irreparable complex DNA double-strand breaks induce chromosome breakage in organotypic three-dimensional human lung epithelial cell culture*. Nucleic Acids Res, 2011. **39**(13): p. 5474-88.
11. Bals, R., et al., *Isolation and air-liquid interface culture of human large airway and bronchiolar epithelial cells*. J Cyst Fibros, 2004. **3 Suppl 2**: p. 49-51.
12. Beaven, A.W. and T.C. Shea, *Recombinant human keratinocyte growth factor palifermin reduces oral mucositis and improves patient outcomes after stem cell transplant*. Drugs Today (Barc), 2007. **43**(7): p. 461-73.
13. Bernardes de Jesus, B., et al., *The telomerase activator TA-65 elongates short telomeres and increases health span of adult/old mice without increasing cancer incidence*. Aging Cell, 2011. **10**(4): p. 604-21.
14. Bernier, J., E.J. Hall, and A. Giaccia, *Radiation oncology: a century of achievements*. Nat Rev Cancer, 2004. **4**(9): p. 737-47.
15. Bhatia, S., et al., *Breast cancer and other second neoplasms after childhood Hodgkin's disease*. N Engl J Med, 1996. **334**(12): p. 745-51.
16. Bickley, L.S., *Bates' Guide to Physical Examination and History-Taking*. Eleventh ed. 2012: Wolters Kluwer Health; Lippincott Williams & Wilkins.
17. Blenkinsopp, W.K., *Proliferation of respiratory tract epithelium in the rat*. Exp Cell Res, 1967. **46**(1): p. 144-54.
18. Bonanno, L., A. Favaretto, and R. Rosell, *Platinum drugs and DNA repair mechanisms in lung cancer*. Anticancer Res, 2014. **34**(1): p. 493-501.
19. Borek, C., et al., *Selenium and vitamin E inhibit radiogenic and chemically induced transformation in vitro via different mechanisms*. Proc Natl Acad Sci U S A, 1986. **83**(5): p. 1490-4.

20. Brambilla, E., et al., *Alterations of expression of Rb, p16(INK4A) and cyclin D1 in non-small cell lung carcinoma and their clinical significance*. J Pathol, 1999. **188**(4): p. 351-60.
21. Brauch, H., et al., *Molecular analysis of the short arm of chromosome 3 in small-cell and non-small-cell carcinoma of the lung*. N Engl J Med, 1987. **317**(18): p. 1109-13.
22. Brown, E.R. and F.A. Shepherd, *Erlotinib in the treatment of non-small cell lung cancer*. Expert Rev Anticancer Ther, 2005. **5**(5): p. 767-75.
23. Caddeo, C., et al., *Effect of resveratrol incorporated in liposomes on proliferation and UV-B protection of cells*. Int J Pharm, 2008. **363**(1-2): p. 183-91.
24. Calveley, V.L., et al., *Genistein can mitigate the effect of radiation on rat lung tissue*. Radiat Res, 2010. **173**(5): p. 602-11.
25. Cardoso, W.V. and J. Lu, *Regulation of early lung morphogenesis: questions, facts and controversies*. Development, 2006. **133**(9): p. 1611-24.
26. Carsten, R.E., et al., *Resveratrol reduces radiation-induced chromosome aberration frequencies in mouse bone marrow cells*. Radiat Res, 2008. **169**(6): p. 633-8.
27. Casas, F. and N. Vinolas, *Toxicity of small cell lung cancer treatment*. Hematol Oncol Clin North Am, 2004. **18**(2): p. 461-81.
28. Cavalheiro, G.R., et al., *c-Myc regulates cell proliferation during lens development*. PLoS One, 2014. **9**(2): p. e87182.
29. Chen, B.J., et al., *Small molecules targeting c-Myc oncogene: promising anti-cancer therapeutics*. Int J Biol Sci, 2014. **10**(10): p. 1084-96.
30. Chiba, I., et al., *Mutations in the p53 gene are frequent in primary, resected non-small cell lung cancer. Lung Cancer Study Group*. Oncogene, 1990. **5**(10): p. 1603-10.
31. Chomienne, C., et al., *Structure-activity relationships of aromatic retinoids on the differentiation of the human histiocytic lymphoma cell line U-937*. Leuk Res, 1986. **10**(11): p. 1301-5.
32. Chomienne, C., et al., *All-trans retinoic acid in acute promyelocytic leukemias. II. In vitro studies: structure-function relationship*. Blood, 1990. **76**(9): p. 1710-7.
33. Cooper, W.A., et al., *Molecular biology of lung cancer*. J Thorac Dis, 2013. **5 Suppl 5**: p. S479-90.
34. Cronkite, E.P., R.A. Conard, and V.P. Bond, *Historical events associated with fallout from Bravo Shot--Operation Castle and 25 Y of medical findings*. Health Phys, 1997. **73**(1): p. 176-86.
35. Crystal, R.G., et al., *Airway epithelial cells: current concepts and challenges*. Proc Am Thorac Soc, 2008. **5**(7): p. 772-7.
36. Cucinotta, F.A. and L.J. Chappell, *Updates to astronaut radiation limits: radiation risks for never-smokers*. Radiat Res, 2011. **176**(1): p. 102-14.
37. Cucinotta, F.A., et al., *Radiation carcinogenesis risk assessments for never-smokers*. Health Phys, 2012. **103**(5): p. 643-51.
38. Cucinotta, F.A., et al., *Space radiation cancer risks and uncertainties for Mars missions*. Radiat Res, 2001. **156**(5 Pt 2): p. 682-8.
39. Dahabreh, I.J., et al., *Somatic EGFR mutation and gene copy gain as predictive biomarkers for response to tyrosine kinase inhibitors in non-small cell lung cancer*. Clin Cancer Res, 2010. **16**(1): p. 291-303.

40. Daroczi, B., et al., *Nuclear factor kappaB inhibitors alleviate and the proteasome inhibitor PS-341 exacerbates radiation toxicity in zebrafish embryos*. Mol Cancer Ther, 2009. **8**(9): p. 2625-34.
41. Day, R.M., et al., *Genistein protects against biomarkers of delayed lung sequelae in mice surviving high-dose total body irradiation*. J Radiat Res, 2008. **49**(4): p. 361-72.
42. Day, R.M., et al., *Enhanced hematopoietic protection from radiation by the combination of genistein and captopril*. Int Immunopharmacol, 2013. **15**(2): p. 348-56.
43. De Bruin, M.L., et al., *Breast cancer risk in female survivors of Hodgkin's lymphoma: lower risk after smaller radiation volumes*. J Clin Oncol, 2009. **27**(26): p. 4239-46.
44. Delgado, O., et al., *Multipotent capacity of immortalized human bronchial epithelial cells*. PLoS One, 2011. **6**(7): p. e22023.
45. Denman, A.R., et al., *Assessment of health risks to skin and lung of elevated radon levels in abandoned mines*. Health Phys, 2003. **85**(6): p. 733-9.
46. di Masi, A., et al., *Retinoic acid receptors: from molecular mechanisms to cancer therapy*. Mol Aspects Med, 2015. **41**: p. 1-115.
47. Downward, J., *Targeting RAS signalling pathways in cancer therapy*. Nat Rev Cancer, 2003. **3**(1): p. 11-22.
48. Du, P., W.A. Kibbe, and S.M. Lin, *lumi: a pipeline for processing Illumina microarray*. Bioinformatics, 2008. **24**(13): p. 1547-8.
49. Duchesne, G.M. and L.K. Hutchinson, *Reversible changes in radiation response induced by all-trans retinoic acid*. Int J Radiat Oncol Biol Phys, 1995. **33**(4): p. 875-80.
50. Durante, M. and F.A. Cucinotta, *Heavy ion carcinogenesis and human space exploration*. Nat Rev Cancer, 2008. **8**(6): p. 465-72.
51. Eferl, R. and E.F. Wagner, *AP-1: a double-edged sword in tumorigenesis*. Nat Rev Cancer, 2003. **3**(11): p. 859-68.
52. Eskiocak, U., et al., *CDDO-Me protects against space radiation-induced transformation of human colon epithelial cells*. Radiat Res, 2010. **174**(1): p. 27-36.
53. Evans, M.J., et al., *Role of nonciliated cells in renewal of the bronchial epithelium of rats exposed to NO2*. Am J Pathol, 1986. **123**(1): p. 126-33.
54. Fedorocko, P. and N.O. Mackova, *Combined modality radioprotection: enhancement of survival and hematopoietic recovery in gamma-irradiated mice by the joint use of liposomal muramyl tripeptide phosphatidylethanolamine (MTP-PE) and indomethacin*. Int J Immunopharmacol, 1996. **18**(5): p. 329-37.
55. Feld, R., et al., *Use of the epidermal growth factor receptor inhibitors gefitinib and erlotinib in the treatment of non-small cell lung cancer: a systematic review*. J Thorac Oncol, 2006. **1**(4): p. 367-76.
56. Fenech, M. and A.A. Morley, *Cytokinesis-block micronucleus method in human lymphocytes: effect of in vivo ageing and low dose X-irradiation*. Mutat Res, 1986. **161**(2): p. 193-8.
57. Ferdinand, R., et al., *Treatments for chronic myeloid leukemia: a qualitative systematic review*. J Blood Med, 2012. **3**: p. 51-76.
58. Ferrara, N., et al., *Discovery and development of bevacizumab, an anti-VEGF antibody for treating cancer*. Nat Rev Drug Discov, 2004. **3**(5): p. 391-400.
59. Fessart, D., H. Begueret, and F. Delom, *3D culture model to distinguish normal from malignant human bronchial epithelial cells*. Eur Respir J, 2013.

60. Forbes, S.A., et al., *COSMIC: exploring the world's knowledge of somatic mutations in human cancer*. Nucleic Acids Res, 2015. **43**(Database issue): p. D805-11.
61. Fortune, *Cancer: The Great Darkness*, in *Fortune*. 1937, Doubleday, Doran.
62. Franzdottir, S.R., et al., *Airway branching morphogenesis in three dimensional culture*. Respir Res, 2010. **11**: p. 162.
63. Freemantle, S.J., K.H. Dragnev, and E. Dmitrovsky, *The retinoic acid paradox in cancer chemoprevention*. J Natl Cancer Inst, 2006. **98**(7): p. 426-7.
64. Fritz, H., et al., *Vitamin A and retinoid derivatives for lung cancer: a systematic review and meta analysis*. PLoS One, 2011. **6**(6): p. e21107.
65. Furuta, Y., et al., *Increase in radioresponse of murine tumors by treatment with indomethacin*. Cancer Res, 1988. **48**(11): p. 3008-13.
66. Gadgeel, S.M., S.S. Ramalingam, and G.P. Kalemkerian, *Treatment of lung cancer*. Radiol Clin North Am, 2012. **50**(5): p. 961-74.
67. Gentleman, R.C., et al., *Bioconductor: open software development for computational biology and bioinformatics*. Genome Biol, 2004. **5**(10): p. R80.
68. Giangreco, A., S.D. Reynolds, and B.R. Stripp, *Terminal bronchioles harbor a unique airway stem cell population that localizes to the bronchoalveolar duct junction*. Am J Pathol, 2002. **161**(1): p. 173-82.
69. Goldberg, R.I., *Protection of irradiated parotid by prostaglandin synthesis inhibitors*. J Am Dent Assoc, 1986. **112**(2): p. 179-81.
70. Grdina, D.J., et al., *Protection against late effects of radiation by S-2-(3-aminopropylamino)-ethylphosphorothioic acid*. Cancer Res, 1991. **51**(16): p. 4125-30.
71. Grdina, D.J., B.J. Wright, and B.A. Carnes, *Protection by WR-151327 against late-effect damage from fission-spectrum neutrons*. Radiat Res, 1991. **128**(1 Suppl): p. S124-7.
72. Greulich, H., et al., *Oncogenic transformation by inhibitor-sensitive and -resistant EGFR mutants*. PLoS Med, 2005. **2**(11): p. e313.
73. Gyori, B.M., et al., *OpenComet: An automated tool for comet assay image analysis*. Redox Biol, 2014. **2**: p. 457-65.
74. Hafer, K., L. Rivina, and R.H. Schiestl, *Cell cycle dependence of ionizing radiation-induced DNA deletions and antioxidant radioprotection in Saccharomyces cerevisiae*. Radiat Res, 2010. **173**(6): p. 802-8.
75. Hafer, K., Y. Rivina, and R.H. Schiestl, *Yeast DEL assay detects protection against radiation-induced cytotoxicity and genotoxicity: adaptation of a microtiter plate version*. Radiat Res, 2010. **174**(6): p. 719-26.
76. Hagiwara, S.I., Y. Ishii, and S. Kitamura, *Aerosolized administration of N-acetylcysteine attenuates lung fibrosis induced by bleomycin in mice*. Am J Respir Crit Care Med, 2000. **162**(1): p. 225-31.
77. Hall EJ, G.A., *Radiobiology for the Radiobiologist*. 6th ed. 2006: Lippincott Williams & Wilkins.
78. Hall, E.J. and C.S. Wuu, *Radiation-induced second cancers: the impact of 3D-CRT and IMRT*. Int J Radiat Oncol Biol Phys, 2003. **56**(1): p. 83-8.
79. Hanahan, D. and R.A. Weinberg, *Hallmarks of cancer: the next generation*. Cell, 2011. **144**(5): p. 646-74.
80. Harley, C.B., et al., *A natural product telomerase activator as part of a health maintenance program*. Rejuvenation Res, 2011. **14**(1): p. 45-56.

81. Hershman, J.M., et al., *Prevention of DNA double-strand breaks induced by radioiodide-(131)I in FRTL-5 thyroid cells*. Endocrinology, 2011. **152**(3): p. 1130-5.
82. Hirsch, F.R., et al., *Epidermal growth factor receptor in non-small-cell lung carcinomas: correlation between gene copy number and protein expression and impact on prognosis*. J Clin Oncol, 2003. **21**(20): p. 3798-807.
83. Honda, T., et al., *Tricyclic compounds containing nonenolizable cyano enones. A novel class of highly potent anti-inflammatory and cytoprotective agents*. J Med Chem, 2011. **54**(6): p. 1762-78.
84. Hong, D.S., et al., *A phase I first-in-human trial of bardoxolone methyl in patients with advanced solid tumors and lymphomas*. Clin Cancer Res, 2012. **18**(12): p. 3396-406.
85. Hong, W.K., et al., *13-cis-retinoic acid in the treatment of oral leukoplakia*. N Engl J Med, 1986. **315**(24): p. 1501-5.
86. Hontzeas, N., K. Hafer, and R.H. Schiestl, *Development of a microtiter plate version of the yeast DEL assay amenable to high-throughput toxicity screening of chemical libraries*. Mutat Res, 2007. **634**(1-2): p. 228-34.
87. Hosseinimehr, S.J., A. Mahmoudzadeh, and S. Akhlagpour, *Captopril protects mice bone marrow cells against genotoxicity induced by gamma irradiation*. Cell Biochem Funct, 2007. **25**(4): p. 389-94.
88. Husgafvel-Pursiainen, K., et al., *p53 mutations and exposure to environmental tobacco smoke in a multicenter study on lung cancer*. Cancer Res, 2000. **60**(11): p. 2906-11.
89. Iggo, R., et al., *Increased expression of mutant forms of p53 oncogene in primary lung cancer*. Lancet, 1990. **335**(8691): p. 675-9.
90. Institute, N.C. *Lung Cancer*. 2015 [cited 2015; Available from: http://www.cancer.gov.
91. J Minna, A.G., *NSCLC full exon sequencing*, M.E.-A. J Shay, Editor. 2012.
92. Jin, C., D. Zhou, and F. Lv, *Beneficial effects of early (but not late) intervention of heme oxygenase-1 on bleomycin-induced pulmonary fibrosis in mice*. Respir Physiol Neurobiol, 2011. **175**(2): p. 239-46.
93. Kaisani, A., et al., *Branching morphogenesis of immortalized human bronchial epithelial cells in three-dimensional culture*. Differentiation, 2014. **87**(3-4): p. 119-26.
94. Karbownik, M. and R.J. Reiter, *Antioxidative effects of melatonin in protection against cellular damage caused by ionizing radiation*. Proc Soc Exp Biol Med, 2000. **225**(1): p. 9-22.
95. Kaul, A., H. Landfermann, and M. Thieme, *One decade after Chernobyl: summing up the consequences*. Health Phys, 1996. **71**(5): p. 634-40.
96. Keith, R.L. and Y.E. Miller, *Lung cancer chemoprevention: current status and future prospects*. Nat Rev Clin Oncol, 2013. **10**(6): p. 334-43.
97. Kim, H.S., et al., *SIRT2 maintains genome integrity and suppresses tumorigenesis through regulating APC/C activity*. Cancer Cell, 2011. **20**(4): p. 487-99.
98. Kim, K., et al., *High throughput screening of small molecule libraries for modifiers of radiation responses*. Int J Radiat Biol, 2011. **87**(8): p. 839-45.
99. Kim, S.B., et al., *Targeting of Nrf2 induces DNA damage signaling and protects colonic epithelial cells from ionizing radiation*. Proc Natl Acad Sci U S A, 2012. **109**(43): p. E2949-55.
100. Kim, Y.H., et al., *Radiation promotes malignant progression of glioma cells through HIF-1alpha stabilization*. Cancer Lett, 2014. **354**(1): p. 132-41.

101. Kimura, J. and G.H. Deutsch, *Key mechanisms of early lung development*. Pediatr Dev Pathol, 2007. **10**(5): p. 335-47.
102. Kolde, R., *pheatmap: Pretty Heatmaps*. 2013.
103. Kong, F.M., et al., *Non-small cell lung cancer therapy-related pulmonary toxicity: an update on radiation pneumonitis and fibrosis*. Semin Oncol, 2005. **32**(2 Suppl 3): p. S42-54.
104. Kosaka, T., et al., *Mutations of the epidermal growth factor receptor gene in lung cancer: biological and clinical implications*. Cancer Res, 2004. **64**(24): p. 8919-23.
105. Koukourakis, M.I., et al., *Amifostine induces anaerobic metabolism and hypoxia-inducible factor 1 alpha*. Cancer Chemother Pharmacol, 2004. **53**(1): p. 8-14.
106. Kozubik, A., M. Pospisil, and J. Netikova, *Enhancement of haemopoietic recovery in sublethally gamma-irradiated mice by the joint use of indomethacin and cystamine*. Folia Biol (Praha), 1990. **36**(6): p. 291-300.
107. Kris, M.G., et al., *Efficacy of gefitinib, an inhibitor of the epidermal growth factor receptor tyrosine kinase, in symptomatic patients with non-small cell lung cancer: a randomized trial*. JAMA, 2003. **290**(16): p. 2149-58.
108. KS Pollard, H.G., Y Ge, S Taylor, S Dudoit, *multtest: Resampling-based multiple hypothesis testing*.
109. Ku, W.W., et al., *Genetic toxicity assessment: employing the best science for human safety evaluation Part VII: Why not start with a single test: a transformational alternative to genotoxicity hazard and risk assessment*. Toxicol Sci, 2007. **99**(1): p. 20-5.
110. Kuntic, V.S., et al., *Radioprotectors - the evergreen topic*. Chem Biodivers, 2013. **10**(10): p. 1791-803.
111. Lamson, D.W. and M.S. Brignall, *Antioxidants in cancer therapy; their actions and interactions with oncologic therapies*. Altern Med Rev, 1999. **4**(5): p. 304-29.
112. Landauer, M.R., et al., *Behavioral toxicity of selected radioprotectors*. Adv Space Res, 1992. **12**(2-3): p. 273-83.
113. Lane, D.P., *Cancer. p53, guardian of the genome*. Nature, 1992. **358**(6381): p. 15-6.
114. Larsen, J.E. and J.D. Minna, *Molecular biology of lung cancer: clinical implications*. Clin Chest Med, 2011. **32**(4): p. 703-40.
115. Lazzaro, D., et al., *The transcription factor TTF-1 is expressed at the onset of thyroid and lung morphogenesis and in restricted regions of the foetal brain*. Development, 1991. **113**(4): p. 1093-104.
116. Le Calvez, F., et al., *TP53 and KRAS mutation load and types in lung cancers in relation to tobacco smoke: distinct patterns in never, former, and current smokers*. Cancer Res, 2005. **65**(12): p. 5076-83.
117. Lee, G.Y., et al., *Three-dimensional culture models of normal and malignant breast epithelial cells*. Nat Methods, 2007. **4**(4): p. 359-65.
118. Lee, T.K. and I. Stupans, *Radioprotection: the non-steroidal anti-inflammatory drugs (NSAIDs) and prostaglandins*. J Pharm Pharmacol, 2002. **54**(11): p. 1435-45.
119. Levine, A.J., *p53, the cellular gatekeeper for growth and division*. Cell, 1997. **88**(3): p. 323-31.
120. Levy, S. and H.J. Forman, *C-Myc is a Nrf2-interacting protein that negatively regulates phase II genes through their electrophile responsive elements*. IUBMB Life, 2010. **62**(3): p. 237-46.

121. Li, F.P. and J.F. Fraumeni, Jr., *Soft-tissue sarcomas, breast cancer, and other neoplasms. A familial syndrome?* Ann Intern Med, 1969. **71**(4): p. 747-52.
122. Liby, K., et al., *The synthetic triterpenoids, CDDO and CDDO-imidazolide, are potent inducers of heme oxygenase-1 and Nrf2/ARE signaling*. Cancer Res, 2005. **65**(11): p. 4789-98.
123. Liby, K., et al., *Triterpenoids CDDO-methyl ester or CDDO-ethyl amide and rexinoids LG100268 or NRX194204 for prevention and treatment of lung cancer in mice*. Cancer Prev Res (Phila), 2009. **2**(12): p. 1050-8.
124. Liby, K., et al., *Prevention and treatment of experimental estrogen receptor-negative mammary carcinogenesis by the synthetic triterpenoid CDDO-methyl Ester and the rexinoid LG100268*. Clin Cancer Res, 2008. **14**(14): p. 4556-63.
125. Liby, K., et al., *The synthetic triterpenoids CDDO-methyl ester and CDDO-ethyl amide prevent lung cancer induced by vinyl carbamate in A/J mice*. Cancer Res, 2007. **67**(6): p. 2414-9.
126. Liby, K.T., *Synthetic triterpenoids can protect against toxicity without reducing the efficacy of treatment with Carboplatin and Paclitaxel in experimental lung cancer*. Dose Response, 2014. **12**(1): p. 136-51.
127. Liby, K.T., et al., *Synthetic triterpenoids prolong survival in a transgenic mouse model of pancreatic cancer*. Cancer Prev Res (Phila), 2010. **3**(11): p. 1427-34.
128. Liby, K.T. and M.B. Sporn, *Synthetic oleanane triterpenoids: multifunctional drugs with a broad range of applications for prevention and treatment of chronic disease*. Pharmacol Rev, 2012. **64**(4): p. 972-1003.
129. Liby, K.T., M.M. Yore, and M.B. Sporn, *Triterpenoids and rexinoids as multifunctional agents for the prevention and treatment of cancer*. Nat Rev Cancer, 2007. **7**(5): p. 357-69.
130. Lippman, S.M., et al., *Randomized phase III intergroup trial of isotretinoin to prevent second primary tumors in stage I non-small-cell lung cancer*. J Natl Cancer Inst, 2001. **93**(8): p. 605-18.
131. Little, M.P., *Cancer and non-cancer effects in Japanese atomic bomb survivors*. J Radiol Prot, 2009. **29**(2A): p. A43-59.
132. Luo, H., et al., *Resveratrol enhances ionizing radiation-induced premature senescence in lung cancer cells*. Int J Oncol, 2013. **43**(6): p. 1999-2006.
133. Maeda, Y., V. Dave, and J.A. Whitsett, *Transcriptional control of lung morphogenesis*. Physiol Rev, 2007. **87**(1): p. 219-44.
134. Mailleux, A.A., et al., *Evidence that SPROUTY2 functions as an inhibitor of mouse embryonic lung growth and morphogenesis*. Mech Dev, 2001. **102**(1-2): p. 81-94.
135. Malkin, D., et al., *Germ line p53 mutations in a familial syndrome of breast cancer, sarcomas, and other neoplasms*. Science, 1990. **250**(4985): p. 1233-8.
136. McDonnell, A.M. and K.L. Lenz, *Palifermin: role in the prevention of chemotherapy- and radiation-induced mucositis*. Ann Pharmacother, 2007. **41**(1): p. 86-94.
137. Meadows, A.T., J.A. Gallagher, and G.R. Bunin, *Late effects of early childhood cancer therapy*. Br J Cancer Suppl, 1992. **18**: p. S92-5.
138. Meng, D., et al., *Prognostic value of K-RAS mutations in patients with non-small cell lung cancer: a systematic review with meta-analysis*. Lung Cancer, 2013. **81**(1): p. 1-10.
139. Milas, L., et al., *Inhibition of radiation carcinogenesis in mice by S-2-(3-aminopropylamino)-ethylphosphorothioic acid*. Cancer Res, 1984. **44**(12 Pt 1): p. 5567-9.

140. Miller, R.C., J.S. Murley, and D.J. Grdina, *Metformin exhibits radiation countermeasures efficacy when used alone or in combination with sulfhydryl containing drugs*. Radiat Res, 2014. **181**(5): p. 464-70.
141. Mitsuishi, Y., H. Motohashi, and M. Yamamoto, *The Keap1-Nrf2 system in cancers: stress response and anabolic metabolism*. Front Oncol, 2012. **2**: p. 200.
142. Molgora, B., et al., *Functional assessment of pharmacological telomerase activators in human T cells*. Cells, 2013. **2**(1): p. 57-66.
143. Morrisey, E.E. and B.L. Hogan, *Preparing for the first breath: genetic and cellular mechanisms in lung development*. Dev Cell, 2010. **18**(1): p. 8-23.
144. Nambiar, D., P. Rajamani, and R.P. Singh, *Effects of phytochemicals on ionization radiation-mediated carcinogenesis and cancer therapy*. Mutat Res, 2011. **728**(3): p. 139-57.
145. Nateri, A.S., B. Spencer-Dene, and A. Behrens, *Interaction of phosphorylated c-Jun with TCF4 regulates intestinal cancer development*. Nature, 2005. **437**(7056): p. 281-5.
146. National Lung Screening Trial Research, T., et al., *Reduced lung-cancer mortality with low-dose computed tomographic screening*. N Engl J Med, 2011. **365**(5): p. 395-409.
147. Netter, F.H., *Atlas of Human Anatomy*. 6th ed. Netter Basic Science. 2014: Saunders Elsevier Inc.
148. Newhauser, W.D. and M. Durante, *Assessing the risk of second malignancies after modern radiotherapy*. Nat Rev Cancer, 2011. **11**(6): p. 438-48.
149. Nicolatou-Galitis, O., et al., *Systematic review of amifostine for the management of oral mucositis in cancer patients*. Support Care Cancer, 2013. **21**(1): p. 357-64.
150. Northway, M.G., et al., *Radiation esophagitis in the opossum: radioprotection with indomethacin*. Gastroenterology, 1980. **78**(5 Pt 1): p. 883-92.
151. Okabe, T., et al., *Differential constitutive activation of the epidermal growth factor receptor in non-small cell lung cancer cells bearing EGFR gene mutation and amplification*. Cancer Res, 2007. **67**(5): p. 2046-53.
152. Oken, M.M., et al., *Screening by chest radiograph and lung cancer mortality: the Prostate, Lung, Colorectal, and Ovarian (PLCO) randomized trial*. JAMA, 2011. **306**(17): p. 1865-73.
153. Pageau, S.C., et al., *The effect of stromal components on the modulation of the phenotype of human bronchial epithelial cells in 3D culture*. Biomaterials, 2011. **32**(29): p. 7169-80.
154. Pandey, K.B. and S.I. Rizvi, *Plant polyphenols as dietary antioxidants in human health and disease*. Oxid Med Cell Longev, 2009. **2**(5): p. 270-8.
155. Pearce, M.S., et al., *Radiation exposure from CT scans in childhood and subsequent risk of leukaemia and brain tumours: a retrospective cohort study*. Lancet, 2012. **380**(9840): p. 499-505.
156. Pergola, P.E., et al., *Bardoxolone methyl and kidney function in CKD with type 2 diabetes*. N Engl J Med, 2011. **365**(4): p. 327-36.
157. Perl, M., et al., *Pathogenesis of indirect (secondary) acute lung injury*. Expert Rev Respir Med, 2011. **5**(1): p. 115-26.
158. Pike, M.C. and T. Alper, *A Method for Determining Dose-Modification Factors*. Br J Radiol, 1964. **37**: p. 458-62.
159. Pillsbury, H.C., 3rd, W.P. Webster, and J. Rosenman, *Prostaglandin inhibitor and radiotherapy in advanced head and neck cancers*. Arch Otolaryngol Head Neck Surg, 1986. **112**(5): p. 552-3.

160. Pirker, R., et al., *Cetuximab plus chemotherapy in patients with advanced non-small-cell lung cancer (FLEX): an open-label randomised phase III trial*. Lancet, 2009. **373**(9674): p. 1525-31.
161. Pirola, L. and S. Frojdo, *Resveratrol: one molecule, many targets*. IUBMB Life, 2008. **60**(5): p. 323-32.
162. Prasanna, P.G., et al., *Normal tissue protection for improving radiotherapy: Where are the Gaps?* Transl Cancer Res, 2012. **1**(1): p. 35-48.
163. Predrag Slijepcevic, G.J., *Investigation of Radioprotective Effects of TA-65 in Human Lymphocytes*, J. Shay, Editor.
164. Presta, L.G., et al., *Humanization of an anti-vascular endothelial growth factor monoclonal antibody for the therapy of solid tumors and other disorders*. Cancer Res, 1997. **57**(20): p. 4593-9.
165. Preston, D.L., et al., *Solid cancer incidence in atomic bomb survivors: 1958-1998*. Radiat Res, 2007. **168**(1): p. 1-64.
166. Probst, B., *Keap1 mutations in cancer cells*, M.E.-A. J Shay, Editor. 2013.
167. R. Tibshirani, G.C., B. Narasimhan and J. Li *samr: SAM: Significance Analysis of Microarrays*. 2011.
168. Radford, E.P., *Human health effects of low doses of ionizing radiation: the BEIR III controversy*. Radiat Res, 1980. **84**(3): p. 369-94.
169. Radiation., U.N.S.C.o.t.E.o.A., *Sources and effects of ionizing radiation*. Vol. 1 & 2. 2000: United Nations Publications.
170. Radvansky, L.J., M.B. Pace, and A. Siddiqui, *Prevention and management of radiation-induced dermatitis, mucositis, and xerostomia*. Am J Health Syst Pharm, 2013. **70**(12): p. 1025-32.
171. Ramirez, R.D., et al., *Immortalization of human bronchial epithelial cells in the absence of viral oncoproteins*. Cancer Res, 2004. **64**(24): p. 9027-34.
172. Ramos-Gomez, M., et al., *Sensitivity to carcinogenesis is increased and chemoprotective efficacy of enzyme inducers is lost in nrf2 transcription factor-deficient mice*. Proc Natl Acad Sci U S A, 2001. **98**(6): p. 3410-5.
173. Rawlins, E.L. and B.L. Hogan, *Epithelial stem cells of the lung: privileged few or opportunities for many?* Development, 2006. **133**(13): p. 2455-65.
174. Rawlins, E.L., et al., *The role of Scgb1a1+ Clara cells in the long-term maintenance and repair of lung airway, but not alveolar, epithelium*. Cell Stem Cell, 2009. **4**(6): p. 525-34.
175. Rawlins, E.L., et al., *Lung development and repair: contribution of the ciliated lineage*. Proc Natl Acad Sci U S A, 2007. **104**(2): p. 410-7.
176. Ray, P.D., B.W. Huang, and Y. Tsuji, *Reactive oxygen species (ROS) homeostasis and redox regulation in cellular signaling*. Cell Signal, 2012. **24**(5): p. 981-90.
177. Revesz, L. and B. Palcic, *Radiation dose dependence of the sensitization by oxygen and oxygen mimic sensitizers*. Acta Radiol Oncol, 1985. **24**(3): p. 209-17.
178. Rivina, Y., *Discovery and Characterization of Radiation Mitigator Yel002*, in *Molecular Toxicology*. 2013, UCLA.
179. Robert H. Schiestl, L.R., Alexandra Miller, Wei Chen, Mo Kang,, *Novel Therapeutic Compounds Yel001 and Yel002 Mitigate Radiation-induced Toxicity*, J.S. Mariam El-Ashmawy, Editor. 2012.
180. Rock, J.R. and B.L. Hogan, *Epithelial progenitor cells in lung development, maintenance, repair, and disease*. Annu Rev Cell Dev Biol, 2011. **27**: p. 493-512.

181. Rock, J.R., S.H. Randell, and B.L. Hogan, *Airway basal stem cells: a perspective on their roles in epithelial homeostasis and remodeling*. Dis Model Mech, 2010. **3**(9-10): p. 545-56.
182. Ryan, J.L., et al., *Decreasing the adverse effects of cancer therapy: an NCI Workshop on the preclinical development of radiation injury mitigators/protectors*. Radiat Res, 2011. **176**(5): p. 688-91.
183. Sadler, T., *Langman's Medical Embryology*. 13th ed. 2014: Lippincott Wolters Kluwer.
184. Sakai, T., M. Larsen, and K.M. Yamada, *Fibronectin requirement in branching morphogenesis*. Nature, 2003. **423**(6942): p. 876-81.
185. Sarma, L. and P.C. Kesavan, *Protective effects of vitamins C and E against gamma-ray-induced chromosomal damage in mouse*. Int J Radiat Biol, 1993. **63**(6): p. 759-64.
186. Sarna, L., et al., *Clinically meaningful differences in patient-reported outcomes with amifostine in combination with chemoradiation for locally advanced non-small-cell lung cancer: an analysis of RTOG 9801*. Int J Radiat Oncol Biol Phys, 2008. **72**(5): p. 1378-84.
187. Sato, M., Lee, W., Girard, L., Xie, Y., Xie, X-J., Yan, J., Smith, A.L., Shames, D.S., Ramirez, R.D., Gazdar, A.F., Shay, and J.W., Minna, J.D. *The Combination of Five Changes (Telomerase, p16/Rb Bypass, p53 Knockdown, Mutant KRASV12, c-Myc) Together With Serum-induced Epithelial Mesenchymal Transition Progresses Normal Human Bronchial Epithelial Cells to Full Malignancy*. . 2009. University of Texas Southwestern Medical Center in Dallas.
188. Sato, M., et al., *Multiple oncogenic changes (K-RAS(V12), p53 knockdown, mutant EGFRs, p16 bypass, telomerase) are not sufficient to confer a full malignant phenotype on human bronchial epithelial cells*. Cancer Res, 2006. **66**(4): p. 2116-28.
189. Scagliotti, G.V., et al., *The biology of epidermal growth factor receptor in lung cancer*. Clin Cancer Res, 2004. **10**(12 Pt 2): p. 4227s-4232s.
190. Scarlatti, F., et al., *Resveratrol sensitization of DU145 prostate cancer cells to ionizing radiation is associated to ceramide increase*. Cancer Lett, 2007. **253**(1): p. 124-30.
191. Seifter, E., et al., *Role of vitamin A and beta carotene in radiation protection: relation to antioxidant properties*. Pharmacol Ther, 1988. **39**(1-3): p. 357-65.
192. Sekine, K., et al., *Fgf10 is essential for limb and lung formation*. Nat Genet, 1999. **21**(1): p. 138-41.
193. Shamir, E.R. and A.J. Ewald, *Three-dimensional organotypic culture: experimental models of mammalian biology and disease*. Nat Rev Mol Cell Biol, 2014. **15**(10): p. 647-64.
194. Shankar, S., G. Singh, and R.K. Srivastava, *Chemoprevention by resveratrol: molecular mechanisms and therapeutic potential*. Frontiers in bioscience : a journal and virtual library, 2007. **12**: p. 4839-54.
195. Shanmugam, M.K., et al., *Oleanolic acid and its synthetic derivatives for the prevention and therapy of cancer: preclinical and clinical evidence*. Cancer Lett, 2014. **346**(2): p. 206-16.
196. Shaw, A.T., et al., *Crizotinib versus chemotherapy in advanced ALK-positive lung cancer*. N Engl J Med, 2013. **368**(25): p. 2385-94.
197. Shaw, L.M., H. Bonner, and R. Lieberman, *Pharmacokinetic profile of amifostine*. Semin Oncol, 1996. **23**(4 Suppl 8): p. 18-22.

198. Shay, J.W., et al., *Spontaneous in vitro immortalization of breast epithelial cells from a patient with Li-Fraumeni syndrome*. Mol Cell Biol, 1995. **15**(1): p. 425-32.
199. Shay, J.W., et al., *The frequency of immortalization of human fibroblasts and mammary epithelial cells transfected with SV40 large T-antigen*. Exp Cell Res, 1993. **209**(1): p. 45-52.
200. Shepherd, F.A., et al., *Erlotinib in previously treated non-small-cell lung cancer*. N Engl J Med, 2005. **353**(2): p. 123-32.
201. Shimoi, K., et al., *Radioprotective effect of antioxidative flavonoids in gamma-ray irradiated mice*. Carcinogenesis, 1994. **15**(11): p. 2669-72.
202. Siegel, R.L., K.D. Miller, and A. Jemal, *Cancer statistics, 2015*. CA Cancer J Clin, 2015. **65**(1): p. 5-29.
203. Simsek, G., et al., *Protective effects of resveratrol on salivary gland damage induced by total body irradiation in rats*. Laryngoscope, 2012. **122**(12): p. 2743-8.
204. Simsek, Y., et al., *Ameliorative effects of resveratrol on acute ovarian toxicity induced by total body irradiation in young adult rats*. J Pediatr Adolesc Gynecol, 2012. **25**(4): p. 262-6.
205. Singh, A., et al., *Dysfunctional KEAP1-NRF2 interaction in non-small-cell lung cancer*. PLoS Med, 2006. **3**(10): p. e420.
206. Slavotinek, A., T.J. McMillan, and C.M. Steel, *Measurement of radiation survival using the MTT assay*. Eur J Cancer, 1994. **30A**(9): p. 1376-82.
207. Smyth, G., *Limma: linear models for microarray data*, in *Bioinformatics and Computational Biology Solutions using R and Bioconductor*. 2005, Springer: New York. p. 397-420.
208. Solis, L.M., et al., *Nrf2 and Keap1 abnormalities in non-small cell lung carcinoma and association with clinicopathologic features*. Clin Cancer Res, 2010. **16**(14): p. 3743-53.
209. Sporn, M.B., *Approaches to prevention of epithelial cancer during the preneoplastic period*. Cancer Res, 1976. **36**(7 PT 2): p. 2699-702.
210. Stenmark, K.R. and S.H. Abman, *Lung vascular development: implications for the pathogenesis of bronchopulmonary dysplasia*. Annu Rev Physiol, 2005. **67**: p. 623-61.
211. Suit, H., et al., *Secondary carcinogenesis in patients treated with radiation: a review of data on radiation-induced cancers in human, non-human primate, canine and rodent subjects*. Radiat Res, 2007. **167**(1): p. 12-42.
212. Sun, S., J.H. Schiller, and A.F. Gazdar, *Lung cancer in never smokers--a different disease*. Nat Rev Cancer, 2007. **7**(10): p. 778-90.
213. Takahashi, T., et al., *p53: a frequent target for genetic abnormalities in lung cancer*. Science, 1989. **246**(4929): p. 491-4.
214. Tamba, M. and A. Torreggiani, *Free radical scavenging and copper chelation: a potentially beneficial action of captopril*. Free Radic Res, 2000. **32**(3): p. 199-211.
215. Team, R.C., *R: A language and environment for statistical computing*. 2013, R Foundation for Statistical Computing: Vienna, Austria.
216. Tili, E. and J.J. Michaille, *Resveratrol, MicroRNAs, Inflammation, and Cancer*. Journal of nucleic acids, 2011. **2011**: p. 102431.
217. Travis, E.L., et al., *NRF2 deficiency reduces life span of mice administered thoracic irradiation*. Free Radic Biol Med, 2011. **51**(6): p. 1175-83.
218. Travis, L.B., et al., *Aetiology, genetics and prevention of secondary neoplasms in adult cancer survivors*. Nat Rev Clin Oncol, 2013. **10**(5): p. 289-301.

219. Tsao, M.S., et al., *Erlotinib in lung cancer - molecular and clinical predictors of outcome*. N Engl J Med, 2005. **353**(2): p. 133-44.
220. Tyldesley, S., et al., *Estimating the need for radiotherapy for lung cancer: an evidence-based, epidemiologic approach*. Int J Radiat Oncol Biol Phys, 2001. **49**(4): p. 973-85.
221. Uma Devi, P., et al., *Radiation protection by the ocimum flavonoids orientin and vicenin: mechanisms of action*. Radiat Res, 2000. **154**(4): p. 455-60.
222. V Kumar, A.A., N Fausto, RN Mitchell, *Robbins Basic Pathology*. 8th ed. 2007: Saunders, Elsevier Inc.
223. Valachovicova, T., V. Slivova, and D. Sliva, *Cellular and physiological effects of soy flavonoids*. Mini Rev Med Chem, 2004. **4**(8): p. 881-7.
224. Vasan, N., J.L. Boyer, and R.S. Herbst, *A RAS renaissance: emerging targeted therapies for KRAS-mutated non-small cell lung cancer*. Clin Cancer Res, 2014. **20**(15): p. 3921-30.
225. Vaughan, M.B., et al., *A three-dimensional model of differentiation of immortalized human bronchial epithelial cells*. Differentiation, 2006. **74**(4): p. 141-8.
226. Vijayalaxmi, et al., *Melatonin and radioprotection from genetic damage: in vivo/in vitro studies with human volunteers*. Mutat Res, 1996. **371**(3-4): p. 221-8.
227. Vijayalaxmi, R.J. Reiter, and M.L. Meltz, *Melatonin protects human blood lymphocytes from radiation-induced chromosome damage*. Mutat Res, 1995. **346**(1): p. 23-31.
228. Vijayalaxmi, et al., *Melatonin as a radioprotective agent: a review*. Int J Radiat Oncol Biol Phys, 2004. **59**(3): p. 639-53.
229. Wang, P., et al., *The two isomers of HDTIC compounds from Astragali Radix slow down telomere shortening rate via attenuating oxidative stress and increasing DNA repair ability in human fetal lung diploid fibroblast cells*. DNA Cell Biol, 2010. **29**(1): p. 33-9.
230. Wang, Y.Y., H. Zhe, and R. Zhao, *Preclinical evidences toward the use of triterpenoid CDDO-Me for solid cancer prevention and treatment*. Mol Cancer, 2014. **13**: p. 30.
231. Wansleeben, C., et al., *Stem cells of the adult lung: their development and role in homeostasis, regeneration, and disease*. Wiley Interdiscip Rev Dev Biol, 2013. **2**(1): p. 131-48.
232. Ward, J.F., *DNA damage produced by ionizing radiation in mammalian cells: identities, mechanisms of formation, and reparability*. Prog Nucleic Acid Res Mol Biol, 1988. **35**: p. 95-125.
233. Wasserman, T.H. and D.M. Brizel, *The role of amifostine as a radioprotector*. Oncology (Williston Park), 2001. **15**(10): p. 1349-54; discussion 1357-60.
234. Weaver, M., N.R. Dunn, and B.L. Hogan, *Bmp4 and Fgf10 play opposing roles during lung bud morphogenesis*. Development, 2000. **127**(12): p. 2695-704.
235. Weiss, J.F. and M.R. Landauer, *Protection against ionizing radiation by antioxidant nutrients and phytochemicals*. Toxicology, 2003. **189**(1-2): p. 1-20.
236. Weissman, I.L., D.J. Anderson, and F. Gage, *Stem and progenitor cells: origins, phenotypes, lineage commitments, and transdifferentiations*. Annu Rev Cell Dev Biol, 2001. **17**: p. 387-403.
237. Wellmann, K.F., *[Smoking and Health. On the Report of the Advisory Committee to the Surgeon General of the Public Health Service]*. Dtsch Med Wochenschr, 1964. **89**: p. 1085-6.
238. Whitsett, J.A., S.E. Wert, and T.E. Weaver, *Diseases of pulmonary surfactant homeostasis*. Annu Rev Pathol, 2015. **10**: p. 371-93.

239. WM Thurlbeck, A.C., *Pathology of the Lung*. Second ed. 1995: Thieme Medical Publishers, Inc.
240. Wu, X., et al., *Human bronchial epithelial cells differentiate to 3D glandular acini on basement membrane matrix*. Am J Respir Cell Mol Biol, 2011. **44**(6): p. 914-21.
241. Wyman, C. and R. Kanaar, *DNA double-strand break repair: all's well that ends well*. Annu Rev Genet, 2006. **40**: p. 363-83.
242. Xie, Y., *MBCB: MBCB (Model-based Background Correction for Beadarray)*. 2010: http://www.utsouthwestern.edu.
243. Yuhas, J.M., *Protective drugs in cancer therapy: optimal clinical testing and future directions*. Int J Radiat Oncol Biol Phys, 1982. **8**(3-4): p. 513-7.
244. Zhang, H., et al., *Resveratrol ameliorates ionizing irradiation-induced long-term hematopoietic stem cell injury in mice*. Free Radic Biol Med, 2013. **54**: p. 40-50.
245. Zilfou, J.T. and S.W. Lowe, *Tumor suppressive functions of p53*. Cold Spring Harb Perspect Biol, 2009. **1**(5): p. a001883.